

INFORMATION TO USERS

This manuscript has been reproduced from the microfilm master. UMI films the text directly from the original or copy submitted. Thus, some thesis and dissertation copies are in typewriter face, while others may be from any type of computer printer.

The quality of this reproduction is dependent upon the quality of the copy submitted. Broken or indistinct print, colored or poor quality illustrations and photographs, print bleedthrough, substandard margins, and improper alignment can adversely affect reproduction.

In the unlikely event that the author did not send UMI a complete manuscript and there are missing pages, these will be noted. Also, if unauthorized copyright material had to be removed, a note will indicate the deletion.

Oversize materials (e.g., maps, drawings, charts) are reproduced by sectioning the original, beginning at the upper left-hand corner and continuing from left to right in equal sections with small overlaps. Each original is also photographed in one exposure and is included in reduced form at the back of the book.

Photographs included in the original manuscript have been reproduced xerographically in this copy. Higher quality 6" x 9" black and white photographic prints are available for any photographs or illustrations appearing in this copy for an additional charge. Contact UMI directly to order.

UMI[®]

Bell & Howell Information and Learning
300 North Zeeb Road, Ann Arbor, MI 48106-1346 USA
800-521-0600

University of Alberta

A Mechanical Model of the Normal Human Spine

by

Steven Tong



A thesis submitted to the Faculty of Graduate Studies and Research in partial fulfillment
of the requirements for the degree of Master of Science.

Department of Mechanical Engineering

Edmonton, Alberta
Spring, 1999



National Library
of Canada

Acquisitions and
Bibliographic Services

395 Wellington Street
Ottawa ON K1A 0N4
Canada

Bibliothèque nationale
du Canada

Acquisitions et
services bibliographiques

395, rue Wellington
Ottawa ON K1A 0N4
Canada

Your file *Votre référence*

Our file *Notre référence*

The author has granted a non-exclusive licence allowing the National Library of Canada to reproduce, loan, distribute or sell copies of this thesis in microform, paper or electronic formats.

The author retains ownership of the copyright in this thesis. Neither the thesis nor substantial extracts from it may be printed or otherwise reproduced without the author's permission.

L'auteur a accordé une licence non exclusive permettant à la Bibliothèque nationale du Canada de reproduire, prêter, distribuer ou vendre des copies de cette thèse sous la forme de microfiche/film, de reproduction sur papier ou sur format électronique.

L'auteur conserve la propriété du droit d'auteur qui protège cette thèse. Ni la thèse ni des extraits substantiels de celle-ci ne doivent être imprimés ou autrement reproduits sans son autorisation.

0-612-40118-9

University of Alberta

Library Release Form

Name of Author: Steven Tong

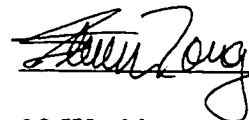
Title of Thesis: A Mechanical Model of the Normal Human Spine

Degree: Master of Science

Year this Degree Granted: 1999

Permission is hereby granted to the University of Alberta Library to reproduce single copies of this thesis and to lend or sell such copies for private, scholarly or scientific research purposes only.

The author reserves all other publication and other rights in association with the copyright in the thesis, and except as hereinbefore provided, neither the thesis nor any substantial portion thereof may be printed or otherwise reproduced in any material form whatever without the author's prior written permission.



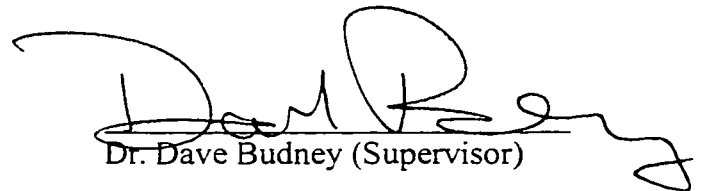
10 Washington Place
St. Albert, Alberta
Canada, T8N 3E8

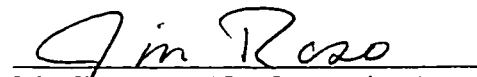
April 15, 99


University of Alberta

Faculty of Graduate Studies and Research

The undersigned certify that they have read, and recommended to the Faculty of Graduate Studies and Research for acceptance, a thesis entitled A Mechanical Model of the Normal Human Spine submitted by Steven Tong in partial fulfillment of the requirements for the degree of Master of Science


Dr. Dave Budney (Supervisor)


Mr. Jim Raso (Co-Supervisor)


Dr. Nelson Durdle


Mr. Mark Ackerman

April 7, 99

For Dad

ABSTRACT

The mechanics of operative treatment of scoliosis and spinal fixation is not clearly understood. The methodology and procedures of treatment are mostly based on empirical information inherently containing a great deal of uncertainty. Variability in deformation severity, spinal shape and geometry, and methods of treatment contribute to this uncertainty. In addition, the complex nature of vertebrae geometry within a motion segment, which results in coupling of loads and responses, leads to added difficulty in determining the required treatment.

To begin understanding the mechanics of the spine, a mechanical model of the normal thoracolumbar spine has been developed using a finite element package. Experimental data taken from published literature was used to define the shape of the normal spine and geometry of the vertebrae. The vertebrae are modeled using solid brick elements with very high modulus and behave essentially as rigid bodies. Ligaments and intervertebral discs are modeled by spring elements using material properties derived from experiment results found in literature. This model is the first step in creating a mechanical model of a scoliotic spine. A scoliotic spine configuration may ultimately be developed from the normal spine model using parametric relationships. These models could eventually lead to a better understanding of the biomechanics involved with spinal instrumentation and scoliotic corrective surgery.

TABLE OF CONTENTS

CHAPTER 1	1
1.1 Introduction.....	1
1.2 Objective of study.....	3
1.3 Overview of chapters.....	3
CHAPTER 2 - Anatomy of the normal spine.....	5
2.1 Normal spine anatomy.....	5
2.2 The vertebrae.....	7
2.3 The intervertebral discs.....	10
2.4 Ligaments.....	12
CHAPTER 3 - Biomechanics of the normal spine.....	16
3.1 The intervertebral discs.....	16
3.2 The vertebrae.....	20
3.3 The ligaments.....	24
CHAPTER 4 - Scoliosis.....	28
CHAPTER 5 - Literature review.....	34
5.1 Vertebrae geometry.....	34

5.2 Material properties of the spine.....	40
5.3 Spine models.....	42
CHAPTER 6 - Geometry of the normal spine model.....	46
6.1 Overall spinal shape.....	46
6.2 Vertebra body geometry.....	50
6.3 Spinal canal geometry.....	60
6.4 Facet geometry and orientation.....	63
6.5 Transverse and spinous process geometry.....	75
CHAPTER 7 - The normal spine model.....	81
7.1 General model description.....	81
7.2 “Rigid” body representation in the model.....	84
7.3 The vertebrae.....	84
7.4 The posterior elements.....	86
7.5 The intervertebral discs.....	88
7.6 The spinal ligaments.....	89
7.7 Facet “suspension” system.....	94
CHAPTER 8 - Material properties and model validation.....	99
8.1 The vertebrae.....	99
8.2 Spinal ligaments.....	100

8.3 Ligaments - “Secondary” stiffness values.....	101
8.4 Ligaments - Initial displacement stiffness values.....	107
8.5 Intervertebral discs.....	108
8.6 Model validation.....	110
CHAPTER 9 - Results.....	112
9.1 Initial testing.....	112
9.2 Bi-linear lumbar spinal model.....	114
9.3 Lumbar flexion.....	116
9.4 Lumbar extension.....	118
9.5 Lateral bending in the lumbar region.....	121
9.6 Axial rotation in the lumbar region.....	125
9.7 Thoracic spinal units.....	130
9.8 Thoracic flexion.....	130
9.9 Thoracic extension.....	133
9.10 Lateral bending in the thoracic region.....	137
9.11 Axial rotation in the thoracic region.....	142
CHAPTER 10 - Discussion of results.....	148
10.1 Flexion of lumbar and thoracic units.....	149
10.2 Extension of lumbar and thoracic units.....	150
10.3 Lateral bending of lumbar and thoracic units.....	151

10.4 Axial rotation of lumbar and thoracic units.....	152
CHAPTER 11 - Future work and conclusions.....	155
11.1 Future work.....	155
11.2 Conclusions.....	158
REFERENCES.....	160

LIST OF TABLES

Table 8.1 Ligament initial stiffness values.....	108
Table 8.2 Disc stiffness parameters.....	109
Table 9.1 Initial trial results.....	114

LIST OF FIGURES

Figure 2-1 The spinal regions.....	5
Figure 2-2 The vertebra.....	7
Figure 2-3 The vertebra anatomy.....	8
Figure 2-4 The intervertebral disc.....	11
Figure 2-5 The annulus fibrosis.....	11
Figure 2-6 The ligaments.....	13
Figure 2-7 The ligaments - cross sectional view.....	14
Figure 3-1 Disc load vs. displacement.....	16
Figure 3-2 Disc axial loading.....	17
Figure 3-3 Disc flexion and extension.....	18
Figure 3-4 Disc torque vs. rotation.....	19
Figure 3-5 Three column structure.....	20
Figure 3-6 Lumbar facets.....	21
Figure 3-7 Thoracic facets.....	23
Figure 3-8 Ligament load vs. deformation.....	25
Figure 3-9 The spinal ligaments.....	26
Figure 4-1 Scoliosis description.....	28
Figure 4-2 Scoliosis patterns.....	30
Figure 4-3 Scoliosis and vertebrae rotation.....	31
Figure 4-4 Scoliotic vertebra.....	32
Figure 4-5 Scoliotic back hump.....	33

Figure 6-1 Vertebral body centroid.....	47
Figure 6-2 Coordinate system.....	48
Figure 6-3 Overall spinal shape.....	49
Figure 6-4 Vertebral body dimensions.....	51
Figure 6-5a Endplate width.....	52
Figure 6-5b Endplate width.....	52
Figure 6-6a Endplate depth.....	53
Figure 6-6b Thoracic endplate depth.....	54
Figure 6-6c Lumbar endplate depth.....	54
Figure 6-7a Body posterior height.....	55
Figure 6-7b Thoracic vertebral body posterior height.....	56
Figure 6-7c Lumbar vertebral body posterior height.....	56
Figure 6-8 Endplate angles.....	57
Figure 6-9 Endplate parameters.....	58
Figure 6-10 “Kidney bean” endplate shape.....	60
Figure 6-11a Spinal canal width and depth.....	61
Figure 6-11b Spinal canal width.....	62
Figure 6-11c Spinal canal depth.....	62
Figure 6-12 Facet card angles.....	64
Figure 6-13a Facet angle alpha.....	65
Figure 6-13b Thoracic facet angle alpha.....	65
Figure 6-13c Lumbar facet angle alpha.....	66

Figure 6-14a Facet angle beta.....	66
Figure 6-14b Thoracic facet angle beta.....	67
Figure 6-14c Lumbar facet angle alpha.....	67
Figure 6-15a Facet surface centers - lateral distance.....	68
Figure 6-15b Facet surface centers - lateral distance.....	69
Figure 6-16a Facet surface centers - posterior distance.....	69
Figure 6-16b Thoracic facet surface centers - posterior distance.....	70
Figure 6-16c Lumbar facet surface centers - posterior distance.....	70
Figure 6-17a Facet surface centers - vertical distance.....	71
Figure 6-17b Superior thoracic facet surface centers - vertical distance.....	71
Figure 6-17c Superior lumbar facet surface centers - vertical distance.....	72
Figure 6-17d Inferior thoracic facet surface centers - vertical distance.....	72
Figure 6-17e Inferior lumbar facet surface centers - vertical distance.....	73
Figure 6-18a Facet surface areas.....	74
Figure 6-18b Thoracic facet surface areas.....	74
Figure 6-18c Lumbar facet surface areas.....	75
Figure 6-19a Transverse process width.....	76
Figure 6-19b Thoracic transverse process width.....	76
Figure 6-19c Lumbar transverse process width.....	77
Figure 6-20a Spinous process declination angle.....	78
Figure 6-20b Lumbar spinous process declination angle.....	79
Figure 6-21a Spinous process length.....	79

Figure 6-21b Lumbar spinous process length.....	80
Figure 7-1 Normal spine model.....	83
Figure 7-2 A modeled vertebra.....	85
Figure 7-3 Disc structure.....	88
Figure 7-4a ALL and PLL.....	90
Figure 7-4b Posterior ligaments.....	91
Figure 7-4c Intervertebral discs.....	92
Figure 7-5a Facet “suspension” system.....	95
Figure 7-5b Facet “suspension” system enlargement.....	96
Figure 7-6 Normal spine model with facet “suspension” system	97
Figure 8-1 Ligament sigmoid shaped load-displacement curve.....	101
Figure 8-2 Anterior longitudinal ligament stiffness.....	103
Figure 8-3 Posterior longitudinal ligament stiffness.....	104
Figure 8-4 Ligamentum flavum stiffness.....	105
Figure 8-5 Facet joint capsule stiffness.....	106
Figure 8-6 Inter/supraspinous ligament stiffness.....	107
Figure 8-7 Constraints and loads.....	111
Figure 9-1 Sigmoid shaped load-displacement curve.....	113
Figure 9-2 Bi-linear stiffness representation.....	115
Figure 9-3 Lumbar flexion comparison graph.....	117
Figure 9-4 Lumbar functional unit in flexion.....	117
Figure 9-5 Lumbar ligaments during flexion.....	118

Figure 9-6 Lumbar extension comparison graph.....	119
Figure 9-7 Lumbar functional unit in extension.....	120
Figure 9-8 Lumbar ligaments during extension.....	121
Figure 9-9 Lumbar lateral bending comparison graph.....	122
Figure 9-10 Lumbar functional unit in lateral bending.....	122
Figure 9-11 Coupling in lumbar functional unit - lateral bending.....	124
Figure 9-12 Lumbar ligaments during lateral bending	125
Figure 9-13 Lumbar axial rotation comparison graph.....	126
Figure 9-14 Lumbar functional unit in axial rotation.....	127
Figure 9-15 Coupling in lumbar functional unit - axial rotation.....	128
Figure 9-16 Lumbar ligaments during axial rotation	129
Figure 9-17 Load-displacement sample for thoracic flexion.....	131
Figure 9-18 Thoracic flexion comparison graph.....	131
Figure 9-19 Thoracic functional unit in flexion.....	132
Figure 9-20 Thoracic ligaments during flexion.....	133
Figure 9-21 Load-displacement sample for thoracic extension.....	134
Figure 9-22 Thoracic extension comparison graph.....	135
Figure 9-23 Thoracic functional unit in extension	136
Figure 9-24 Thoracic ligaments during extension.....	137
Figure 9-25 Load-displacement sample for thoracic lateral bending.....	138
Figure 9-26 Thoracic lateral bending comparison graph.....	139
Figure 9-27 Thoracic functional unit in lateral bending.....	140

Figure 9-28 Coupling in thoracic functional unit - lateral bending.....	141
Figure 9-29 Thoracic ligaments during lateral bending.....	142
Figure 9-30 Load-displacement sample for thoracic axial rotation.....	143
Figure 9-31 Thoracic axial rotation comparison graph.....	144
Figure 9-32 Thoracic functional unit in axial rotation.....	145
Figure 9-33 Coupling in thoracic functional unit - axial rotation.....	146
Figure 9-34 Thoracic ligaments during axial rotation.....	147

CHAPTER 1

1.1 INTRODUCTION

Scoliosis is defined as a lateral curvature of the spine in the frontal plane. (36) It usually consists of an original abnormal curve in addition to a compensatory curve in the opposite direction. Lateral curvature is regularly accompanied by an obligatory rotation of the spine in the vertical axis and deformation in the sagittal plane. Deformation in the sagittal plane is frequently a reduction of natural kyphosis and lordosis in the thoracic and lumbar region. The abnormal curvatures which occurs in both the frontal and sagittal planes, in addition to the rotation of the vertebrae about the vertical axis, is caused by the inherent coupling characteristics of motion segments in the spine.

Treatment of severe forms of this condition in many cases involves surgery where spinal instrumentation is used to achieve correction. Spinal instrumentation inherently increases the stiffness of the spine and prevents further curvature progression. The majority of correction failures are not due to breakdowns of instrumentation devices, but rather errors made by the surgeon in choosing the type of instrumentation and method of application to a given patient. (2) Since methods of treatment are almost entirely based on empirical information, a thorough understanding of the biomechanics of the scoliotic spine, and how it compares to the normal spine, would greatly facilitate any future development in scoliosis treatment.

The preeminent goal of corrective surgery is to manipulate the scoliotic spine into a normal spine configuration as closely as possible. Ultimately, a model capable of simulating a pre-operative scoliotic spine configuration, the mechanics of the interaction between the spine and the instrumentation, as well as the post-operative short and long term response of the spine would be a powerful tool in optimizing scoliotic corrective surgery. Such a model would incorporate a relationship (if one exists) between the geometry and behavior of a scoliotic spine and a normal spine. This relationship would describe the progression of a normal spine into a scoliotic configuration and how, with surgery, the scoliotic spine is manipulated back towards a normal configuration via spinal instrumentation. From this model, the forces and moments needed to achieve correction of the spine could be determined. This comprehensive model would also predict the tissue loading and response to correction. The model would ultimately permit surgeons to simulate surgical procedures, which in turn, would assist them in determining the best method of treatment.

Our approach to begin building this “ultimate” model was to create a mechanical model of the “generic” normal spine. The model was created within a finite element package. Given the presently available resources and experimental data for the normal spine, a mechanical model of the normal spine evidently appeared to be the best initial step towards creating the “ultimate” model. Eventually, the scoliotic spine model could be produced from the normal spine model using parametric relationships.

1.2 OBJECTIVE OF STUDY

The objective of this thesis is to develop and validate a mechanical model of the normal human spine. This model incorporates the 17 vertebrae in the thoracic and lumbar region. The interconnecting spinal ligaments and intervertebral discs are included in this model, but the ribs, sternum, muscle tissue, and fascia surrounding the spine are not included.

1.3 OVERVIEW OF CHAPTERS

The anatomy of the normal human spine will first be discussed in Chapter 2. The objective of this chapter is to familiarize the reader with key physiological features of the spine, and introduce vocabulary describing spinal anatomy. Chapter 3 will cover the functional biomechanics of the normal spine and its components. This chapter will discuss the mechanics of ligaments and intervertebral discs as found in literature. In Chapter 4, the condition of scoliosis is explored since scoliosis is the original motivation for the work done in this thesis. Different causes, general characteristics, and variations of the spinal deformity will be discussed. The literature review is covered in Chapter 5. Chapter 6 then discusses the geometry of the normal spine model. The methods in which the data were gathered to create the three-dimensional configuration of a normal spine are presented in this chapter. Chapter 7 and 8 present the mechanical model of the normal spine and its material properties. This is followed by the model's validation and results in Chapter 9 and 10. Finally,

conclusions and recommendations for future work regarding the normal spine model are considered in Chapter 11.

CHAPTER 2 - ANATOMY OF THE NORMAL SPINE

2.1 THE NORMAL SPINE

The spine is the primary skeletal support structure in the human body and functions as a complex linkage that also provides protection for the spinal cord. The term normal spine implies a state in which the spine is free of disease, deformity, or surgical treatment. The spine extends from the base of the skull to the pelvis, and has many functions within the body. From a mechanical perspective, it plays a primary role in postural control, body support, and locomotion. (19) The spinal column can be divided into 5 regions, of which only 3 regions permit movement.

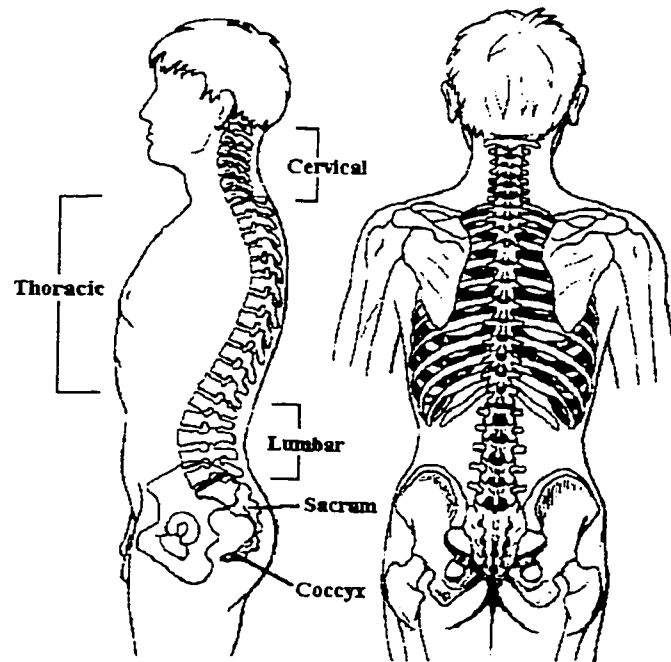


Figure 2-1. A mid-sagittal plane view and a frontal plane view (posterior aspect) of the spine within the body. Modified from Kapandji. (11)

The upper or superior region of the spine, extending from the skull to the base of the neck, is called the cervical region. In this region, there are 7 vertebrae termed Cervical 1 to Cervical 7 (C1 to C7). Inferior to, or down from the cervical region is the thoracic region. Within this region is the thorax, encompassing the part of the body between the base of the neck and the diaphragm. The thoracic spine has 12 vertebrae, Thoracic 1 to Thoracic 12 (T1 to T12). Each vertebra in the thoracic region is connected to a pair of ribs. Ribs numbered 1 to 7 connecting to vertebrae T1 to T7, are termed “true” ribs, and attach directly to the sternum by means of their own costal cartilage. Ribs 8 to 12 attaching to vertebra T8 to T12 are called “false” ribs. The costal cartilage of “false” ribs 8 to 10 insert into the costal cartilage of the adjacent superior rib. The remaining inferior false ribs 11 and 12 are often called floating ribs and do not insert anteriorly into a superior rib. The lumbar region of the spinal column is inferior to the thoracic region and is characterized by 5 large vertebrae, Lumbar 1 to Lumbar 5 (L1 to L5), which represent the bones in the “small of the back”. The cervical, thoracic, and lumbar regions entail the only spinal segments capable of motion. The two remaining regions inferior to the lumbar vertebrae are the sacrum and coccyx which fuse together forming a bony mass. The large osseous sacrum, which is composed of 5 fused sacral vertebrae, transmits body loads to the pelvis via the sacroiliac joints and provides stability to the pelvic girdle. The coccyx attaches to the inferior aspect of the sacrum and contains 4 fused coccygeal vertebrae. These small bones form the “tailbone” of the lower back.

The normal spine, as seen in the frontal plane, is symmetric about a vertical mid-line. In the mid-sagittal plane, the cervical and lumbar region both have concave curvature towards the posterior aspect of the body. Curvature of this nature is termed lordosis. In contrast, the thoracic region of the spine is concave towards the anterior aspect of the body. This type of curvature is called kyphosis.

2.2 THE VERTEBRAE

Since the normal spine mechanical model for this thesis only incorporates the thoracic and lumbar regions, detailed anatomy for only these regions will be discussed. Vertebrae in the thoracic and lumbar region are generally similar in shape. However, there are distinct differences in geometry between thoracic and lumbar vertebrae.

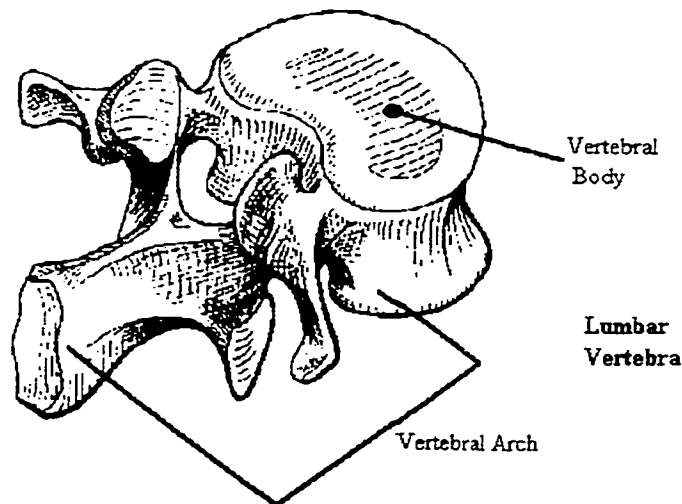


Figure 2-2. Posterior oblique view of a lumbar vertebra made up of the vertebral body and vertebral arch structures. Modified from Kapandji. (11)

A vertebra consists of two parts, the vertebral body, and the vertebral arch. The vertebral body is the large, kidney bean shaped block which occupies the anterior portion of the vertebra. Its primary function is to support loading on the spine including body weight. A lumbar vertebral body is noticeably larger than a thoracic vertebral body. Generally, the size of the body increases from the superior thoracic region to the inferior lumbar region. A characteristic feature of any thoracic vertebral body is a smooth costal facet on either side of the vertebral body which serve as articulating surfaces for the heads of ribs.

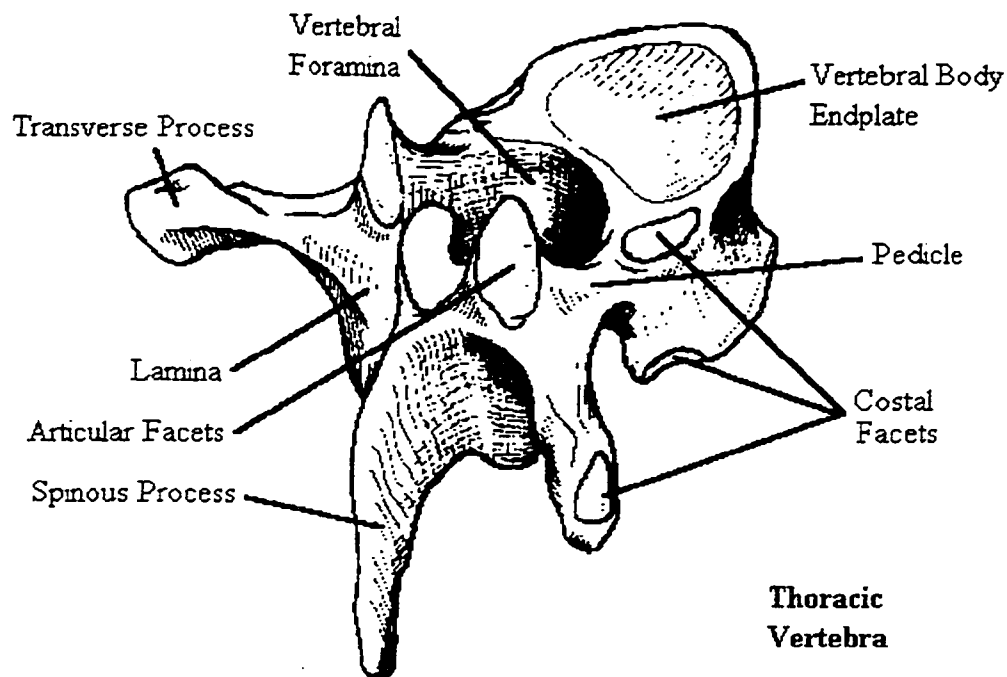


Figure 2-3. Posterior oblique view of a thoracic vertebra and its parts. Modified from Kapandji. (11)

The core of the vertebral body is composed of porous cancellous bone while the exterior is made up of harder, denser cortical bone. The superior and inferior surfaces of the vertebral bodies are called endplates. Endplates tend to have flat, rough surfaces with exception of the perimeter, which is a harder, smoother bony rim. The endplates serve as attachment surfaces for the intervertebral discs.

The vertebral arch is formed by the posterior elements in a vertebra. These elements play a key role in controlling the range of motions of the spinal column. The core interior of the vertebral arch is composed of cancellous bone while its smooth exterior is made up of cortical bone. The arch encloses the vertebral foramina, an opening which forms the spinal canal which houses and protects neural tissues including the spinal cord. The posterior elements extending immediately off the posterior aspect of the vertebral body are called the pedicles and form the base of the vertebral arch. Connecting the two pedicles together are the laminae, thus completing the enclosure of the arch. These sweeping flat bony plates extend posteromedially and slightly inferiorly from the ends of the pedicles. The spinous process branches off the vertebral arch where the two laminae join, and extends in the posteroinferior direction in the symmetrical median plane of the vertebra. This process serves as an attachment point for the inter and supraspinous ligaments as well as numerous muscles in the back. Thoracic spinous processes are distinctly longer than their stubbier lumbar counterparts and actually overlap along the spine. The transverse processes branch off the vertebral arch at the junction where the pedicles and laminae meet, extending posteriolaterally on

either side of the arch. The transverse processes serve as attachment points for the intertransverse ligaments as well as some deep muscles in the back. The transverse processes of the thoracic vertebrae have smooth facets on the ends which articulate with the tubercle of the ribs. The articular processes or zygapophyses also branch off the pedicle-laminae junction. Articular processes extend off the vertebral arch in both the superior and inferior direction. At the ends of these processes are articular facet surfaces, which form the facet or zygapophyseal joints in a functional motion segment. The perimeter of these facet surfaces serve as attachment points for the capsular ligaments of a facet joint. Articular processes help prevent anterior shearing of a superior vertebra over an adjacent inferior one, and play a key role in controlling flexion, extension, and lateral bending of the spine.

2.3 THE INTERVERTEBRAL DISCS

Interconnecting the endplate surfaces of the vertebrae are the intervertebral discs. (Figure 2-4 and 2-5) The discs are the stiffest interconnecting structures between adjacent vertebra. Intervertebral discs vary in size, but generally increase in thickness and diameter from the thoracic to lumbar region.

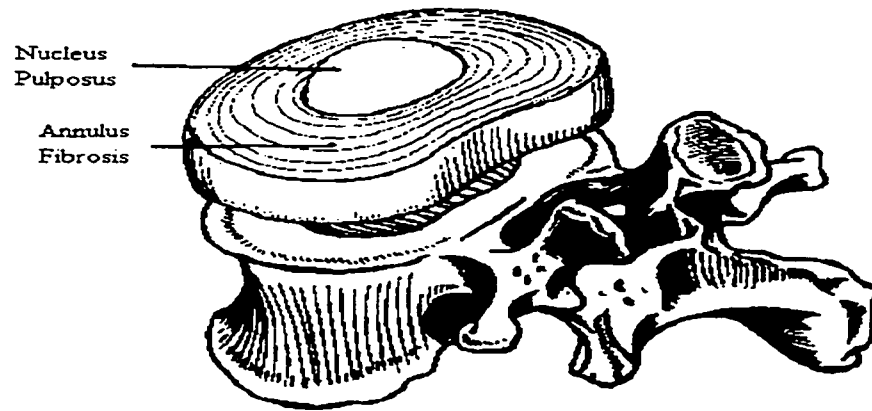


Figure 2-4. Representation of an intervertebral disc structure detached from the superior endplate of a typical lumbar vertebra. Modified from Kapandji. (11)

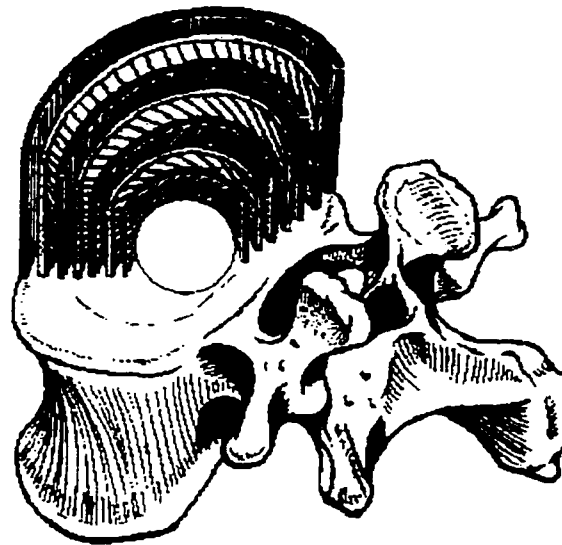


Figure 2-5. Representation of the layered structure in the annulus fibrosis on a typical lumbar vertebra. Modified from Kapandji. (11)

The core of the intervertebral disc is composed of a soft, gelatinous material called the nucleus pulposus. The nucleus has a high water content (70% - 90%) (39)

and is confined in the superior and inferior direction by hyaline cartilage plates which cover the rough endplates of the vertebral bodies. Enclosing the nucleus core is the annulus fibrosis, a series of layered concentric fibrous ligaments. Parallel annulus ligament fibers in each layer insert into the bony perimeter rim of the vertebral body endplates. The annulus fibers extend approximately 30 degrees from the horizontal plane of the endplates and are oriented 120 degrees with the adjacent neighboring layer. The intervertebral discs comprise approximately 1/4 of the total axial height of the spinal column and play a significant role in shock absorption while transmitting loads to the bony vertebral bodies in the spine.

2.4 THE INTERCONNECTING LIGAMENTS

Adjacent vertebral arches are interconnected by seven spinal ligaments. These include the anterior and posterior longitudinal ligaments, the facet or joint capsular ligaments, the ligamentum flavum, the intertransverse ligaments, the interspinous ligaments, and the supraspinous ligaments. (Figure 2-6 and 2-7)

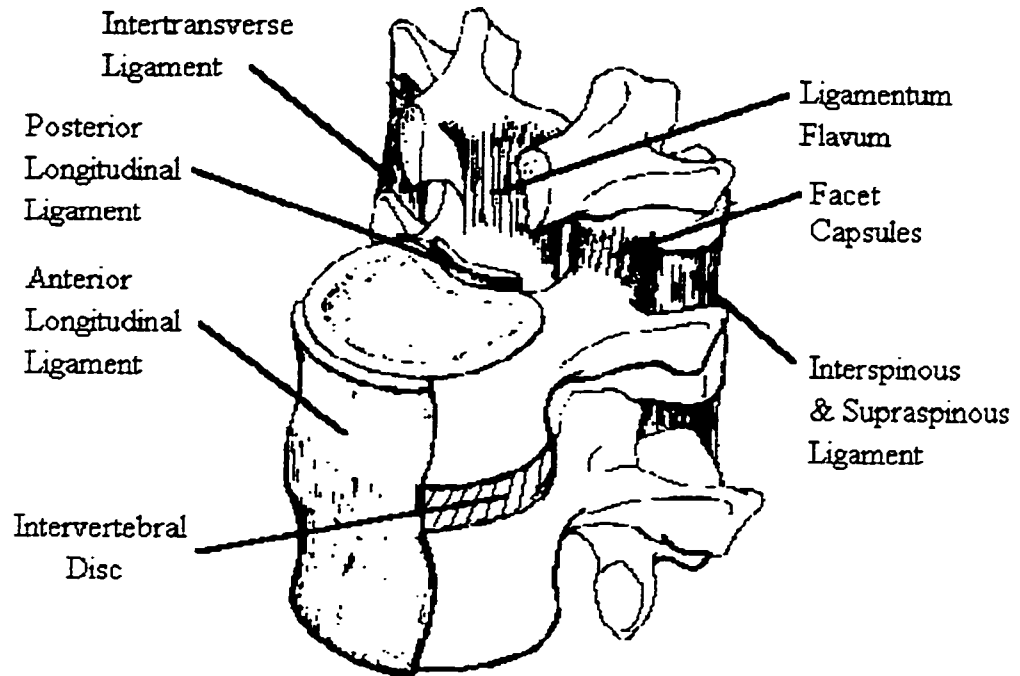


Figure 2-6. The interconnecting spinal ligaments. Modified from White & Panjabi. (39)

The anterior longitudinal ligament is a wide fibrous band lining the anterior aspect of the vertebrae bodies in the spine. This ligament inserts into each vertebra body near the endplate regions and firmly attaches to each intervertebral disc. The anterior longitudinal ligament primarily aids in preventing hyperextension of the spine and provides stability between adjacent vertebrae.

The posterior longitudinal ligament is similar to the anterior longitudinal ligament but covers the posterior aspect of the vertebrae bodies inside the spinal canal. This narrow fibrous band attaches firmly to the posterior aspect of the intervertebral

discs, and inserts into every vertebral body. The posterior longitudinal ligament provides stability and aids in preventing hyperextension of the spine.

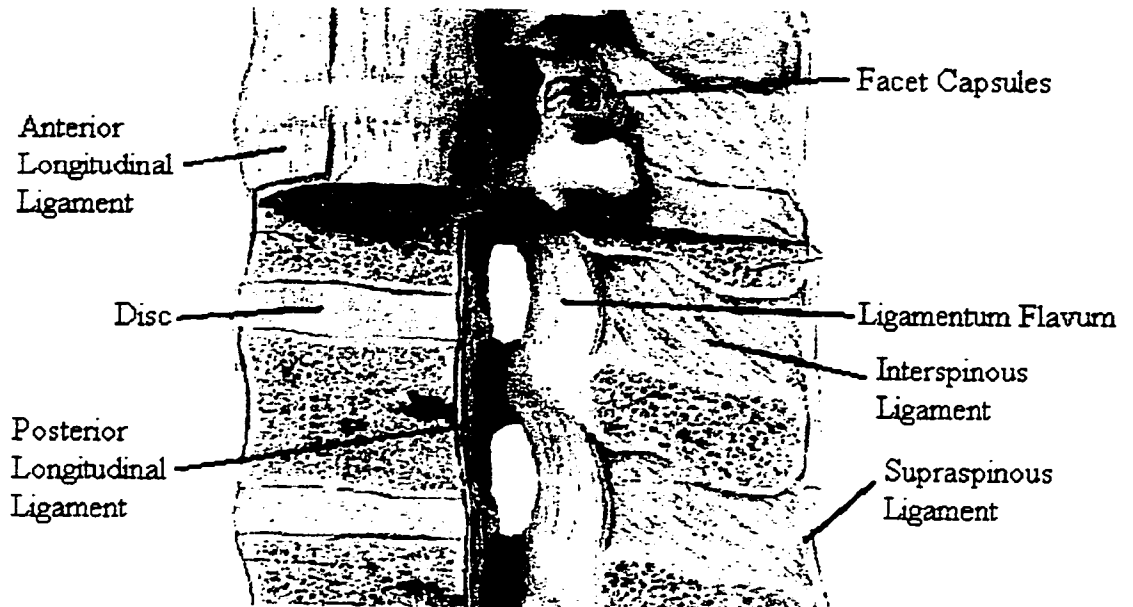


Figure 2-7. Lateral cross sectional view of the spinal column with interconnecting ligaments and disc. Modified from Netter. (21)

The facet capsular ligaments join adjacent superior and inferior articular process surfaces. These fibrous ligaments insert into the perimeter of mating facet surfaces creating an enclosed “capsule”. The facet surfaces inside the capsules are lined with hyaline cartilage that works in conjunction with synovial fluid within the joint to minimize friction. The capsular ligaments play a key role in controlling extension, flexion, and rotation between adjacent vertebrae but also allow gliding movements to

occur between facet surfaces. During axial compression on an extended spine, the facet joints carry a small portion of the compressive load which would otherwise be taken by the intervertebral discs.

The ligamentum flavum is a discontinuous ligament band interconnecting the inferior aspect of a lamina in a superior vertebra to the superior aspect of a lamina in an inferior vertebra. This highly elastic ligament helps to straighten the spine from a flexed position and provides some protection for the spinal cord inside the spinal canal.

Intertransverse ligaments connect the ends of adjacent transverse processes in the spine. Within the thoracic spine, these ligaments are composed of a few small fibers, but become increasingly more substantial in the lumbar region.

Interspinous ligaments are discontinuous thin fibrous ligaments lining and connecting adjacent spinous processes together. Overlaying the spinous process tips is the supraspinous ligament, a continuous cord-like ligament which inserts into the posterior ends of each spinous process and intertwines with the interspinous ligaments. Together these ligaments control rotation between adjacent vertebrae and prevent hyperflexion of the spine.

CHAPTER 3 - BIOMECHANICS OF THE NORMAL SPINE

3.1 THE INTERVERTEBRAL DISCS

During normal activity, the spine can undergo flexion, extension, axial rotation, and lateral bending. These movements subject the intervertebral discs to a multitude of forces and moments including compressive, tensile, torsion, and shear loads. The most apparent function of the intervertebral discs is to sustain, in conjunction with the facet joints, the axial compressive loading on the spine.

When subject to compression, the load-displacement curve of the disc is sigmoid in shape. (Figure 3-1) (39) The disc offers little resistance to small loads and displacements, but quickly increases resistance when subjected to larger loads.

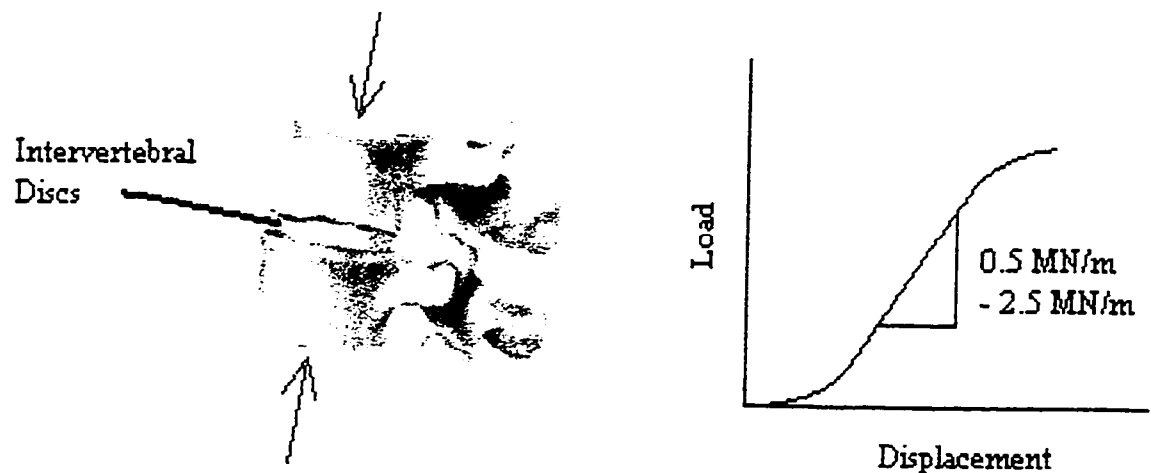


Figure 3-1. Sigmoid shaped load - displacement graph for intervertebral discs.

This behavior allows unimpeded motion during normal physiological ranges of motion, but provides increased resistance and stability during higher loading situations. When a uniform compressive load is applied to the vertebral bodies in a motion segment (with excised posterior elements), the nearly incompressible nucleus pulposus is flattened and displaced outwards, which in turn causes the annulus fibrosis to “bulge” outwards placing the annulus fibers in tension. (Figure 3-2)

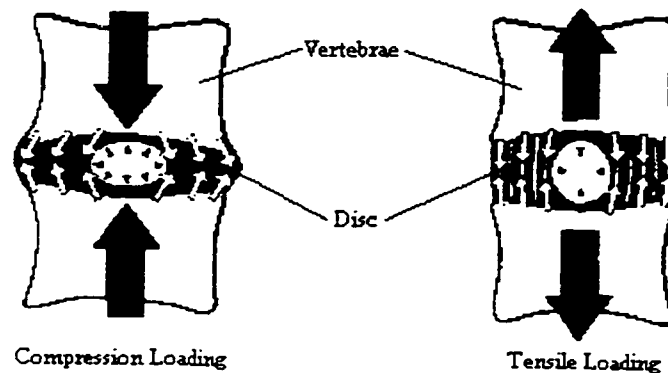


Figure 3-2. Disc behavior when spine subjected to compressive and tensile loads.

Tensile loads are experienced by the fibers in the annulus. Modified from Kapandji. (11)

Uniform tensile loading on the intervertebral disc rarely occurs during normal physiological motions. More often, only a section of the intervertebral disc is placed in tension during flexion, extension, and bending movements. In the rare case that a disc undergoes uniform traction, the annulus fibers are placed in tension resisting the axial load. The nucleus pulposus, enclosed by the annulus and vertebrae body endplates, changes from a flattened sphere, into an elongated egg-like shape. (Figure 3-2) When

the spine is subjected to bending movements such as flexion, the relatively incompressible nucleus pulposus is shifted towards the posterior region of the intervertebral disc. This places the posterior annulus fibers in tension and causes the disc to bulge posteriorly outwards. The opposite arises during extension movements where the nucleus is “squeezed” towards the anterior region of the disc causing the disc to bulge anteriorly outwards. (Figure 3-3)

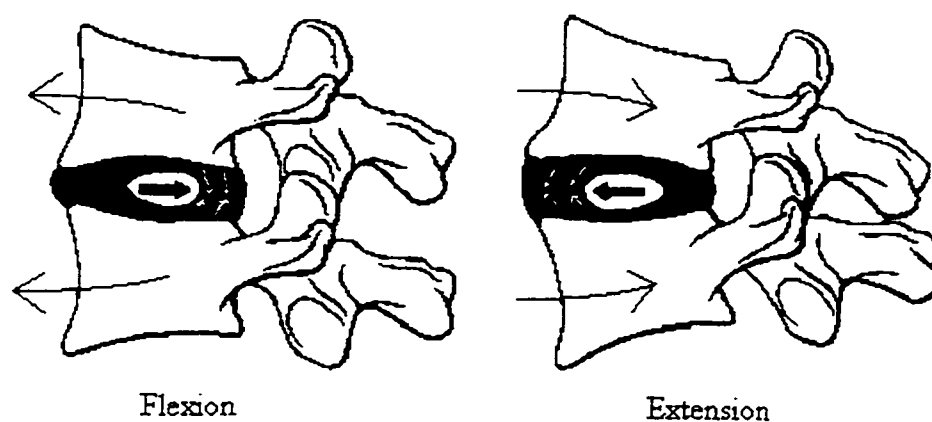


Figure 3-3. Disc behavior when spine subjected to flexion or extension. Modified from Kapandji. (11)

When the intervertebral disc is subjected to torsion, the diagonally oriented annulus fibers are placed in tension. The torque-angle of rotation graph for an intervertebral disc is sigmoid in shape. (39) At low angles of rotation (1 - 3 degrees), the disc offers very little resistance to torsion. Higher angles of rotation (4 - 12 degrees) produce a linear torque-angle of rotation relationship, with failure of the disc usually occurring at 20 degrees. (Figure 3-4) (39)

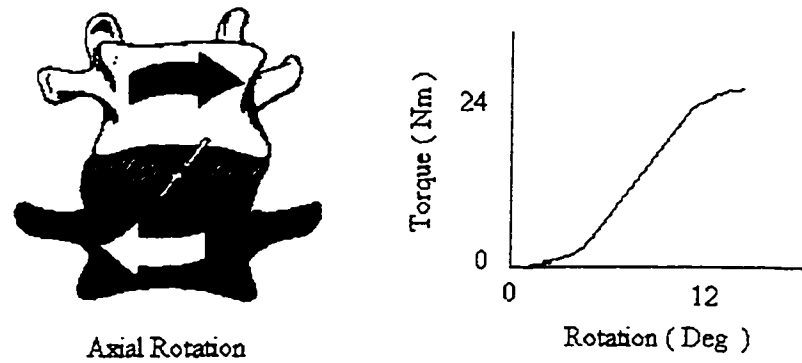


Figure 3-4. Torque vs. axial rotation for an intervertebral disc. Fibers in the annulus are loaded in one direction only. Modified from Kapandji. (11)

The torsional behavior of the disc allows the spine to rotate freely during normal physiological movements, but under higher loads, the disc behavior limits the range of motion of the spine by providing increased resistance.

The intervertebral discs exhibit viscoelastic properties and are sensitive to rate of loading. At quick axial loading rates, the force-displacement graph of an intervertebral disc exhibits a higher stiffness than that of a slower loading rate. The discs are also susceptible to the phenomena of creep and relaxation. This time dependent behavior is a built in defense mechanism protecting the spine during abrupt trauma situations.

3.2 THE VERTEBRAE

As mentioned before, a vertebrae is composed of two components, the vertebral body and the vertebral arch. To analyze how the shape of a vertebra contributes to the behavior of a functional unit, the spine can be thought of as a three column structure. (Figure 3-5) The main anterior column is made up of the rigid vertebral bodies interconnected by intervertebral discs, while the two minor posterior columns are made up of the articular processes interconnected by facet capsules.

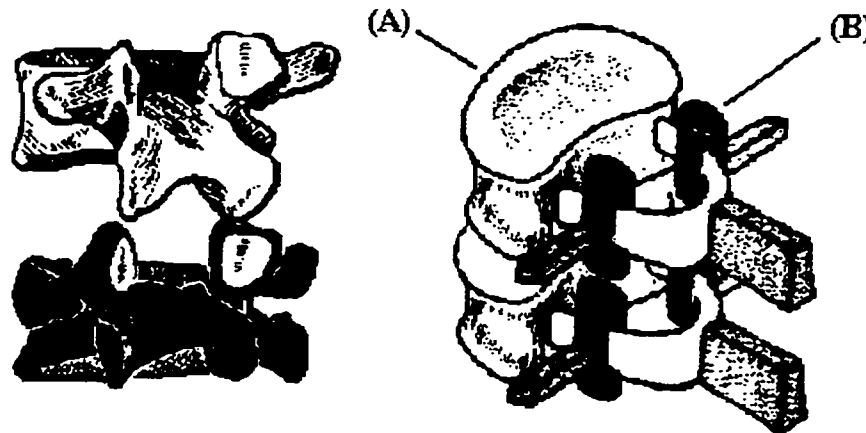


Figure 3-5. The spine modeled as a three column structure composed of the vertebral bodies and articular processes. Column (A) transmits loads through the intervertebral disc whereas column (B) transmits loads through the facet joints. Modified from Kapandji. (11)

The anterior column is the primary support member in the spine and its behavior is dictated by the swivel joint-like action of the intervertebral discs. The two posterior columns, made up of the articular processes and facet surfaces, are only involved in

supporting axial loads when the spine is extended. These processes do however extensively affect how vertebrae move relative to one another.

The facet surface orientations in the lumbar spine differ significantly from the thoracic spine. In a typical lumbar vertebra, the superior facet surfaces face medially, and slightly posteriorly. The inferior facets face laterally, and slightly anteriorly. (Figure 3-6) In a functional lumbar unit, the orientation of mating superior and inferior facet surfaces act to inhibit rotation of one adjacent vertebra relative to the other.

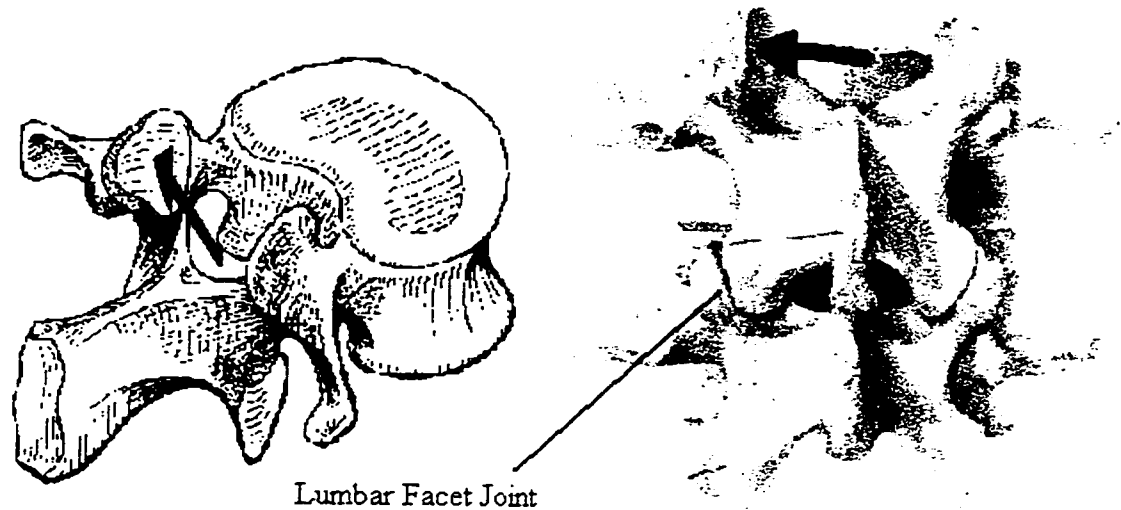


Figure 3-6. The typical lumbar facet's normal orientation is in the direction of the black arrows shown above. Modified from Kapandji. (11)

Any minor rotation in a lumbar functional unit causes the facet surfaces to come into contact, preventing further movement. Because of this, very little rotation is seen in the lumbar spine during normal physiological movements. Flexion of the lumbar spine

occurs when mating lumbar facet surfaces glide over one another. During flexion, the facet joint capsules are placed in tension, controlling to some degree the range of motion in the lumbar spine. The mechanical properties of capsular ligaments, which exhibit viscoelastic behavior like intervertebral discs, aid in preventing hyper-flexion and possible damage to the spine. Extension movements on the other hand, relieve capsular ligaments of tensile loads, and eventually causes contact of the mating superior and inferior facets. Facet surface contact prevents hyper-extension and signifies the end of the lumbar spine's normal range of extension. Further extension of the spine becomes increasingly difficult, and can eventually result in damage to the articular processes.

The orientation of thoracic articular facets enables flexion, extension, and rotations of vertebrae to occur. The superior facets of a thoracic vertebra face in the posterior direction, slightly superiorly and laterally, while the inferior facets face in the anterior direction, slightly inferiorly and medially. (Figure 3-7)

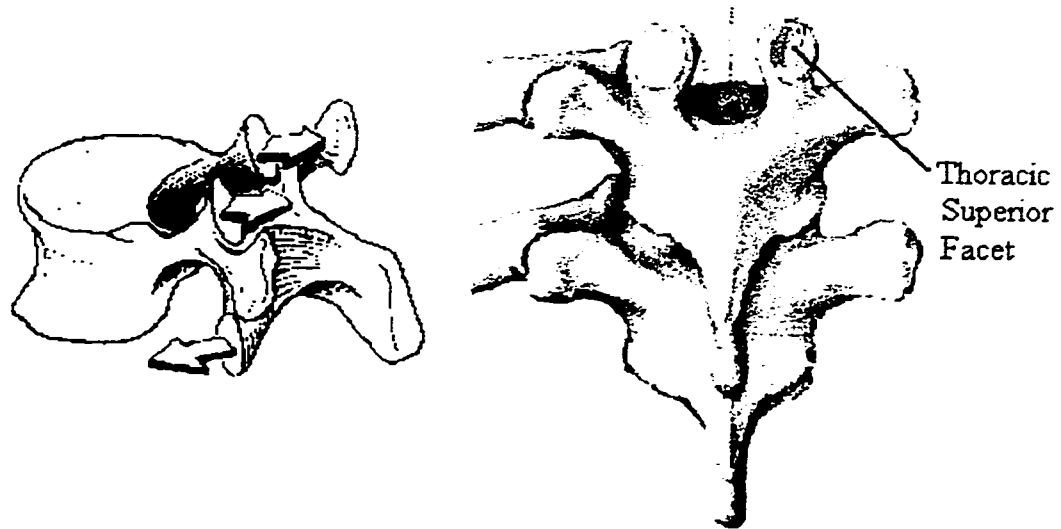


Figure 3-7. Thoracic facet orientation enables rotation, flexion, and to some degree extension. Modified from Kapandji. (11)

Flexion movements in the thoracic spine cause thoracic facet surfaces to glide relative to one another. Elongation and stretching of thoracic joint capsules place limits on flexion ranges. Extension movements in the thoracic region cause thoracic joint capsule ligaments to become slack, relieving any tensile loads. The limits of extension are reached when the facet surfaces of superior and inferior articular processes come into contact. Rotations within a thoracic motion segment result in facet surfaces gliding over one another. The limits of rotation are not influenced by contacting facet surfaces as in the lumbar region, but are determined by the mechanical properties of the facet joint capsules, intervertebral discs and interconnecting ligaments.

The transverse and spinous processes, extending off the vertebral arch, both serve as attachment points for interconnecting ligaments and muscles. In a functional unit, rotation of one vertebra relative to another occurs about the intervertebral disc. Long moment arms created by the transverse and spinous processes allow spinal muscles to apply significant leverage for extension or lateral bending of the spine. Connecting the ends of the transverse and spinous processes in adjacent vertebrae, are cable-like intervertebral ligaments, including the intertransverse, interspinous, and supraspinous ligaments. These ligaments limit the allowable distance between adjacent process end points and help to control movements in the spine.

3.3 THE LIGAMENTS

Interconnecting ligaments of vertebrae contribute to spinal stability and govern, to some degree, the spine's range of motion. The spinal ligaments include the anterior and posterior longitudinal ligament, the ligamentum flavum, the articular process capsules, the intertransverse ligaments, and the inter and supraspinous ligaments.

Ligaments are uniaxial structures which behave somewhat like rubber bands. They are composed of groups of tissue fibers oriented in parallel. This construction yields a highly anisotropic structure which is capable of supporting high tensile loads but buckles under compression. The load-displacement graph of ligaments is non-linear in shape. (Figure 3-8) (39)

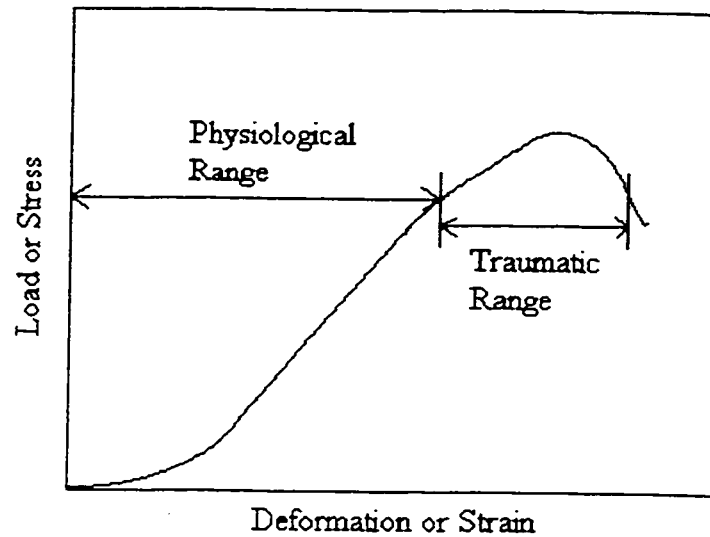


Figure 3-8. Typical load-deformation graph for an interconnecting spinal ligament.

When subjected to gradually increasing tensile loads, ligaments initially extend freely under small loads but progressively increase in stiffness under higher load. Eventually, the ligament's stiffness become somewhat linear until loads reach a "yielding" point where the stiffness suddenly decreases. A ligament also exhibits creep, relaxation, and viscoelastic behavior and is thus sensitive to rates of loading. Ligaments subjected to increased tensile loading rates display higher stiffness values. Those subjected to slow loading rates exhibit a lower stiffness. This defense mechanism characteristic of many in vivo tissues, protects the body from sudden loads experienced during shock or trauma situations.

Placements of the various spinal ligaments contribute to the manner in which the spine behaves. The center of rotation, or swivel point, of a functional unit is located near the center of the nucleus pulposus. The perpendicular distance of an interconnecting ligament to the center of rotation yields a specific moment arm distance for that ligament.

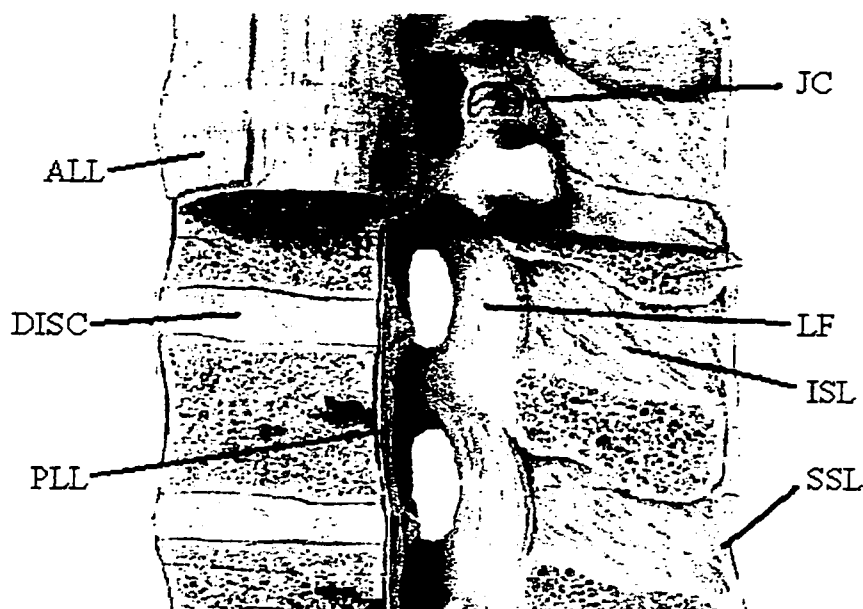


Figure 3-9. Spinal ligaments - ALL (anterior longitudinal ligament). PLL (posterior longitudinal ligament). JC (articular joint capsules). LF (ligamentum flavum). ISL (interspinous ligament). SSL (supraspinous ligament).

Modified from Netter (21)

Looking at a functional unit in the midsagittal plane (Figure 3-9), the ligaments with the largest moment arm are the inter and supraspinous ligaments. The ligaments closest to the center of rotation are the anterior and posterior longitudinal ligaments, while the

ligaments having “medium” length moment arms are the intertransverse ligament, ligamentum flavum, and articular joint capsules. The farther away a ligament is from the center of the intervertebral disc, the longer its moment arm. This implies that the stability of the spine could possibly be more easily affected by the smaller inter and supraspinous ligaments rather than the stronger anterior longitudinal ligaments.

CHAPTER 4 - SCOLIOSIS

Scoliosis is a significant amount of abnormal lateral curvature and deviation of the spine from the vertical mid-line in the frontal plane. (36) Although the deformation in the frontal plane is the most noticeable aspect of the disease, it is regularly accompanied by a “flattening” of the spine in the sagittal plane. (Figure 4-1)

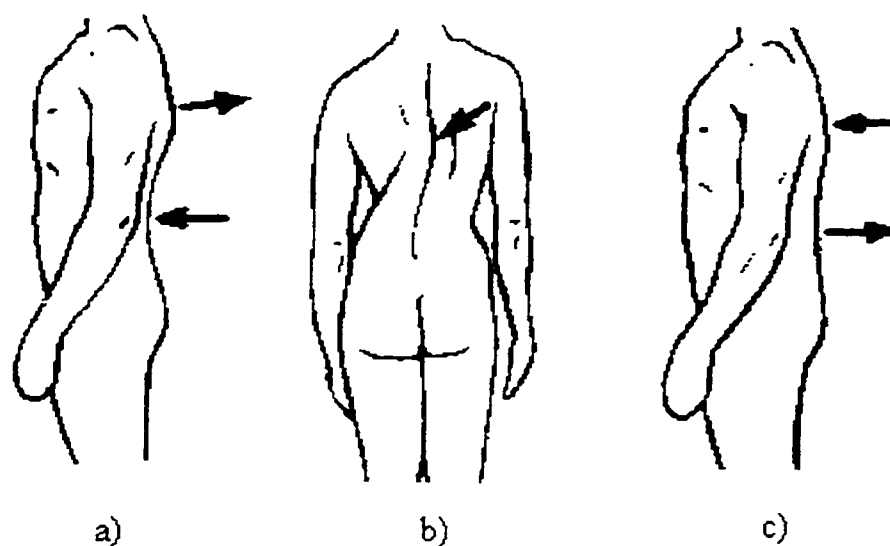


Figure 4-1. a) Lateral view of normal spine curvature. b) Posterior view of scoliotic spine
c) Lateral view of scoliotic spine with a “flattening” of the back

A scoliotic spine compared with a normal spine will usually have a reduction in lumbar lordosis and thoracic kyphosis. Rotations of individual vertebrae about the longitudinal axis of the spine also accompany the abnormal curvature, and are a result of coupling effects in motion segments.

The various causes of scoliosis may be classified into 3 groups; idiopathic, neuromuscular, and congenital. The cause of neuromuscular scoliosis is related to the nerves and muscles, whereas congenital scoliosis refers to lateral curvature present at birth. Of the three, idiopathic scoliosis is by far the most common, and accounts for 80 - 90% of scoliosis cases.(12) Idiopathic scoliosis, which denotes scoliosis of unknown cause, occurs mostly in adolescent females. This disease may arise for no apparent reason in an otherwise healthy individual, but has been loosely linked with people pertaining a family history of scoliosis.

The majority of scoliosis cases fall into 5 curve patterns. (Figure 4-2) The most common curve is the double major curve usually consisting of a right thoracic curve and a compensatory left lumbar curve. Once in a while, the curves are reversed with a left thoracic and right lumbar curve.

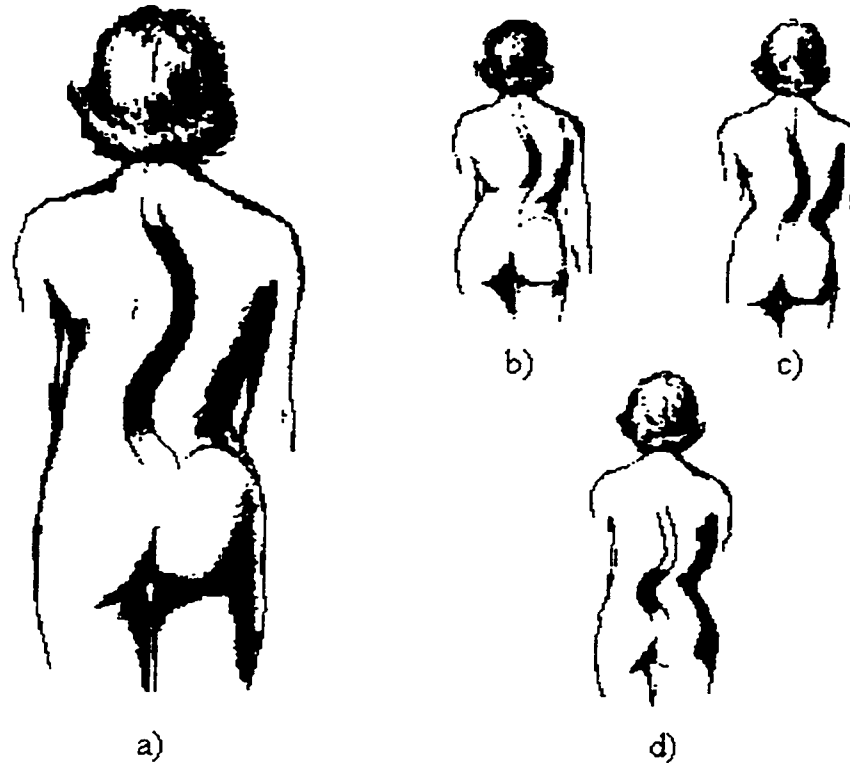


Figure 4-2. a) A double major curve scoliotic spine, the most popular case. b) single thoracic curve, c) single thoracolumbar curve, and d) single lumbar scoliotic curve.

Modified from Keim. (12)

Frequently, an individual who acquires a double curve pattern initially develops a single right thoracic curve. The individual, in an attempt to align the head with the sacrum in the pelvis, develops a compensatory lumbar curve in the opposite direction. The lumbar curve eventually progresses, resulting in a double major curve configuration. Scoliosis of this type leads to a shortening of the trunk, and in mild cases is only a cosmetic problem. If curve progression is critical, leading to respiratory or cardiopulmonary malfunction, surgery is necessary. Other less common curve patterns

are single curves in the thoracic, thoracolumbar, lumbar, and cervicothoracic regions of the spine. (Figure 4-2) These curves may also require surgery in extreme cases.

In a normal spine, the coupling effect within motion segments causes a rotation of individual vertebrae when lateral bending occurs. During lateral bending, the vertebrae rotate along the longitudinal axis of the spine such that the spinous processes point towards the convexity of the curve. This pattern is consistently noted in the cervical and superior to mid-thoracic region, but not so in the inferior thoracic or lumbar region. In a scoliotic spine, the opposite occurrence is noted where the spinous processes point towards the concavity of the curve. (Figure 4-3)

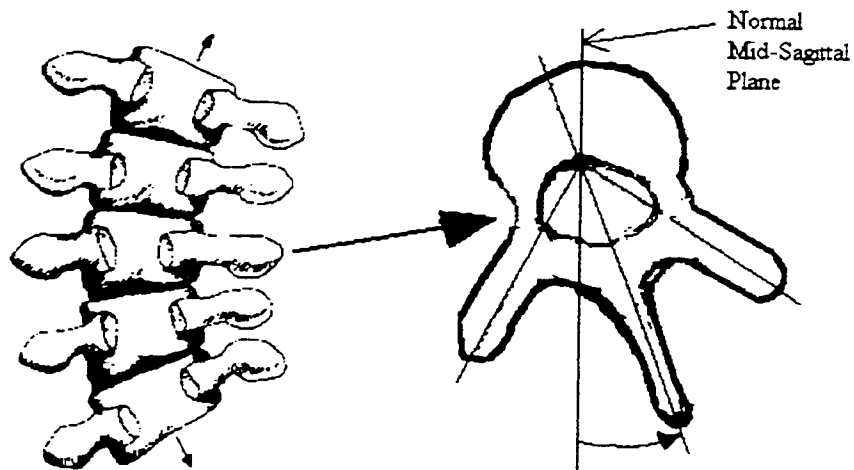


Figure 4-3. In the scoliotic spine, vertebrae rotate such that the spinous processes point towards the concavity of the curve.

In addition to overall spinal curvature, scoliosis is also manifested by a distortion of individual vertebrae. In a scoliotic vertebra, the vertebral body and

posterior elements are both affected. The scoliotic vertebral body as seen in the frontal plane, has a lateral wedge angle between superior and inferior endplates. In the transverse plane, the vertebral body is asymmetrical, and no longer retains the uniform kidney bean shape. (Figure 4-4)

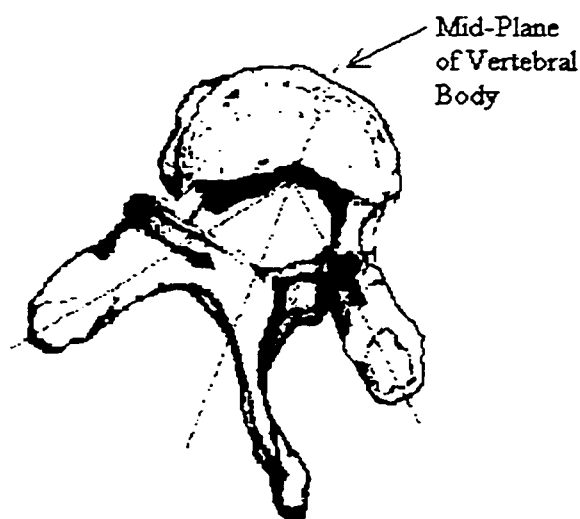


Figure 4-4. Superior view of a scoliotic vertebra. The vertebral body and posterior elements are non-symmetrical. Modified from Keim. (12)

The posterior elements are also deformed to some extent. The pedicles become wider and longer on one side of the vertebra and shorter on the other side. The spinous processes, articular processes, and transverse processes are also no longer symmetrical about the mid-line of the vertebra and differ in size and length from one side to another.

The abnormally rotated thoracic vertebrae of a scoliotic spine are normally accompanied by deformed ribs. (Figure 4-5) This rotation produces a posterior

“bulge” or back hump on the convex side of the curve and is characteristic of scoliosis.

The hump is most noticeable from a posterior view during flexion of the spine.

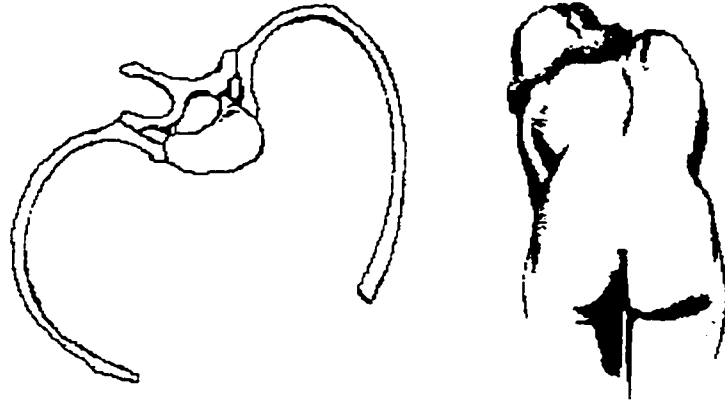


Figure 4-5. Deformed scoliotic vertebrae and ribs produce a pronounced back hump with uneven shoulder heights. Modified from Keim. (12)

Treatment of scoliosis may begin with bracing where pressure is applied to strategic areas on the ribs by means of a body casing, in hope of preventing further curve progression. In more serious cases, surgery is necessary where instrumentation is employed to achieve correction. Spinal instrumentation inherently increases the strength of the spine and prevents further curvature progression. Presently, the methods and procedures of this surgery are based on empirical information containing a high degree of variability. It is the aim of this thesis is to build a normal spine model that could eventually be incorporated to better understand the mechanics of scoliotic surgery.

CHAPTER 5 - LITERATURE REVIEW

The past 30 years have seen an emergence of spinal models which study and contribute to understanding the mechanics of the spine. Recently, more advanced tools for creating complex spinal models have come forth, but the present lack of experimental data on geometry and mechanical properties of physiological spine components, inhibits the progress of creating a complete and thorough mechanical model of the normal spine. In this chapter, various studies regarding spine mechanics are reviewed to gain insight into different techniques and methodologies which could possibly be used in creating and validate the normal spine model of this thesis.

5.1 VERTEBRAE GEOMETRY

Lavaste et al. (14) developed a method to model the three dimensional geometry of a normal lumbar spine segment. After doing a morphological analysis on 40 lumbar vertebrae from 8 lumbar spines, Lavaste et al. determined that the geometry of each vertebra could be mathematically reconstructed using six parameters measured from a vertebra. These parameters include the width, depth, height, and concavity of the vertebral body, in addition to the total height and depth of the vertebra. A series of secondary parameters are calculated from these six parameters and incorporated into mathematical equations used to define the geometry of a vertebra. The required measurements can be easily obtained from anterioposterior and lateral radiographs.

This geometric modeling method developed by Lavaste et al. potentially allows for quick construction of individualized spine models of patients, using a minimal amount of digitized data from AP and lateral radiographs. The methodology and procedure developed in this study was used to describe the “kidney bean” shape of the vertebral body endplates, and is described in Chapter 6.

A study performed by Panjabi et al. (25, 26) documents the quantitative three-dimensional morphology of thoracic and lumbar vertebrae. This study was carried out to provide a resource for quantitative geometric data for use in spine models. In total, 204 thoracic and lumbar vertebrae from 12 spines were evaluated. The male and female cadavers from which these vertebrae were excised, ranged in age from 19 to 59 years. The soft tissues attached to, and interconnecting the spinal vertebrae, were initially softened by boiling, then removed by submerging the spines in bleach and ethanol. Each bony vertebra was then scrubbed clean of all tissue matter, dried and rigidly mounted into a stand. After defining an origin at each vertebral body centroid, key points were digitizing along surfaces of the vertebra and translated into various dimensions and areas representative of a vertebra's surface morphology. The data gathered were intended for use in normal thoracolumbar spine models and may provide a better understanding of vertebrae morphology and function. The recorded dimensions for various vertebral features in this study include:

- endplate width, depth, area, and inclination

- vertebral body height
- spinal canal width, depth, and area
- pedicle width, height, area, inclination, and moment of inertia
- costotransverse process articulation area (thoracic region only)
- costovertebral articulation area (thoracic region only)
- pars intra-articularis area
- spinous process length
- transverse process width

Berry et al. (3) performed a morphometric study on selected thoracic vertebrae to provide quantitative data for the development and improvement of spinal implants. Particular emphasis was placed on pedicle and vertebral body morphology as these features are usually the recipients of pedicle fixation screws during corrective spinal surgery. Twenty seven dimensions were measured on selected vertebrae from 30 spines already cleaned and prepared by the Hamann-Todd Osteological Collection in Cleveland, Ohio. The vertebrae were taken from cadavers between 50 and 70 years of age. The vertebral levels evaluated were T2, T7, T12, and L1 to L5. The outside dimensions of the vertebrae were measured using Vernier calipers, while angular measurements were carried out using a goniometer. The dimensions recorded for the vertebral feature at the selected vertebral levels included:

- vertebra total length in lateral plane

- vertebral body width and depth at vertebral body mid-transverse plane, and superior and inferior endplates
- vertebral body anterior and posterior height
- vertebral body endplate angle of declination relative vertebral body mid-transverse plane
- spinal canal width and depth
- pedicle width and height
- pedicle angle relative to vertebral body mid-sagittal plane
- height between superior and inferior articular processes in frontal plane
- spinous process angle of declination relative to vertebral body mid-transverse plane

The overall goal of Berry's et al. study was to provide geometrical information for vertebra reconstruction and modeling. The underlying emphasis of the study was to provide insight into the application of pedicle screw fixation and to investigate spinal instrumentation design possibilities and constraints.

Scoles et al. (34) performed a morphological study on vertebra anatomy at multiple spinal levels to investigate and define geometric ranges in morphometry in normal spines. This study was performed to aid in the development and use of internal spinal fixation techniques for stabilizing spine fractures. The vertebrae of 50 normal post mortem adult spines taken after death were evaluated at the spinal levels T1, T3, T6, T9, T12, L1, L3, and L5. Twenty five male and 25 female adult spines ranging

from 20 to 40 years of age, were evaluated and measured using calipers, protractors, and goniometers. The vertebral features measured in the study include the:

- maximum height of the vertebral body in the sagittal plane
- anteroposterior diameter of the vertebral body in the mid-sagittal plane
- maximum diameter of the superior surface of the vertebral body in the transverse plane
- vertebra-pedicle angle
- pedicle minimum and maximum diameter
- pedicle length and axis length
- spinal canal width and depth
- distance between the inferior facet surface edge and the pedicle center in the transverse plane
- distance between the inferior facet surface edge and the inferior pedicle surface in the transverse plane

The measured data at each vertebral level was averaged, and a linear regression technique was employed to determine data trends as a function of vertebral level. Emphasis was placed on measuring features relevant to the placement of pedicle screws and implants. Scoles et al. found that a high degree of variability is present in posterior element geometry and thus concluded that a universal implant system or instrumentation technique could not be clinically applied.

Dumas (7) investigated the articulating facet joints in the posterior elements of vertebrae. These facets were found to significantly affect the kinematic and mechanical behavior of the spine. For example, the physiological range of axial rotation in a lumbar spine is limited and controlled by facet joints. Facet joints in a spine subjected to axial compression in the extended position, have been found to support up to 35% of the total loading.

The primary purpose of Dumas' study was to provide geometrical data on spinal facets for use in biomechanical models of the spine. Using digitizing equipment, a morphological study was conducted on the spinal facets from 4 embalmed cadavers to determine the shape, orientation, position, and area of the facet surfaces. The facet surfaces in each vertebra of the 4 spine samples were fitted using plane, cylindrical, and dihedral surfaces. Dumas determined that dihedral surfaces provide the best fit for thoracic and cervical facets, while cylindrical surfaces best approximated lumbar facet surfaces. The orientation of the facet surfaces relative to the vertebral bodies were evaluated, averaged, and recorded at each spinal level in terms of card angles. With card angles, 2 angles in a Cartesian coordinate system are required to define the orientation of a surface in three dimensional space. (Figure 6-12) The locations of the facet surface centers were also evaluated in Cartesian coordinates relative to the vertebral body centroids. The center points were digitized and expressed in terms of lateral, posterior, and vertical displacements from the vertebral body centroids at each

spinal level. The facet surface areas were assessed and averaged for the 4 spine samples by spinal region and inferior and superior facets. Dumas found that cervical and thoracic vertebrae have larger superior than inferior facets, while lumbar vertebrae exhibit an opposite trend.

5.2 MATERIAL PROPERTIES

Chazal et al. (4) conducted a biomechanical study on 43 human spinal ligaments. Each ligament in the study was taken from human subjects, ages 30 to 80 years, within one hour postmortem. The ligaments studied at various spinal levels include the anterior and posterior longitudinal ligaments, the ligamentum flavum, the supra and interspinous ligaments, and the intertransverse ligaments. The load displacement properties of the ligaments were evaluated through tensile tests where the ligament specimen was distracted via the bones in which they insert, rather than the ligament itself. This method was used to prevent damage to the ligament and provide a realistic simulation of in vivo conditions where loads are transmitted to ligaments via bony attachments. Chazal et al. found that the ligament specimens have a characteristic sigmoid load-displacement shape (Figure 8-1) when subjected to a slow displacement loading rate of 1mm/min. The initial part of the curve is concave towards the load axis of the graph. Further increase in tensile load results in a linear load-displacement relationship with a slope steeper than the initial region of the curve. Loading beyond the linear region produces a concave curve towards the elongation axis quickly

followed by rupture and failure of the ligament. The load-displacement value for every specimen was recorded and documented at the end of each of the three regions of the sigmoid curve. It was also found that during rapid loading and unloading cycles, ligaments exhibit elastic properties.

Myklebust et al. (20) evaluated spinal ligaments taken from 41 human male cadavers with an average age of 67 years. Each specimen was tested within 1 to 3 days postmortem and kept at a temperature of 2°C until tested. The ligaments were studied in situ by sectioning and excising the intervertebral disc and all interconnecting spinal ligaments from a given functional unit except the ligament to be studied. Tensile loads were then applied to the ligament by pinning the bony vertebrae of the functional unit in a tensile testing apparatus and applying a distraction between the two vertebrae. The anterior and posterior longitudinal ligament, the two articular joint capsules, the interspinous ligament, and the ligamentum flavum were evaluated at each level between C2 to S1. Force deflection curves for all ligaments were found to exhibit a sigmoid shape. (Figure 8-1) Each ligament was tested until failure, where failure was defined as the point where an increase in deflection corresponds to a decrease in load. The average failure load and displacement at each vertebral level was then recorded for each spinal level. The load deflection results of the study are similar to and in agreement with those reported by others. (4, 29)

In a study by Pintar et al. (29), the tensile properties of lumbar spinal ligaments

were investigated using 38 fresh human cadavers ranging in age from 31 to 80 years old. Pintar's et al. objective was to gather data for direct use in mathematical and finite element models. In situ isolation testing was performed on the anterior and posterior longitudinal ligaments, the ligamentum flavum, the articular joint capsules, and the interspinous and supraspinous ligaments at each lumbar spinal level between T12 and L5. The in situ method and procedure used in the study is the same as that of Myklebust et al. (20). For testing, the intervertebral disc and all interconnecting spinal ligaments in the functional unit were removed except the ligament tested. Tensile loads were then applied to the ligament by distraction of vertebrae body pairs to which the ligament was attached. The displacement between the vertebrae was recorded throughout the test to yield a data set representative of a force-displacement curve for the ligament. The resultant curves for all ligaments were then evaluated and averaged at each level in the lumbar spine. To determine the overall stiffness of the ligament, the linear portion of the curve was fitted using a least squares regression.

5.3 FINITE ELEMENT MODELS OF THE SPINE

Descrimes et al. (5) utilized a finite element model of the thoracolumbar spine to better understand the influence of the facet joints on the mechanical behavior of the spine. The overall geometry of the model was obtained using stereoradiographic 3-D reconstructions of a given patient combined with CT scans of cadaveric vertebrae. Each intervertebral disc in the model was represented by a 3-D beam element and

torsion spring. The anterior and posterior longitudinal ligaments of the spine were accounted for by the disc elements, while the remaining interconnecting ligaments were modeled using linear springs. 3-D beam elements were also used to represent the vertebrae, sternum, and rib. The model were evaluated using either plane or cylindrical facet surfaces. These articular surfaces were represented by point-to-surface contact and shell elements while the articular capsule ligaments were modeled by linear springs. The mechanical properties of the beam and spring elements in the model were all taken from various literature sources.

In order to test and validate the model, Describes et al. extracted various functional units from the model, and analyzed the units individually by comparing loading response with cadaveric samples. Each unit was tested for flexion, extension, lateral bending, and axial rotation where loads were applied to the superior vertebra while the inferior vertebra was held fixed. Describes et al. stated that further validation of the entire model as a whole, instead of individual functional units, was required to further test and understand the coupling relationship between the spine and facet joints.

Ueno and Liu (38) created a three-dimensional finite element model of a lumbar functional unit (L4-L5) to investigate failure mechanisms in the intervertebral joint subjected to torsional loading. The individual influence of the spinal ligaments, intervertebral disc, and facet joints during torsional loading on the spine was

investigated as well as stress distributions within the annulus fibers of the disc.

The geometry of the finite element model was obtained by digitizing dried lumbar vertebrae. The intervertebral disc in the model was given a constant thickness of 10mm and assumed to have the same transverse section area as the adjacent endplates of the vertebral bodies. The vertebrae bodies and posterior elements were modeled using solid brick elements where the outermost element layer was given material properties typical of cortical bone, while the inner elements were given properties typical of cancellous bone. The vertebral body endplate surfaces were given cartilaginous properties. For the intervertebral discs, 8 concentric layers of elements representing the annulus fibrosis were used, while the nucleus pulposus was modeled using elements behaving in an incompressible manner incapable of sustaining shear. All interconnecting spinal ligaments were included where the geometry of the insertion points was chosen based on anatomical texts. The material properties used in the model were all linearly elastic and gathered from results found in literature.

Ueno and Liu found that the facet joints in the lumbar functional unit, when subjected to torsion loads, carry 30% to 40% of applied load. Upon removal of the facets, an increase in stress occurs within the intervertebral discs. Throughout the study, resistance to torsion by spinal ligaments were found to be extremely small and were considered negligible. The intervertebral discs exhibited an increase in both pressure within the nucleus pulposus and compressive stresses within the endplate

ground substance. The annulus fibers were found to exhibit tensile stresses with a maximum occurring in the outermost lateral aspect of the disc. It was on this basis that Ueno and Liu concluded that disc herniations, which occur at the posterior and slightly lateral aspect of the disc are not likely caused by torsion loading on the spine.

CHAPTER 6 - GEOMETRY OF NORMAL SPINE MODEL

A quantitative description of the normal spine was compiled from various data found in existing literature. (3, 7, 14, 25, 26, 27, 34) This data enabled the creation of an accurate geometric and mechanical model of a normal spine. In addition to determining the overall curvature and shape of the normal spine, the key anatomical dimensions investigated were:

- the morphology of the vertebral body
- the spinal canal width and depth
- the size and orientation of the articular facets
- the length and orientation of the spinous and transverse process

6.1 OVERALL SPINAL SHAPE

The overall shape of the normal spine model was defined using the locations of the vertebral body centroids from a "generic" normal spine. The "generic" spine was developed using experimental data taken from 4 adolescent female subjects, in which the locations of L5 to T1 vertebral body centroids were described in a 3-D Cartesian coordinate system. (41)

This experimental data was previously found by digitizing the vertebral body centroids of sagittal plane x-rays. In the sagittal plane, the centroids were defined as

the intersection of two straight lines, connecting the anterior superior endplate edge with the posterior inferior endplate edge of a vertebral body and vice versa. (Figure 6-1) For the “generic” spine model, it was assumed the vertebral body centroids were aligned on the vertical z-axis. (Figure 6-2)

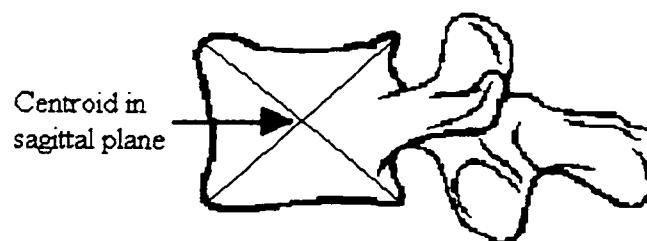


Figure 6-1. The vertebral body centroid is defined as the intersection point of two lines connecting the superior and inferior endplates.

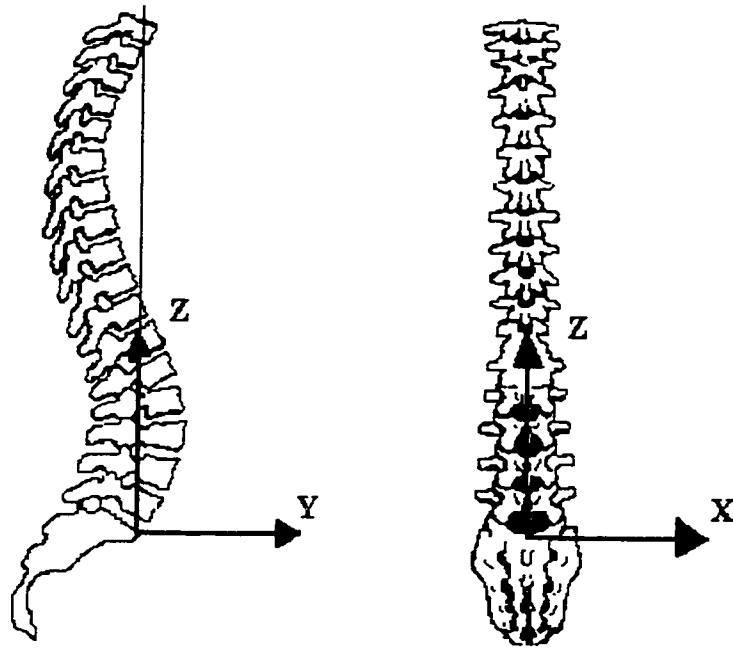


Figure 6-2. Coordinate system used in defining spinal curvature. Origin is located at the anterior aspect of the superior vertebral body endplate of S1. Note that the z axis intersects the vertebral body centroid of T1. Modified from White (39)

The data were expressed in terms a 3-D Cartesian coordinate system with the origin located at the anterior aspect of the superior endplate of S1. The frontal plane of the spine was represented by the z-x plane, while the mid-sagittal plane was represented by the z-y plane. (Figure 6-2) The experimental data was normalized so that the overall geometry and shape of the 4 data cases could be compared with one another. Each spine was positioned such that the location of the origin and T1 vertebral body centroid would lie along the vertical z axis. The distance between the origin, and the vertebral

body centroid of T1 was scaled to a value of 100%, while the deviation of the body centroids from the z axis in the z-y mid-sagittal plane were expressed as a percentage of this distance. The spine was assumed to be symmetrical in the z-x frontal plane with no deviation of vertebral body centroids about the z axis. Data points for the vertebral body centroids of the four spines were curve fitted using a 5th degree polynomial to determine the 3-D geometric shape of the normal spine model. (Figure 6-3)

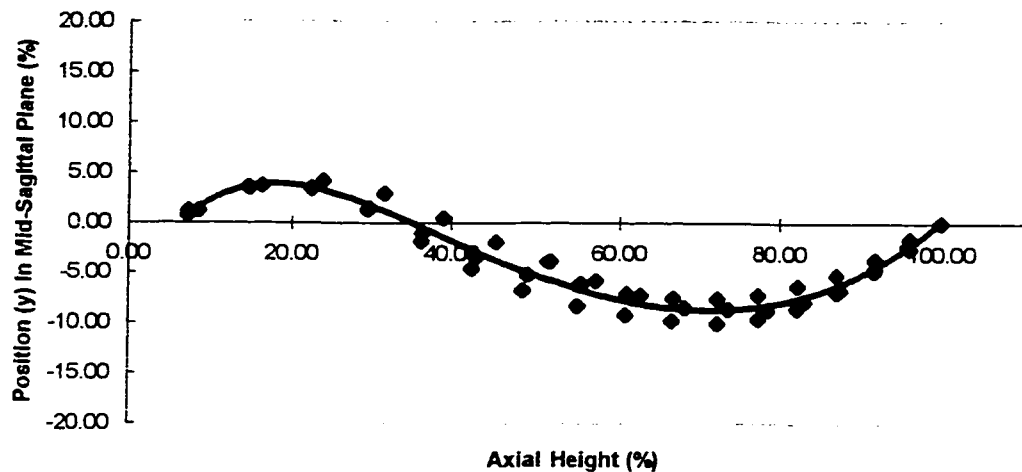


Figure 6-3. Curve fitting of data representing the vertebral body centroids of the normal spines. The y-axis in this figure, represents the “y-axis” in Figure 6-2. The x-axis in this figure, represents the “vertical z-axis” of Figure 6-2. The displacements on the y-axis in this figure, were expressed as a percentage of the axial height between S1 (origin) and T1 (100%) on the x-axis. The curve fitting was done using a 5th degree polynomial, least squares regression.

Z coordinates of the vertebrae centroids at each vertebral levels were averaged to determine the locations of the vertebral body centroids. In this model, the mid-plane of

the individual vertebral bodies are assumed to be perpendicular to the tangent of the curve.

6.2 VERTEBRA BODY GEOMETRY

After defining the overall shape of the normal spine model, the geometry of the individual vertebrae were determined from experimental results reported in literature. The significant dimensions (Figure 6-4) of thoracic and lumbar vertebral bodies were retrieved from literature (3, 14, 25, 26) detailing:

- the maximum superior and inferior vertebral body endplate widths in the transverse plane. (Figure 6-4 - Dimension A)
- the maximum superior and inferior vertebral body endplate depths along the symmetrical mid-line in the transverse plane. (Figure 6-4 - Dimension B)
- the anterior and posterior height or distance between endplates in the mid-sagittal plane. (Figure 6-4 - Dimension C)
- the superior and inferior endplate inclination or declination relative to the transverse mid-plane of the vertebral body. (Figure 6-4 - Dimension D)
- a method of defining the kidney bean shape of the superior and inferior endplates of the vertebral bodies using mathematical plane curves. (14)

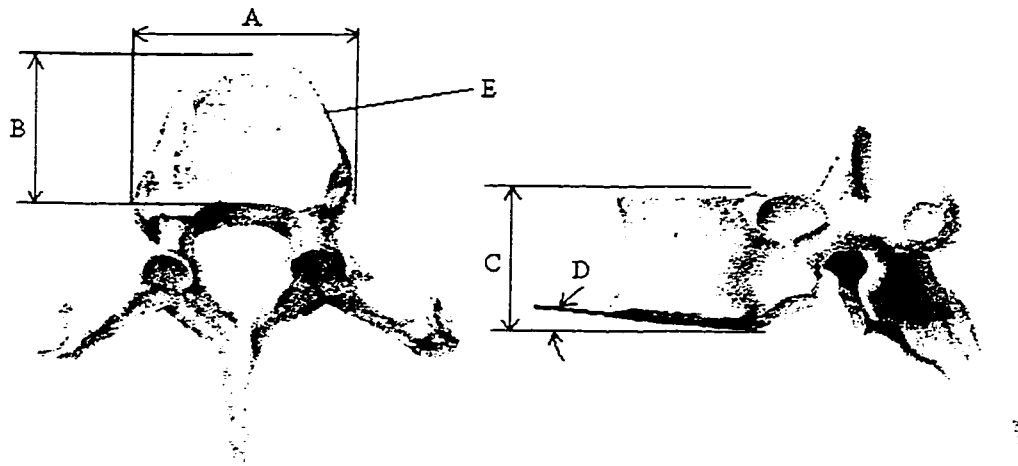


Figure 6-4. Relevant dimensions in the vertebral body. A - Superior and inferior body width.
 B - Superior and inferior body depth. C - Anterior and posterior body height.
 D - Superior and inferior endplate angles, and E - Body "kidney bean" like shape

Combining this information, the geometry of the vertebrae in the thoracic and lumbar regions was reconstructed for use in the normal spine model.

The superior and inferior endplate widths and depths of the vertebral bodies were described by Berry et. al. (3), Scoles et. al. (34), and Panjabi et. al. (25, 26) Measured data for the vertebral body widths were specified for the superior and inferior endplates of each vertebrae in the thoracic and lumbar spine. The widths of each pair of inferior and superior adjacent endplates bordering an intervertebral disc were averaged and plotted as a function of vertebral level. The plotted data was then analyzed by linear regression analysis. (Figure 6-5a and 6-5b) From this result, the vertebral body widths for the normal spine model were determined.

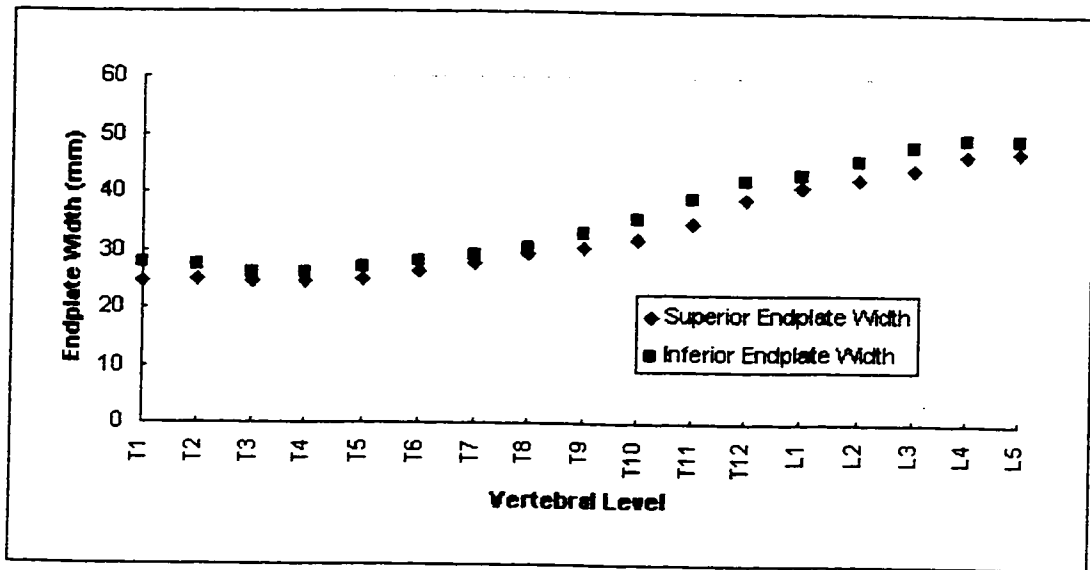


Figure 6-5a. Superior and inferior endplate width data plotted at each vertebral level.

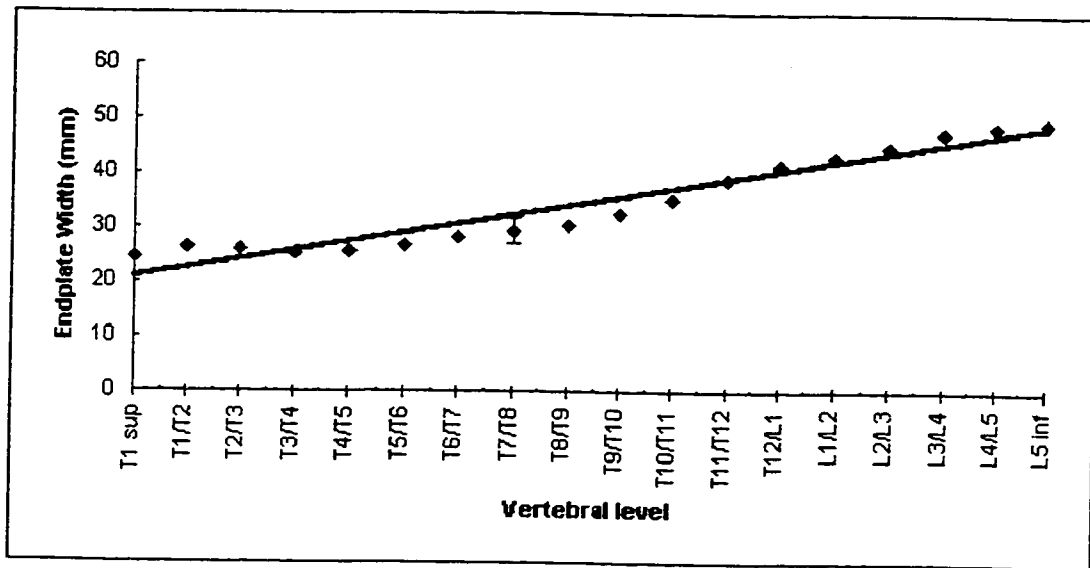


Figure 6-5b. The widths of each endplate bordering an intervertebral disc were averaged and set equal to one another. This subsequent data was then fitted with a linear curve for use in the normal spine model. A typical range for +/- one standard deviation is shown for the averaged result of the T7/T8 data point. The averaged result given at each vertebral level were based on 12 vertebrae.

Measured data for the vertebral body depths were also curve fitted and evaluated using the linear regression technique. (Figure 6-6a, 6-6b, and 6-6c) Again, the depths of the inferior and superior adjacent endplates bordering an intervertebral disc were averaged and assumed to be the same at each vertebral level. It was noted that a change in slope occurred at the thoracolumbar junction when evaluating both thoracic and lumbar regions as a whole. This change in slope represents a distinct geometric variation between thoracic and lumbar vertebrae. Thus, the thoracic and lumbar regions were evaluated separately and the final data used for the normal spine model was taken from the thoracic and lumbar linear curve fits.

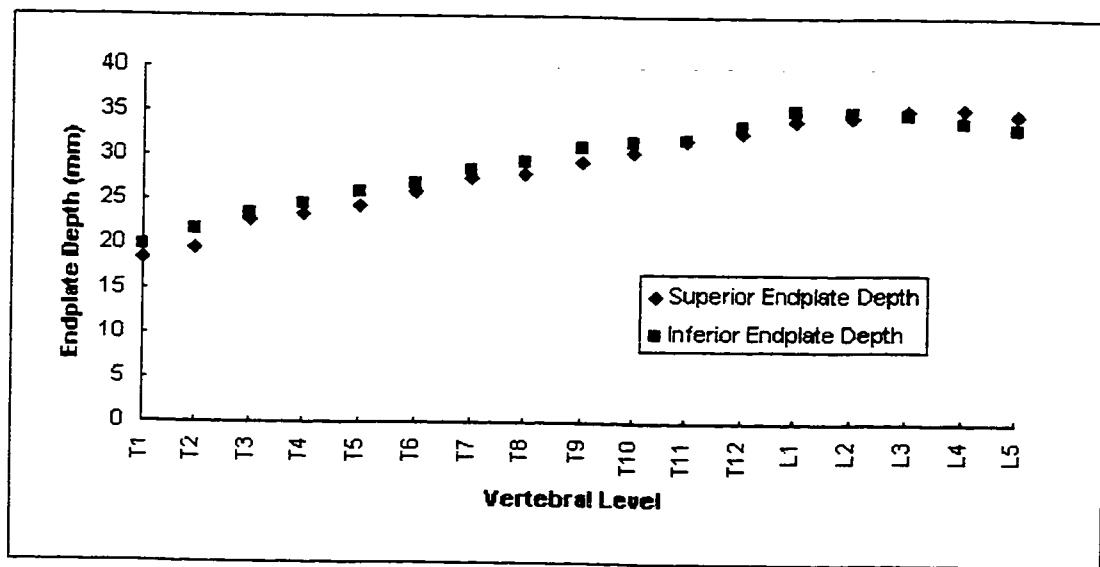


Figure 6-6a. Superior and inferior endplate depth data plotted at each vertebral level.

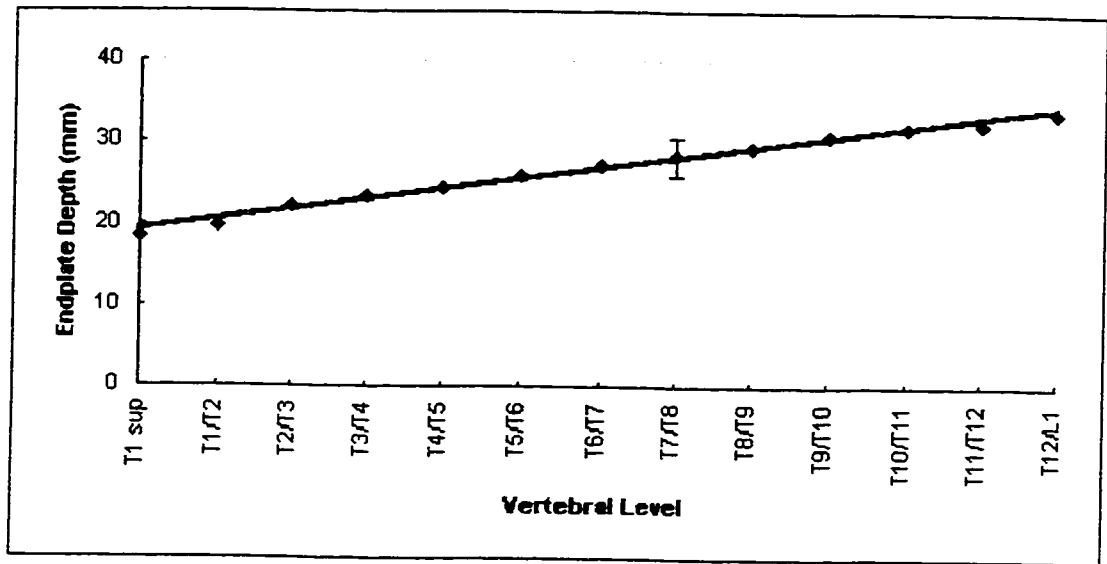


Figure 6-6b. A linear curve fit for the endplate depth data in the thoracic region. A typical range for +/- one standard deviation is shown at T7/T8.

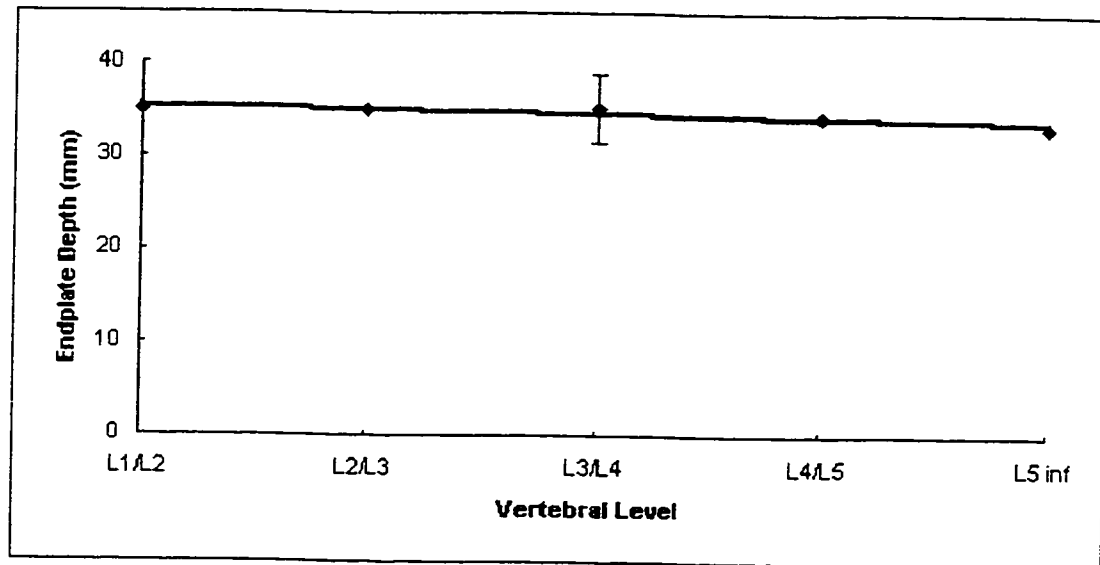


Figure 6-6c. A linear curve fit for the endplate depth data in the lumbar region. A typical range for +/- one standard deviation is shown at L3/L4.

Data points in both Figure 6-6b and 6-6c assume depths of adjacent endplates bordering each intervertebral disc are the same.

Data from Panjabi et. al. (25, 26) detailed the vertebral body posterior heights at each vertebral level along the symmetrical mid-line of the spine. The thoracic and lumbar regions were considered separately because a change in slope was noted at the thoracolumbar junction when plotting the posterior heights as a function of vertebral level. (Figure 6-7a, 6-7b, and 6-7c) The two regions were each curve fitted using the linear regression technique from which the final data for the normal spine model were taken.

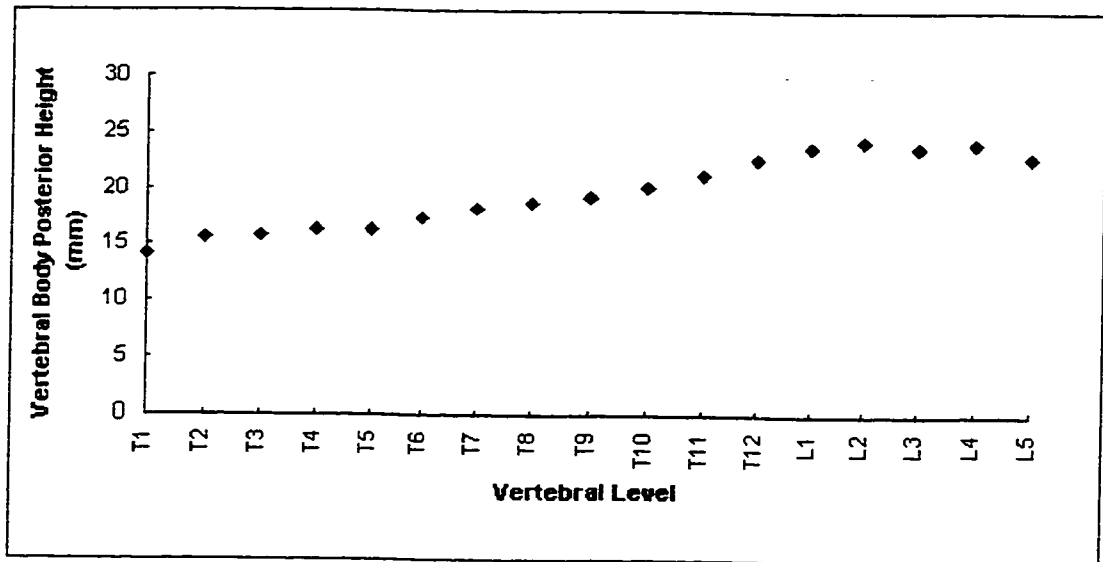


Figure 6-7a. Vertebral body posterior heights as a function of vertebral level.

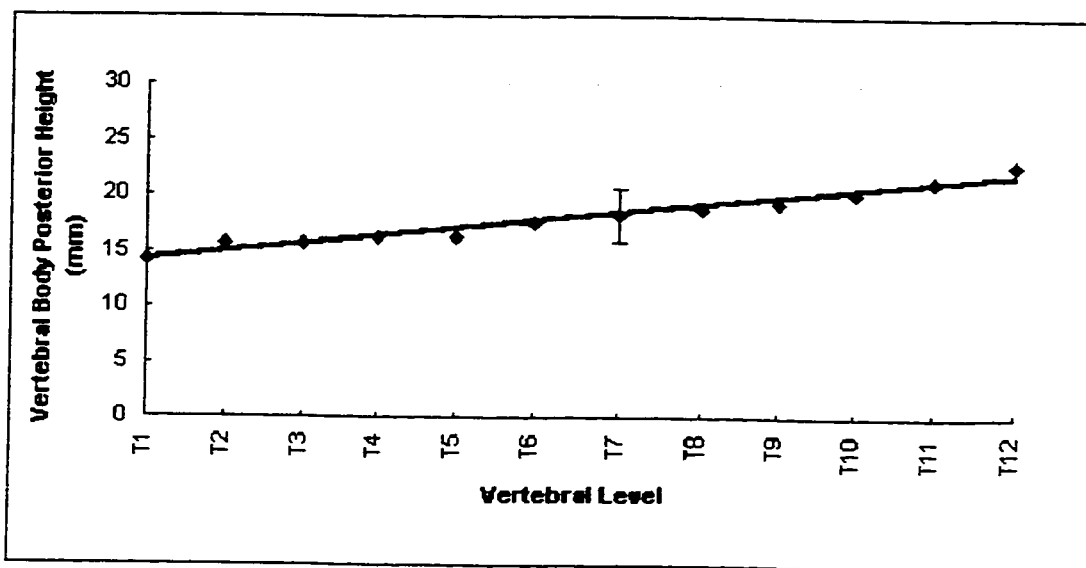


Figure 6-7b. Linear curve fit of vertebral body posterior height data in the thoracic spine.

A typical range for +/- one standard deviation is shown at T7.

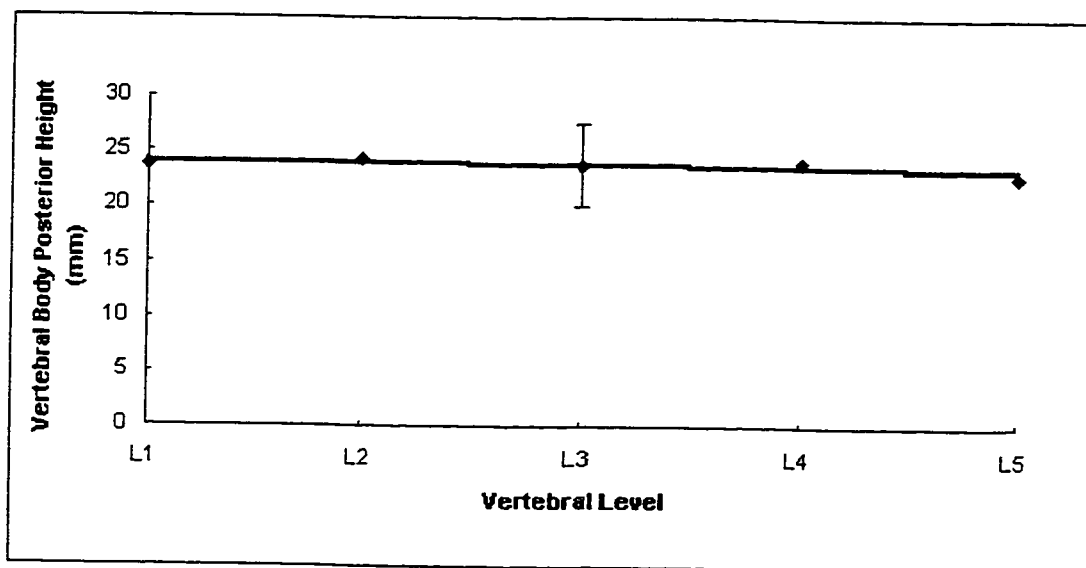


Figure 6-7c. Linear curve fit on vertebral body posterior height data in the lumbar spine.

A typical range for +/- one standard deviation is shown at L3.

When plotted, the superior and inferior endplate angles of inclination data, as found by Panjabi et. al. (25, 26), produced no discernible trend or pattern as a function of vertebral level. (Figure 6-8) This raw data were directly incorporated into the normal spine model, with small alterations to the endplate angles of inclination to visually agree with anatomical drawing and sketches in anatomy texts.

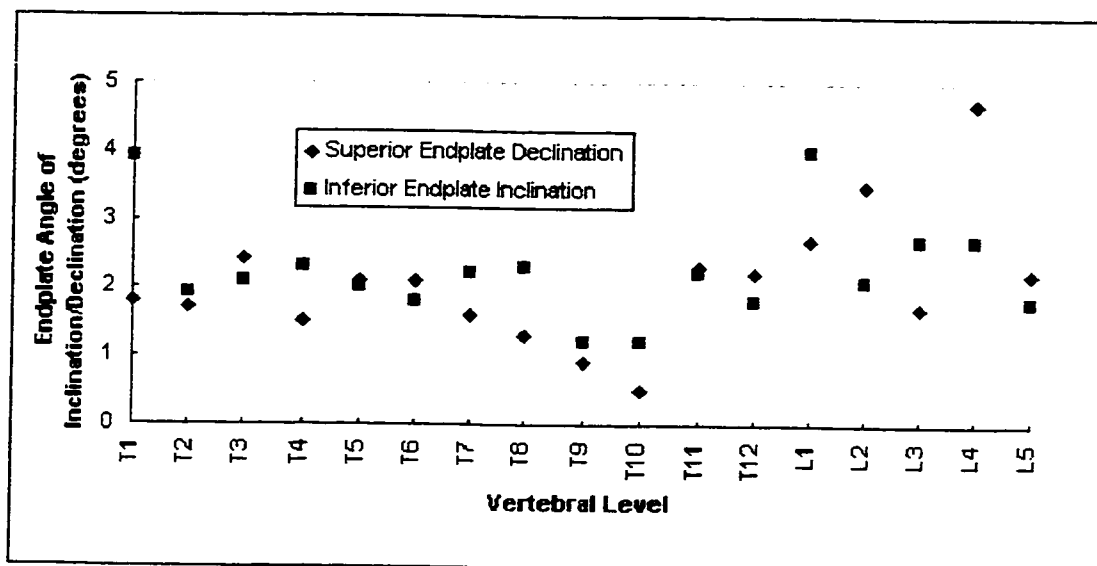


Figure 6-8. Endplate angles relative to the vertebral body transverse mid-plane plotted at each vertebral level.

The kidney bean shape of the endplates in the vertebrae is defined by three superimposed mathematical plane curves (Figure 6-10) developed by F. Lavaste et. al. (14) This was necessary for describing the locations of the intervertebral disc and some ligaments. The plane curves are derived from 4 parameters representing specific dimensions on a vertebral body. These dimensions include the vertebral body width, depth, height, and side wall concavity. (Figure 6-9)

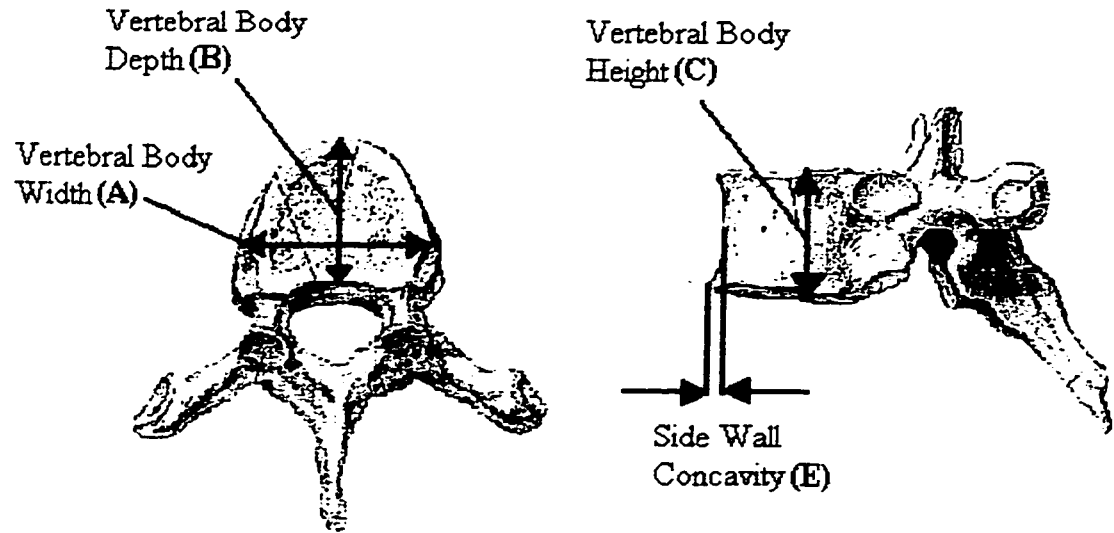


Figure 6-9. Vertebral body dimensions used to parametrically define the endplate shape.

From the four parameters, a series of secondary parameters are calculated and incorporated into the plane curve equations which are expressed in polar coordinates.

The endplate shapes are defined as follows:

Let: Vertebral body width = A

Vertebral body depth = B

Vertebral body height = C

Side wall concavity = E

Then: $U_1 = A$

$U_2 = B - (3 / 2)E$

$\epsilon = 1 / [1 + (A / 2) + (3B / 2)]$

$\alpha = 8\epsilon - 12$

$$\beta = 20\varepsilon - 29.2$$

$$\gamma = 16\varepsilon - 23.4$$

$$\delta = 4\varepsilon - 6.7$$

$$P(\theta) = \alpha X^5 + \beta X^4 + \gamma X^3 + \delta X^2 + 1$$

$$X = 2\theta / \pi$$

Using the above variables, the endplate shape on a vertebra is described by 3 equations expressed in polar coordinates. This method was used in defining the thoracic and lumbar vertebrae vertebral body shapes in the normal spine model. (Figure 6-10)

$$\text{For } \theta = [-\pi / 2, -\pi / 3], R(\theta) = -B / (3 \sin \theta)$$

$$\text{For } \theta = [-\pi / 3, 0], R(\theta) = P(\theta) / [(2\cos\theta / U_1)^2 + (3\sin\theta / (2U_2))^2]^{1/2}$$

$$\text{For } \theta = [0, \pi / 2], R(\theta) = -1 / [(2\cos\theta / U_1)^2 + (3\sin\theta / (2U_2))^2]^{1/2}$$



Figure 6-10. The black line outlining the right aspect of the above vertebra endplate represents the “kidney bean” shaped curves described by three polar equations. Region 1 represents $R(\theta) = -B / (3 \sin \theta)$ for $\theta = [-\pi / 2, -\pi / 3]$. Region 2 represents $R(\theta) = P(\theta) / [(2\cos\theta / U_1)^2 + (3\sin\theta / (2U_2))^2]^{1/2}$ for $\theta = [-\pi / 3, 0]$. and $R(\theta) = -1 / [(2\cos\theta / U_1)^2 + (3\sin\theta / (2U_2))^2]^{1/2}$ for $\theta = [0, \pi / 2]$.

6.3 SPINAL CANAL GEOMETRY

The geometry of the spinal canal width and depth in the transverse plane of the vertebrae were found in literature by Panjabi et. al. (25, 26) Although this information was not directly used to specify the shape and size of the spinal canal in the normal spine model, it was used to describe the posterior location of the spinous process base attachment point to the lamina, relative to the vertebral body. The data for the spinal canal width and depth were plotted as a function of vertebral level between T1 and L5,

and fitted with a third degree polynomial using a least squares regression. The spinal canal depth for each vertebra was determined from the fitted curve and referenced to describe the locations of the base of spinous processes in the normal spine model.

(Figure 6-11a, 6-11b, and 6-11c)

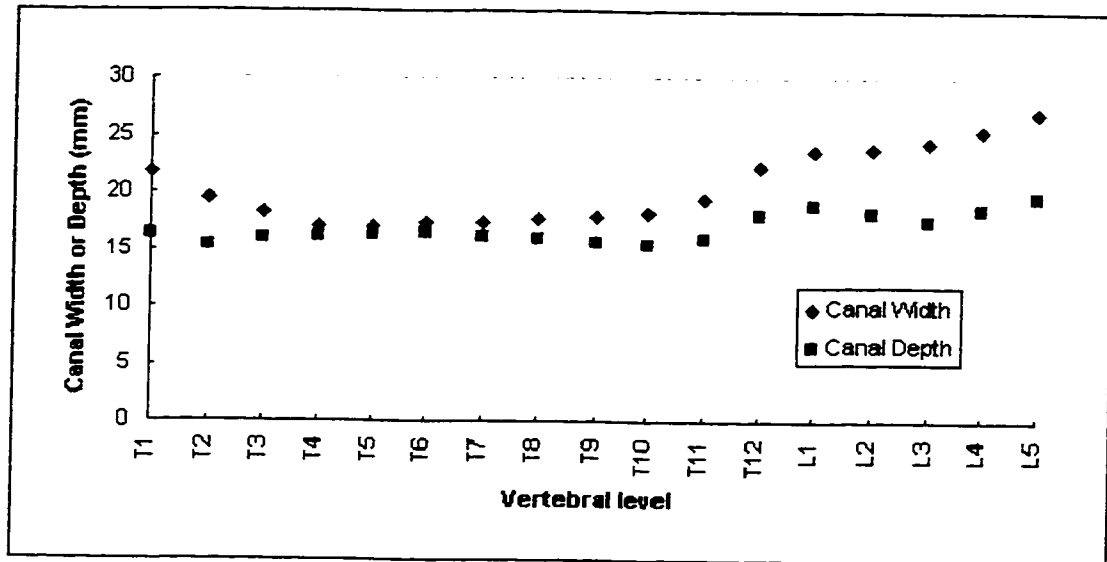


Figure 6-11a. Spinal canal width and depth as a function of vertebral level.

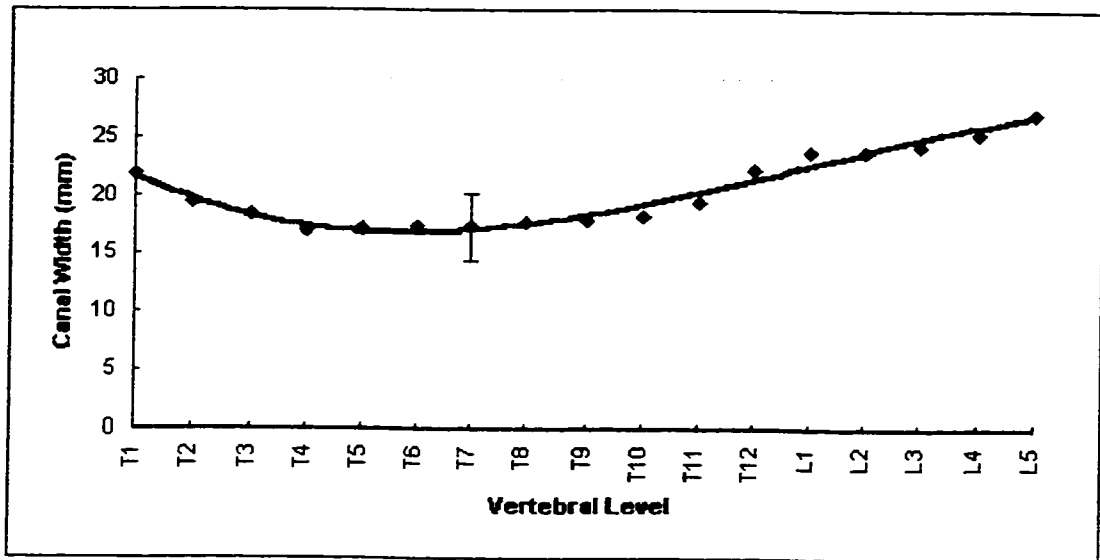


Figure 6-11b. Spinal canal widths, curve fitted with a 3rd degree polynomial. A typical range for +/- one standard deviation is shown at T7.

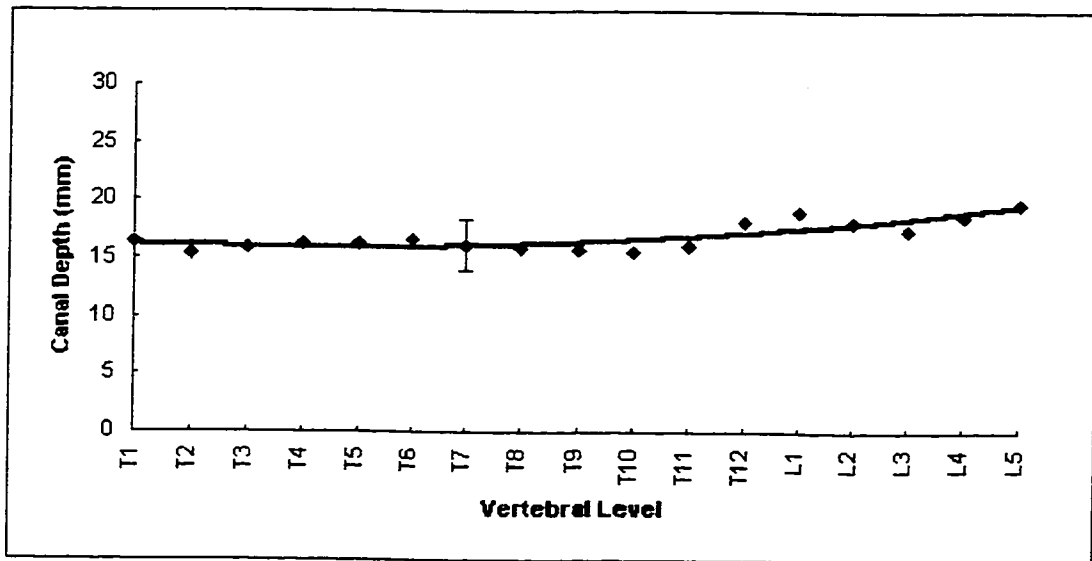


Figure 6-11c. Spinal canal depths, curve fitted with a 3rd degree polynomial. A typical range for +/- one standard deviation is shown at T7.

6.4 FACET GEOMETRY

The facet surfaces in the normal spine model were derived using measured data found in literature (3, 7, 25, 26, 27, 34) and were modeled as circular, plane surfaces.

The data for the thoracic and lumbar facets describe:

- the orientation of the superior and inferior facet surfaces relative to the vertebral bodies in 3-D space, with the assumption that the facets are plane surfaces.
- the 3-D positions of the facet surface centers relative to the vertebral body centroids.
- the surface areas of the facets.

From these data, the geometry and orientation of the facet surfaces in the thoracic and lumbar regions can be defined relative to the vertebral bodies in the normal spine model.

The orientations of the superior and inferior facets in the normal spine were described by G.A. Dumas (7). Using “card angles”, the orientation of a facet surface can be described relative to a vertebra. (Figure 6-12) With this method, two angles between the facet plane and the frontal (angle α) and transverse (angle β) plane of a vertebra, are used to define the facet’s orientation.

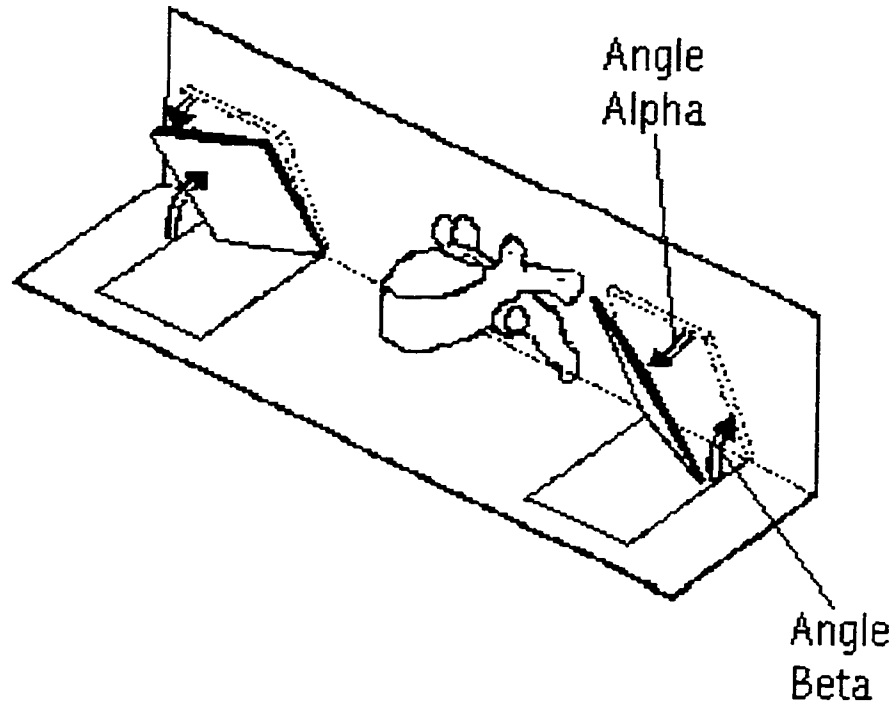


Figure 6-12. Card angles are used to define the facet surface orientations relative to a vertebra using two angles alpha (α) and beta (β).

The orientation of facets in the thoracic region differ considerably from facets in the lumbar region. This was apparent when angles α and β were plotted as a function of vertebral level. (Figures 6-13 to 6-14) As a result, the thoracic and lumbar facet surface angles α and β were both evaluated separately and fitted using a least squares polynomial regression. The fitted polynomial curves were then used to define the facet orientation in the normal spine model.

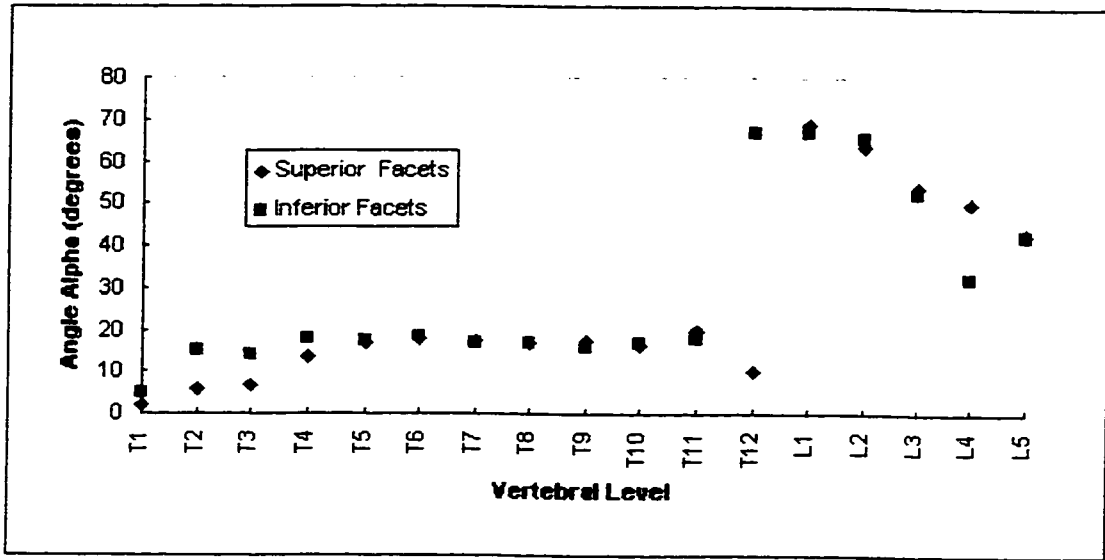


Figure 6-13a. Angles alpha (α) as a function of vertebra level in the normal spine.

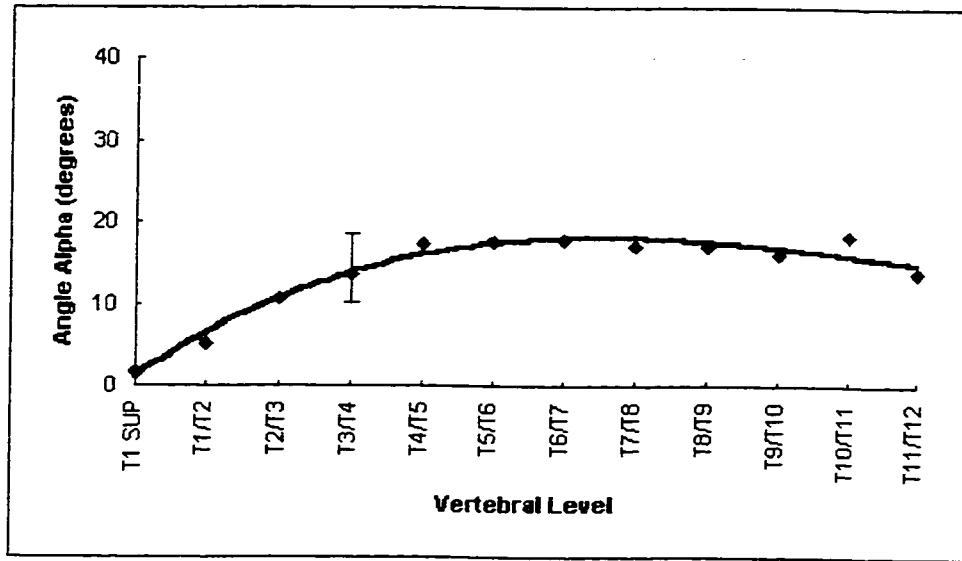


Figure 6-13b. Angles alpha (α) for the thoracic spine curve fitted with a 4th degree polynomial. A range of data, typical of the averaged results in the figure, is shown at T3/T4.

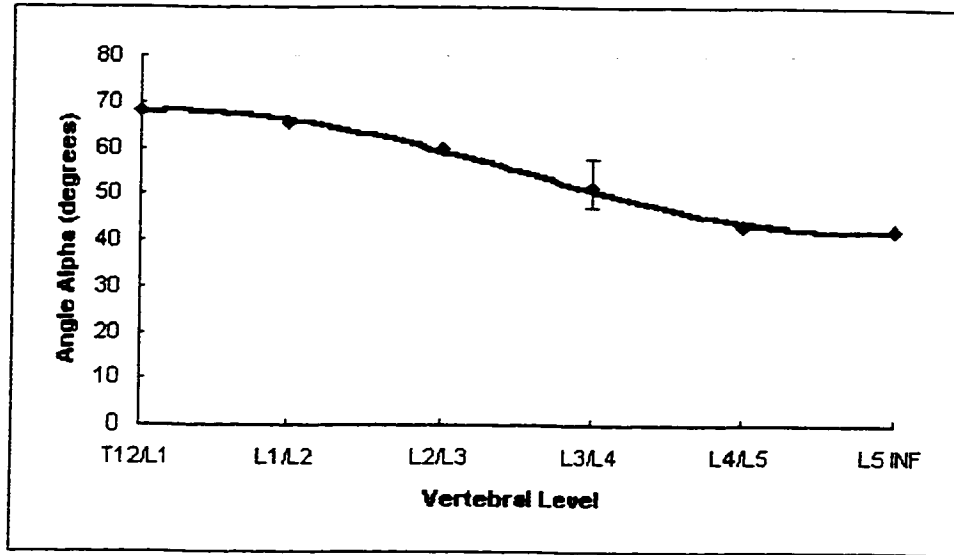


Figure 6-13c. Angles alpha (α) for the lumbar spine curve fitted with a 3rd degree polynomial. A range of data, typical of the averaged results in the figure, is shown at L3/L4.

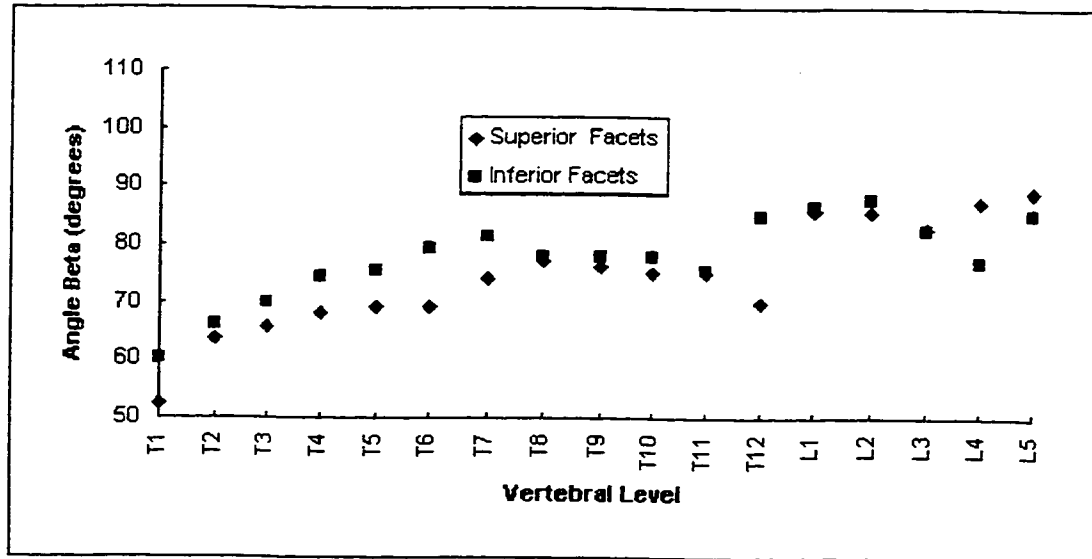


Figure 6-14a. Angles beta (β) as a function of vertebra level in the thoracic and lumbar regions.

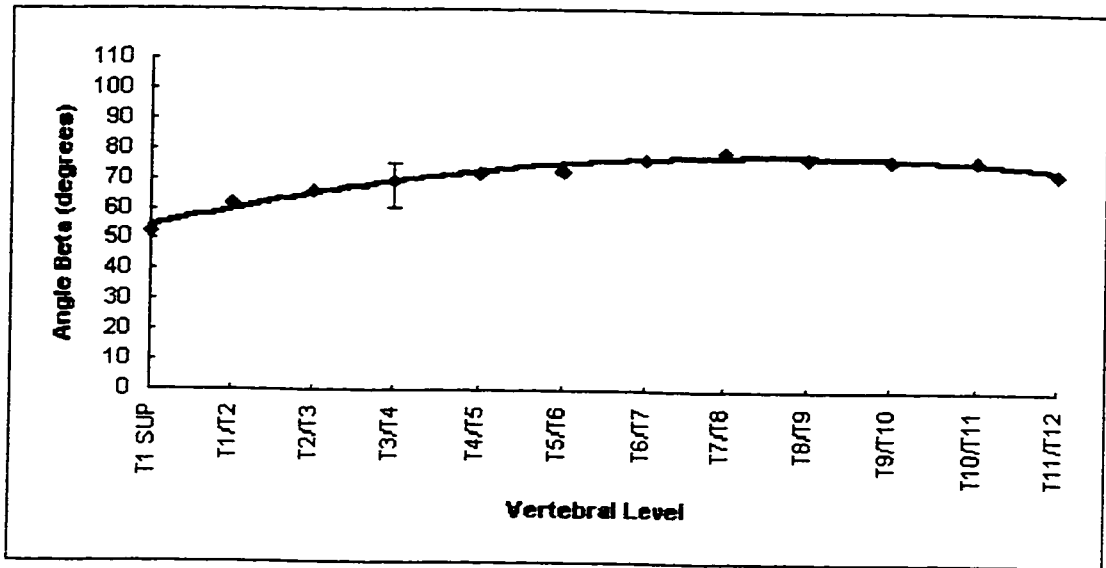


Figure 6-14b. Angles beta (β) for the thoracic spine curve fitted with a 3rd degree polynomial.

A range of data, typical of the averaged results in the figure, is shown at T3/T4.

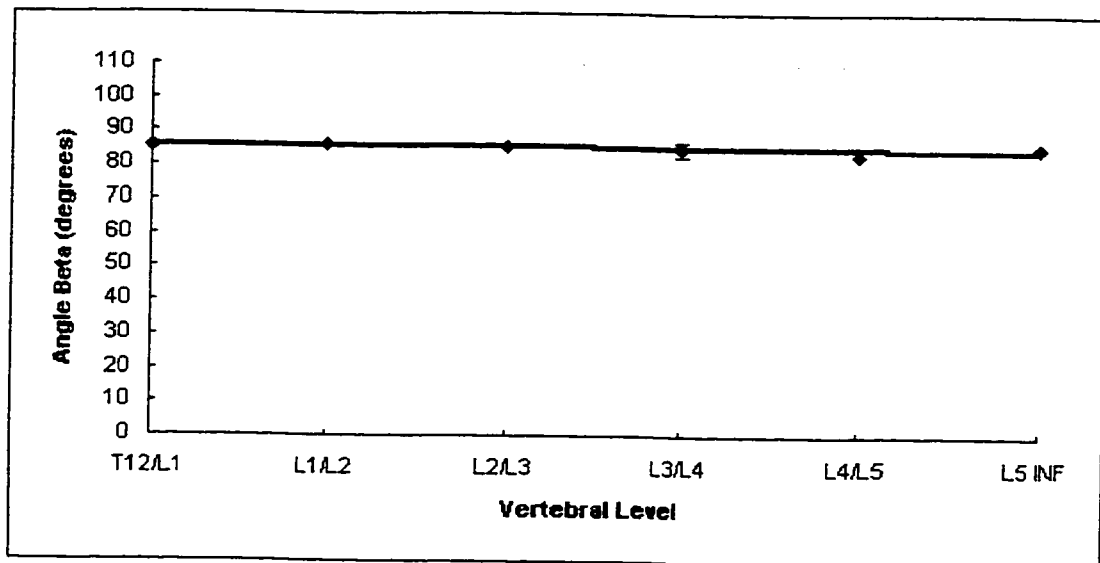


Figure 6-14c. Angles beta (β) for the lumbar spine fitted with a linear curve. A range of data, typical of the averaged results in the figure, is shown at L3/L4.

The position of the facet surface centers relative to the vertebral body was also reported by G.A. Dumas (7). These data included the lateral, posterior, and vertical distance between each superior or inferior facet, and the corresponding vertebral body centroids. The data for the three distances were plotted as a function of vertebral level, and curve fitted using a least squares regression. For each distance, the thoracic and lumbar regions were assessed separately with the exception of the facet to body centroid lateral distance, which did not exhibit an abrupt transition at the thoracolumbar junction. (Figures 6-15, 6-16, and 6-17) The position of the facet surface centers in the normal spine model were then established from these curves. In the model, variations in position and orientation between mating facet surfaces were ultimately averaged at each spinal level to bring mating inferior and superior facets together.

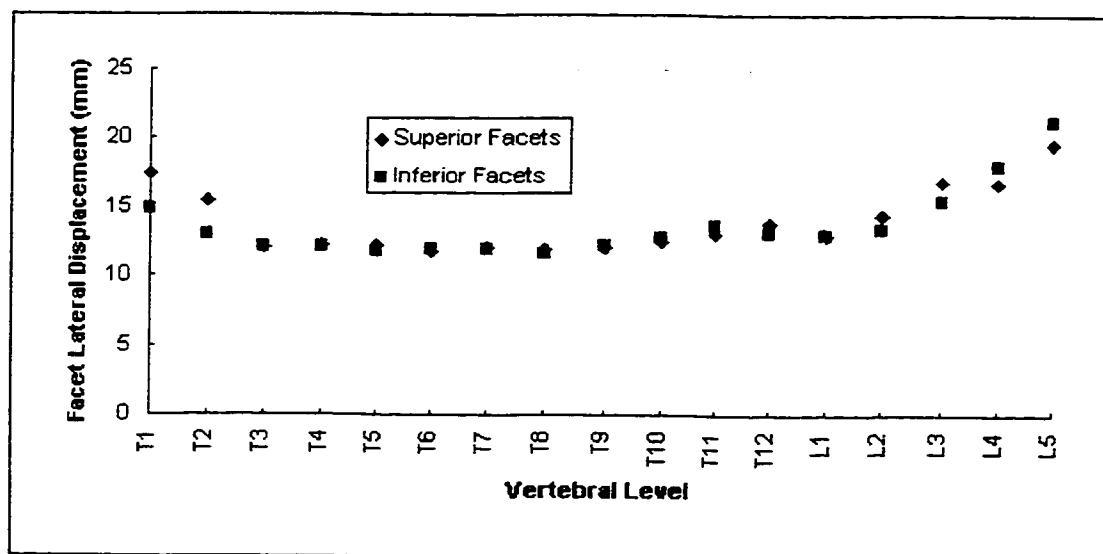


Figure 6-15a. Lateral distance between facet surface centers and vertebral body centroids in the normal spine.

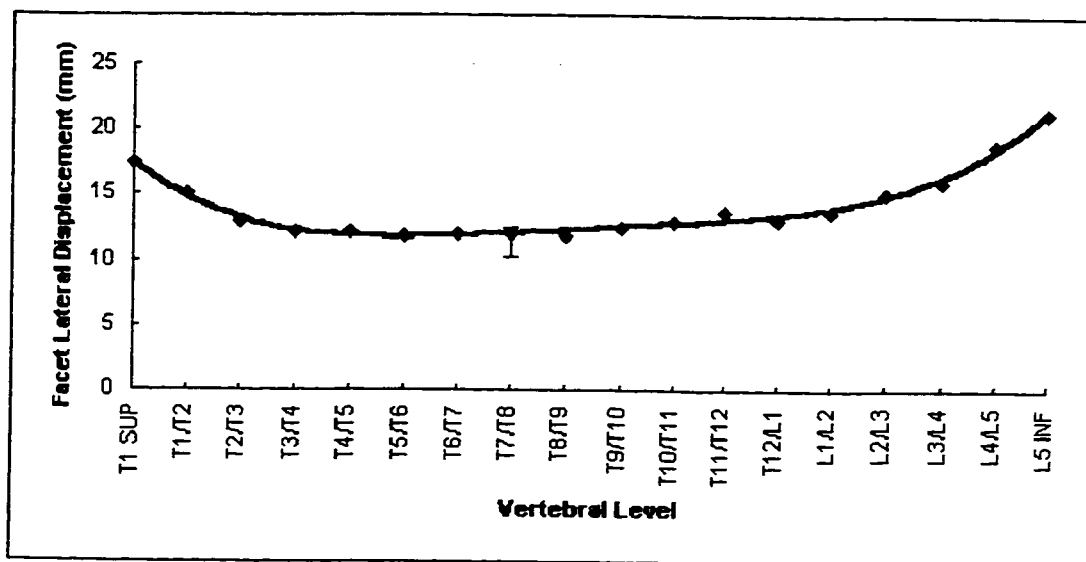


Figure 6-15b. Curve fitted data for the lateral distance between facet surface centers and vertebral body centroids using a 5th degree polynomial. A range of data, typical of the averaged results in the figure, is shown at T7/T8.

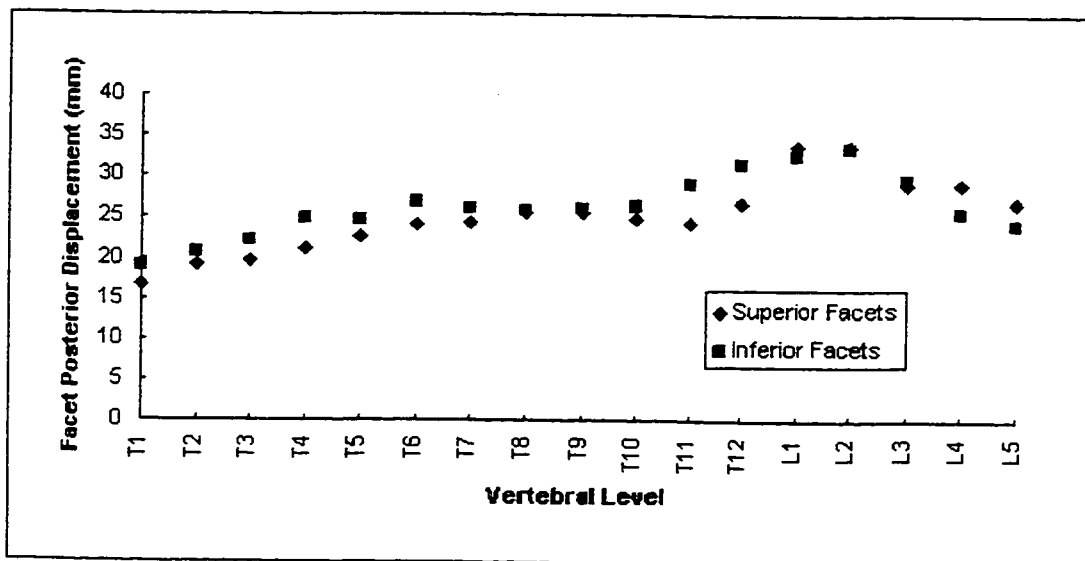


Figure 6-16a. Posterior distance between facet surface centers and vertebral body centroids in the thoracic and lumbar regions.

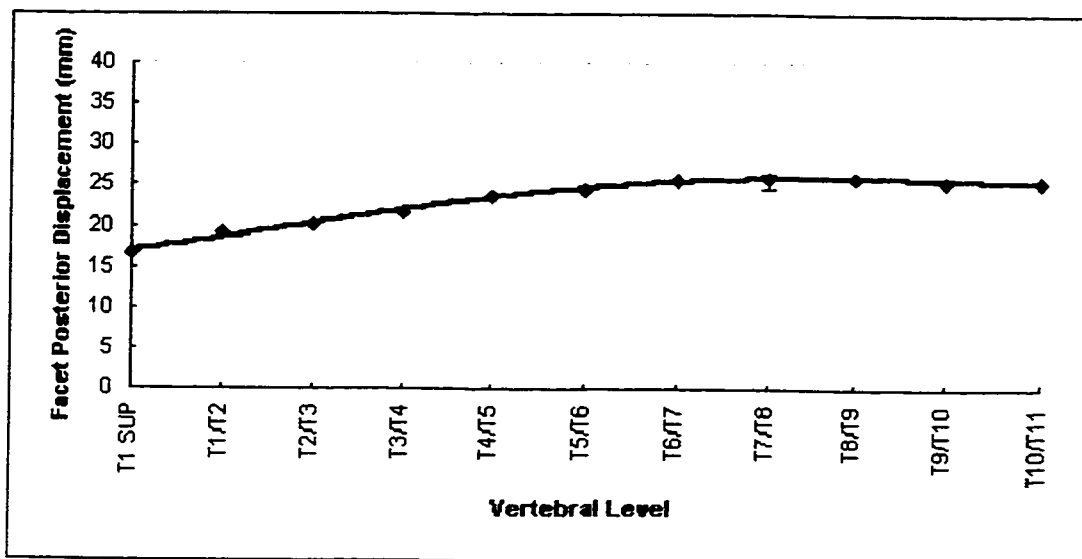


Figure 6-16b. Curve fitted data for the posterior distance between thoracic facet surface centers and vertebral body centroids using a 4th degree polynomial. A range of data, typical of the averaged results in the figure, is shown at T7/T8.

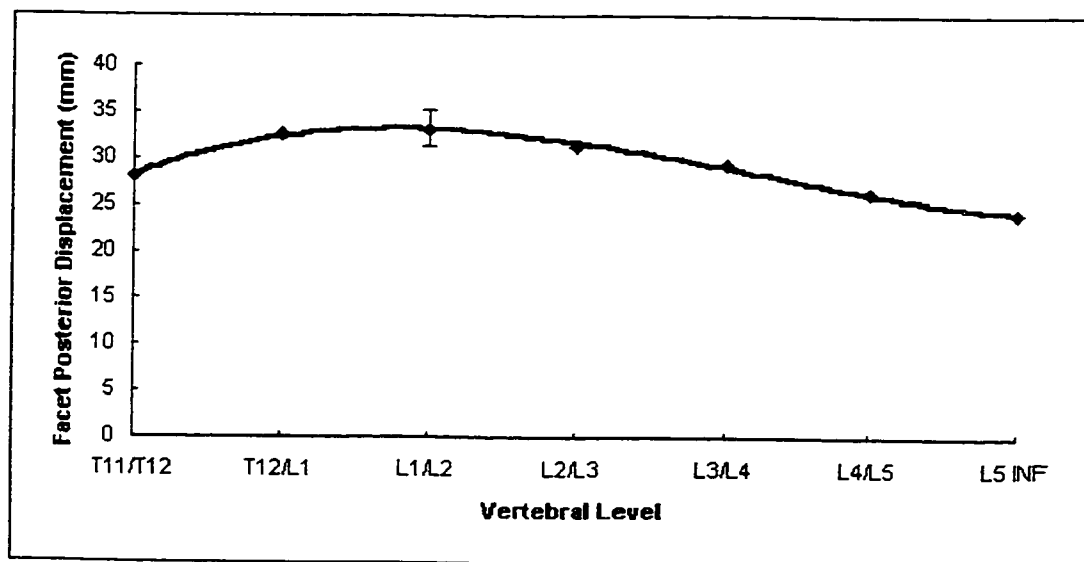


Figure 6-16c. Curve fitted data for the posterior distance between lumbar facet surface centers and vertebral body centroids using a 3rd degree polynomial. A range of data, typical of the averaged results in the figure, is shown at L1/L2.

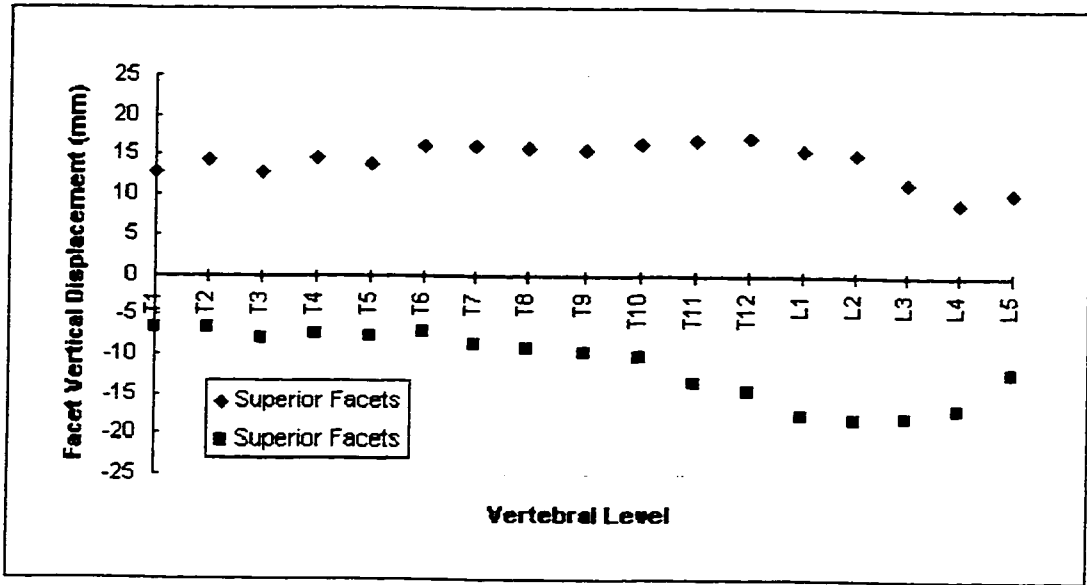


Figure 6-17a. Vertical distances between superior and inferior facet surface centers and vertebral body centroids in the normal spine.

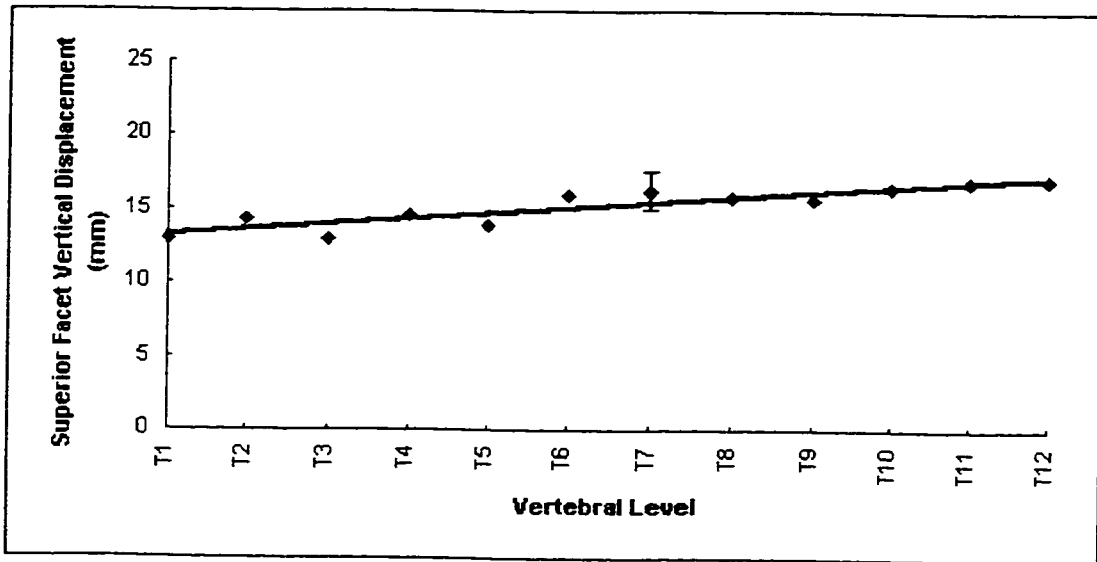


Figure 6-17b. Curve fitted data for the vertical distance between superior thoracic facet surface centers and vertebral body centroids using a linear curve. A range of data, typical of the averaged results in the figure, is shown at T7.

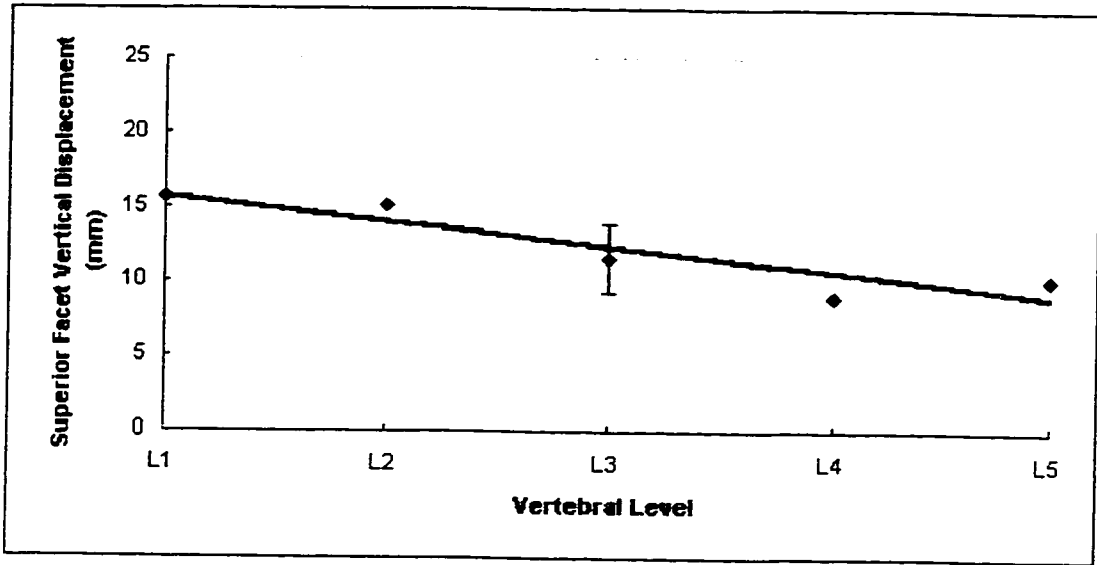


Figure 6-17c. Curve fitted data for the vertical distance between superior lumbar facet surface centers and vertebral body centroids using a linear curve. A range of data, typical of the averaged results in the figure, is shown at L3.

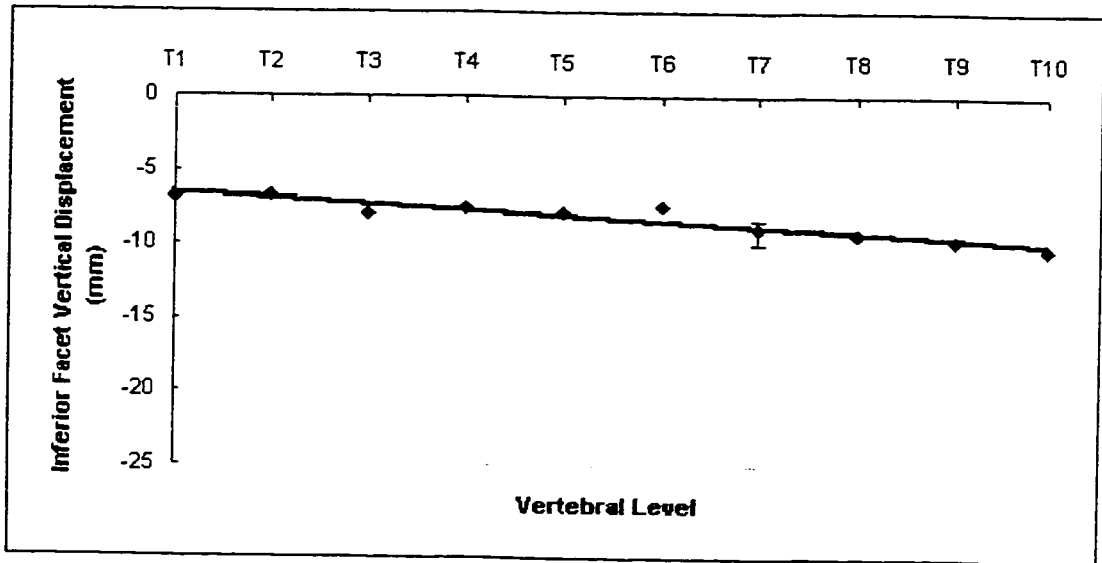


Figure 6-17d. Curve fitted data for the vertical distance between inferior thoracic facet surface centers and vertebral body centroids using a linear curve. A range of data, typical of the averaged results in the figure, is shown at T7.

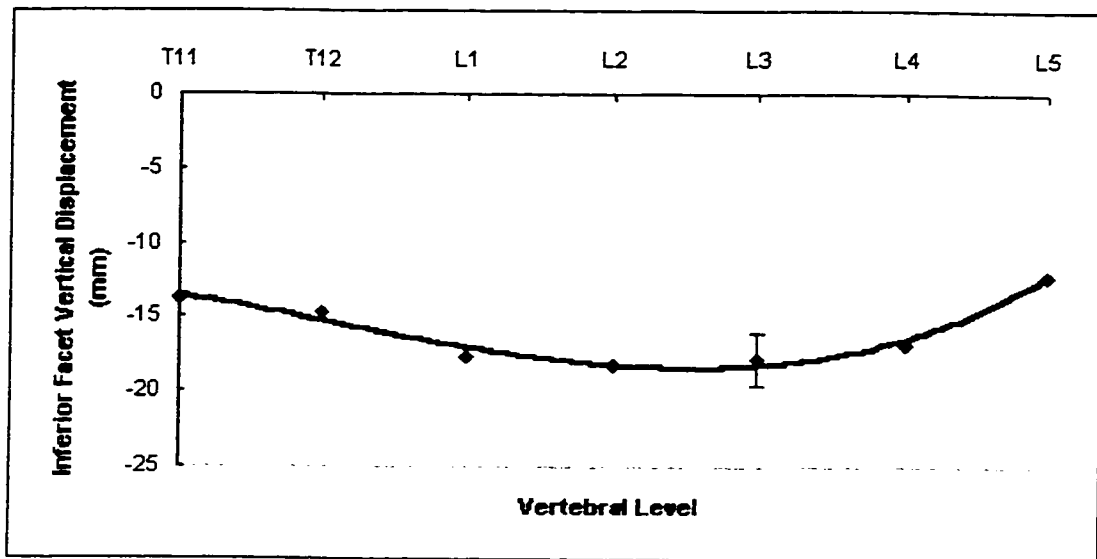


Figure 6-17e. Curve fitted data for the vertical distance between inferior lumbar facet surface centers and vertebral body centroids using a 3rd degree polynomial. A range of data, typical of the averaged results in the figure, is shown at L3.

Panjabi et. al. (27) described the facet surface areas for thoracic and lumbar vertebrae in the normal spine. A plot of facet area versus vertebral level for the thoracic and lumbar spine exhibit a sudden change in slope at the thoracolumbar junction. The thoracic and lumbar regions were curve fitted independently using a least squares regression. A constant facet surface area is noted in the thoracic region, with a linear increase occurring in the lumbar region. (Figure 6-18a, 6-18b, 6-18c) The fitted curves were used to describe the facet surface areas in the normal spine model, which were assumed to be circular planes.

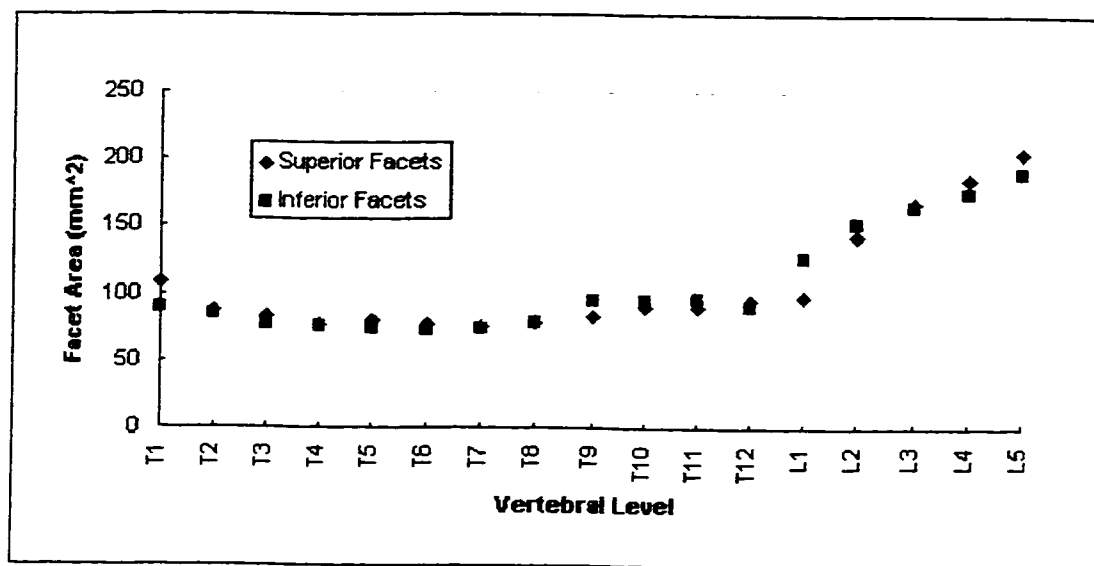


Figure 6-18a. Facet surface areas for the thoracic and lumbar spine.

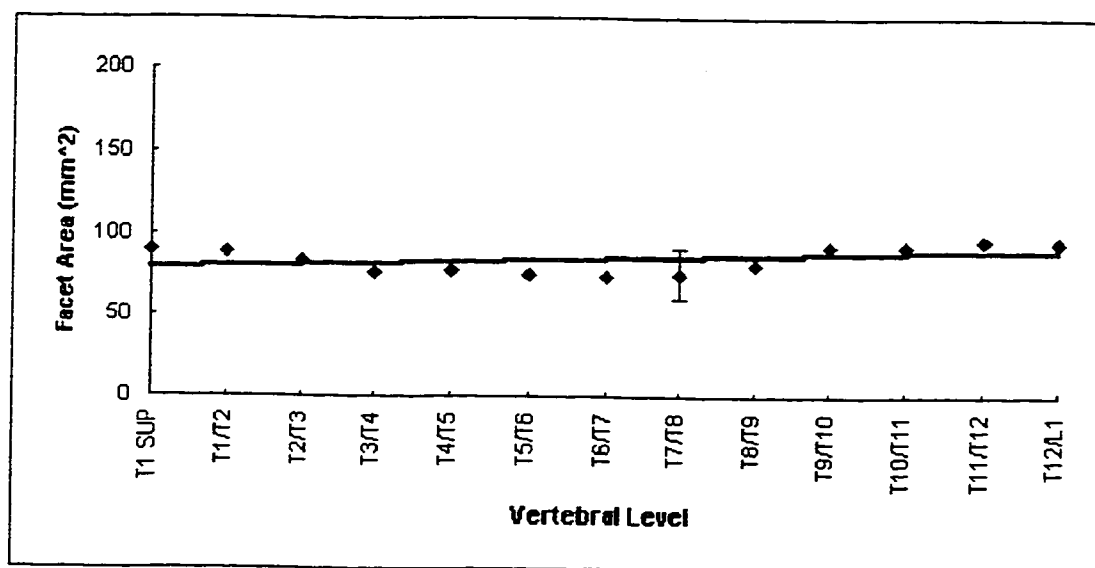


Figure 6-18b. A linear curve fit for the facet surface area data in the thoracic spine. A typical range for +/- one standard deviation is shown at T7/T8.

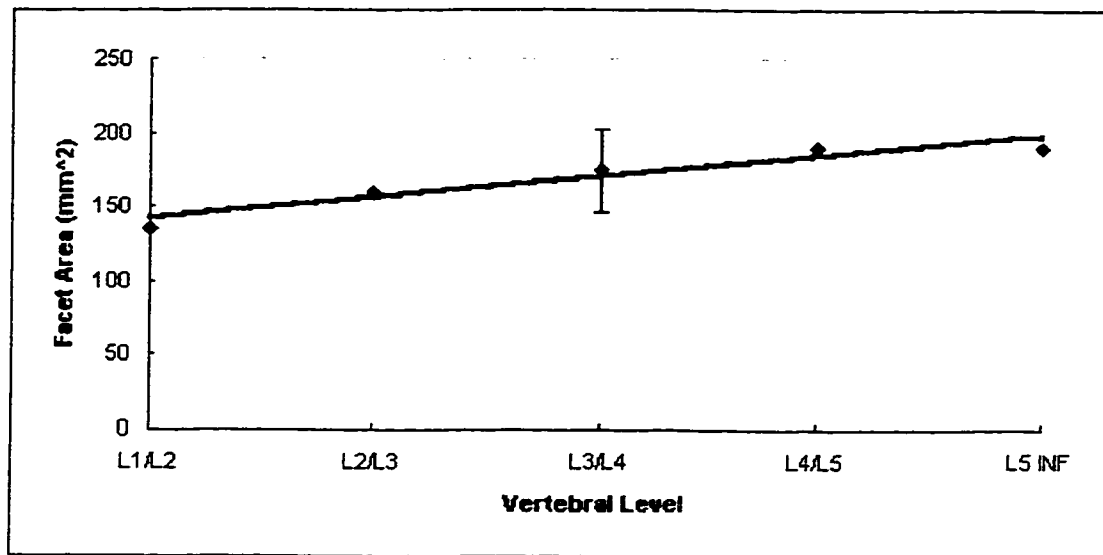


Figure 6-18c. A linear curve fit for the facet surface area data in the lumbar spine. A typical range for +/- one standard deviation is shown at L3/L4.

6.5 TRANSVERSE AND SPINOUS PROCESS GEOMETRY

Measured data on the transverse process width, the width between the two end points of the processes in the frontal plane, are described by Panjabi et. al. (25, 26). The data were plotted against vertebral level, and curve fitted using a 3rd degree polynomial. (Figures 6-19a, 6-19b, 6-19c) The fitted curve was then used to define the position of the transverse process end points in the model as seen in the frontal plane.

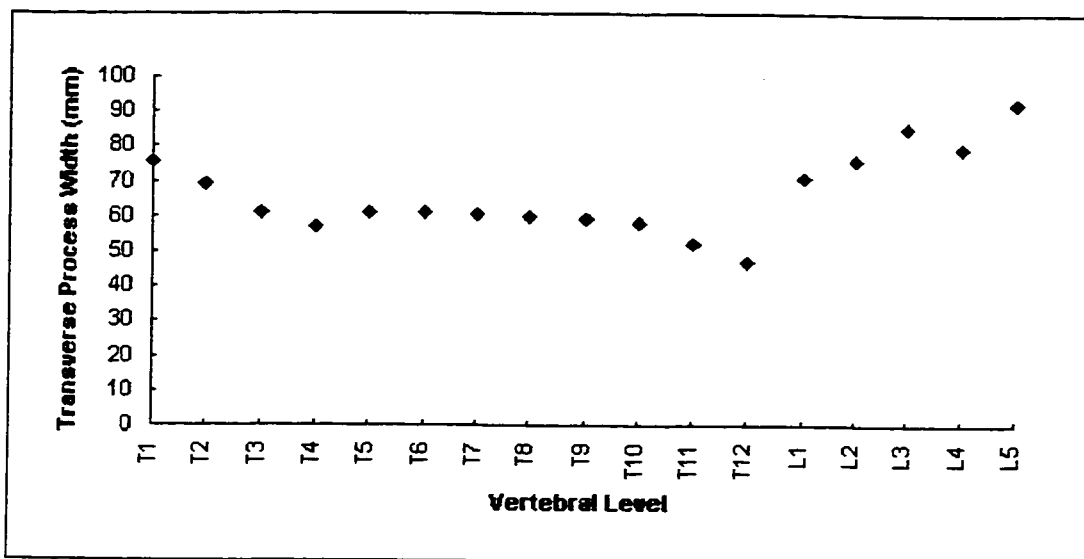


Figure 6-19a - Transverse process width data in the thoracic and lumbar spine. Note the change in width at the thoracolumbar junction.

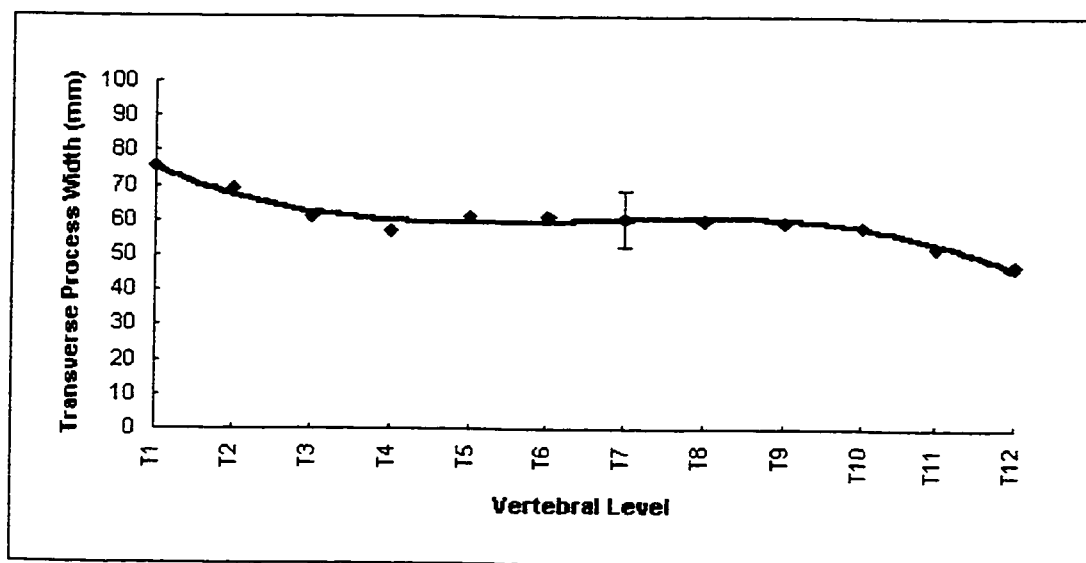


Figure 6-19b. Transverse process width data in the thoracic spine fitted with a 3rd degree polynomial. A typical range for +/- one standard deviation is shown at T7.

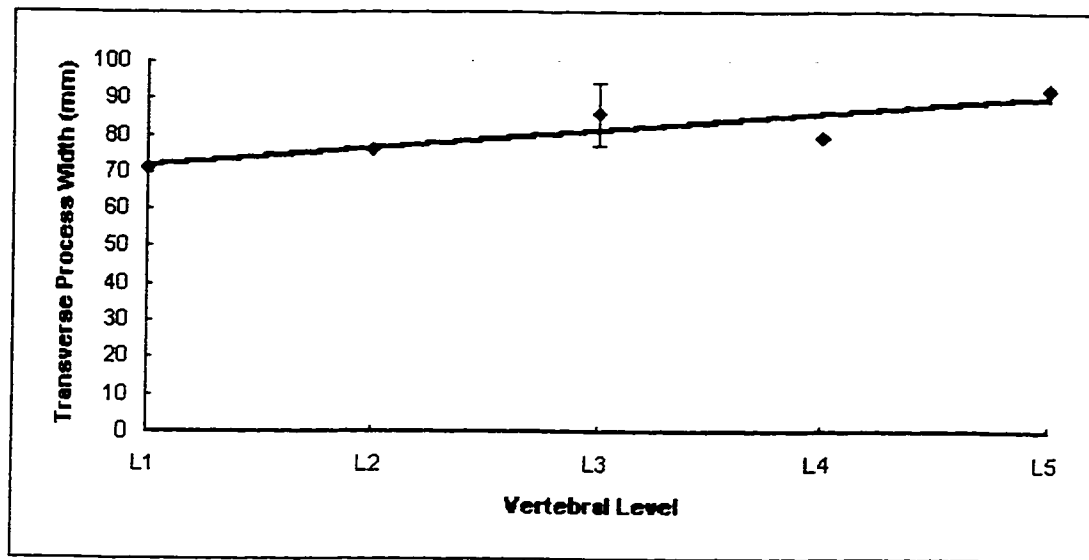


Figure 6-19c. Transverse process width data in the lumbar spine fitted with a linear curve.

A typical range for \pm one standard deviation is shown at L3.

No quantitative data were found in literature describing the position of the transverse process end points in the sagittal plane of the vertebra. Instead, these data were estimated using anatomical drawings found in anatomy texts. (19, 21) Combining the estimated data from the anatomy drawings of the thoracic and lumbar spine with the curve fitted frontal plane data, provided enough information to describe the position of the transverse process end points relative to the vertebral body centroids.

The spinous process lengths and angles of declination relative the vertebral bodies were found in literature by Berry et. al. (3) The data on the spinous processes were given for the whole lumbar region, and three thoracic vertebrae, T2, T7 and T12. Based on this data, it was assumed in thoracic region, that the length and angle of declination varied linearly as a function of vertebral level between T2 to T7 and T7 to

T12. Only the data in the lumbar region were curve fitted and evaluated using a least squares regression. (Figures 6-20a, 6-20b, 6-21a, and 6-21b) Combining the linear relationships in the thoracic region with the fitted curve in the lumbar region provided enough information to describe the geometry and end point location of the spinous processes in the normal spine model.

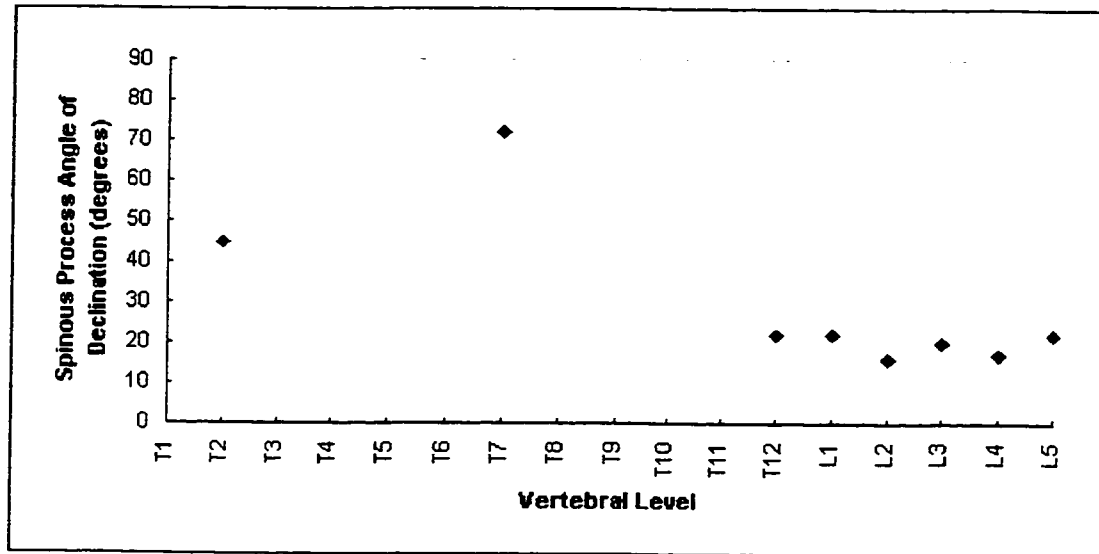


Figure 6-20a. The spinous process angle of declination with respect to the associated vertebral body transverse mid-plane in the normal spine.

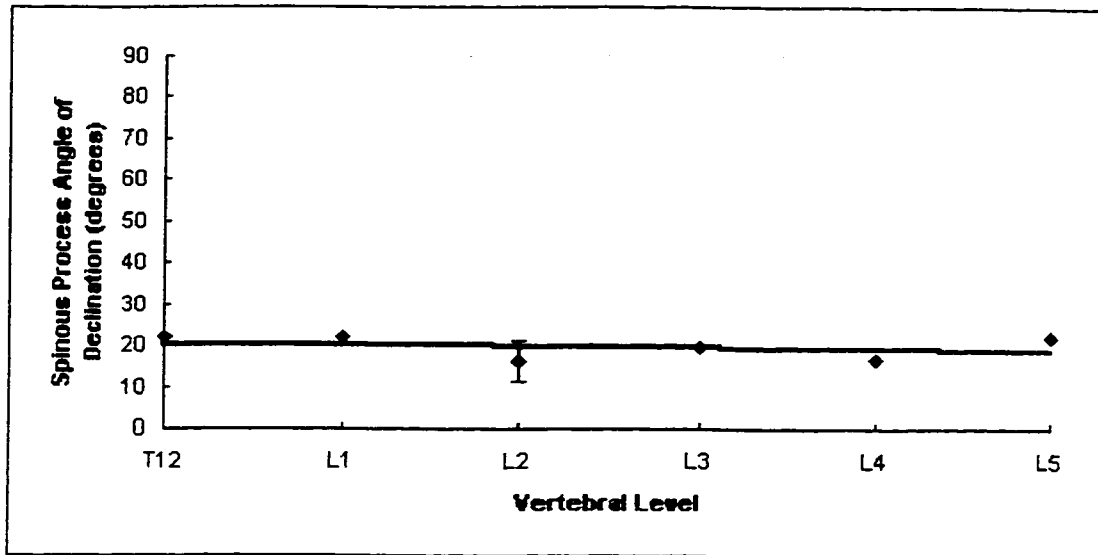


Figure 6-20b. A linear curve fit of the spinous process angle of declination data in the lumbar spine. A typical range for +/- one standard deviation is shown at L2.

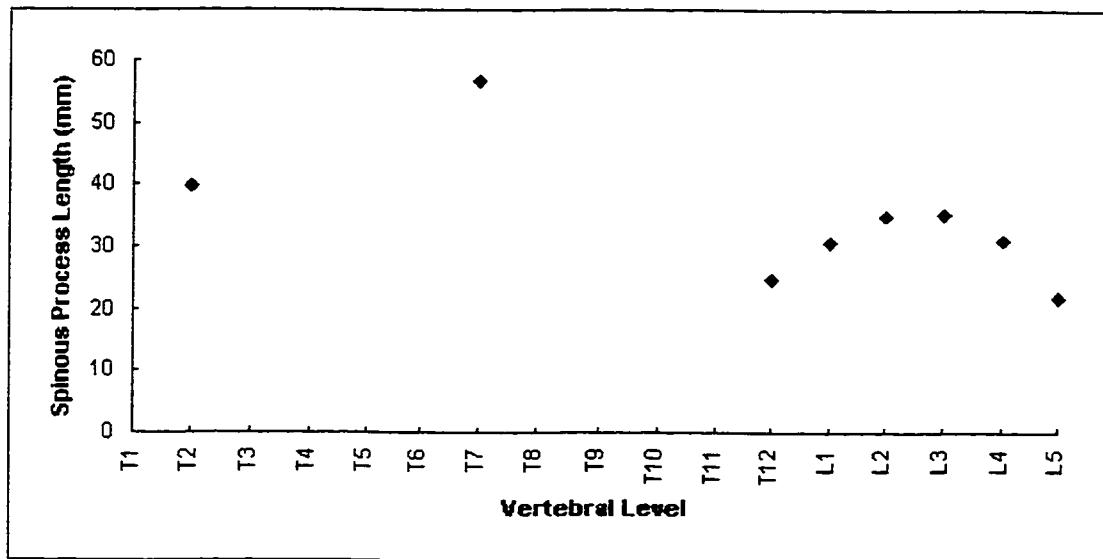


Figure 6-21a. Spinous process length along the angle of declination in the normal spine.

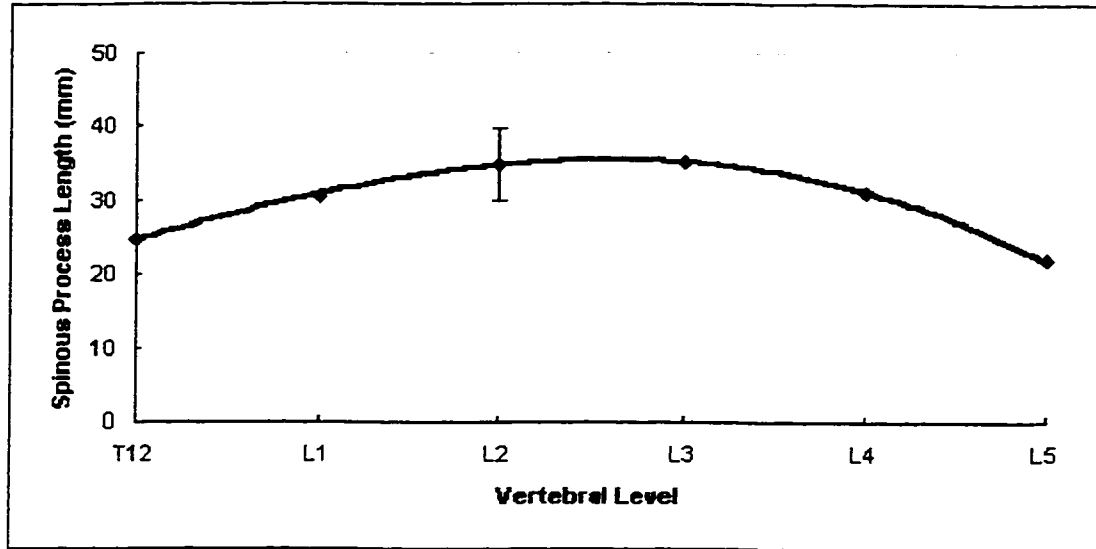


Figure 6-21b. A 3rd degree polynomial curve fit of spinous process length in the lumbar spine. A typical range for +/- one standard deviation is shown at L2.

CHAPTER 7 - THE NORMAL SPINE MODEL

7.1 GENERAL MODEL DESCRIPTION

To study the mechanical behavior of the normal spine, a model was developed within a finite element package (ANSYS). This package was chosen for its convenience compared with preparation and development of original software. The data used to describe the geometry and three-dimensional configuration of the FEM model were taken from the geometric information previously described in Chapter 6.

Anatomical components incorporated into the mechanical model include:

- the thoracic and lumbar vertebrae (T1 - L5)
- the intervertebral discs in the thoracic and lumbar region
- the interconnecting spinal ligaments

Together, these components form a thoracolumbar spinal column absent of spinal cord, ribs, sternum, muscles, and fascia. These spinal components were excluded so that the study could be manageable and to facilitate the validation process of the model.

The objective of this thesis was to create a spine model that reproduces the mechanical behavior of the normal spine. This model provides a foundation for eventual development of a comprehensive model of a scoliotic spine. Due to the present lack of experimental data regarding the geometry and mechanical behavior of

these excluded anatomical parts, especially in the rib-vertebra costal articulation joints and the soft tissues (muscle, fascia, and intercostal membranes), verification of an all inclusive model could not be made at the time this thesis was written. The normal spine mechanical model is shown in Figure 7-1. The configuration of the vertebrae in the model's unloaded equilibrium position, simulates the spinal shape of a person standing upright. In Figure 7-1, only the vertebrae are shown without the ligaments or intervertebral discs.

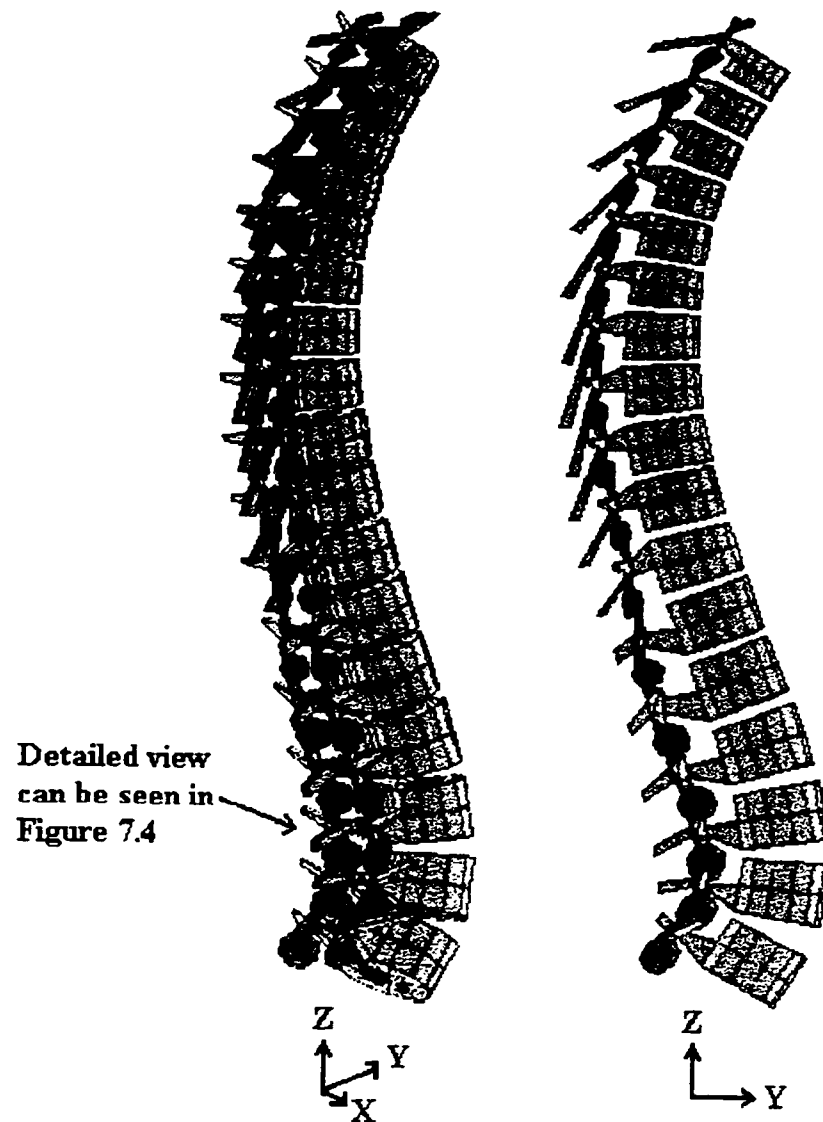


Figure 7-1. FEM model of thoracolumbar spine shown in posterior-oblique, and mid sagittal view. Model is shown without intervertebral discs and ligaments.

In the model, the spine is oriented so that the hypothetical vertebral body centroid location of vertebra S1 falls along the same vertical z axis as the body centroid of vertebra T1. The origin of the Cartesian coordinate system is positioned at the vertebral body centroid of S1 while the corresponding plane of the x and y axis is

oriented perpendicular to the z axis. The y-z plane corresponds with the mid-sagittal plane of the spine, bisecting each vertebra along its individual plane of symmetry, while the x-z plane corresponds to the anatomical frontal plane.

7.2 “RIGID” BODIES IN THE MODEL

Various elements are required to simulate the different properties of the several anatomical components in the normal spine model. Initially, the spine was to be modeled as a series of rigid bodies interconnected by springs which represent the softer intervertebral disc and spinal ligaments. Due to modeling limitations in the FEM software package, rigid bodies could not be simulated. The rigid body constraints equations within the package were not valid during large displacement, steady state, static analysis. To overcome this, the elements used to model the vertebrae were given a high modulus of elasticity when compared with the softer interconnecting ligaments and disc.

7.3 THE VERTEBRAE

The bony vertebrae were modeled using 8 node solid brick elements as seen in Figure 7-2. Each vertebral body is composed of 64 elements symmetrically oriented in a two layer, radial array pattern. The interior core of the vertebral body is comprised of 32 wedge shaped elements surrounded about its outer lateral surfaces by another 32 cube shaped bricks.

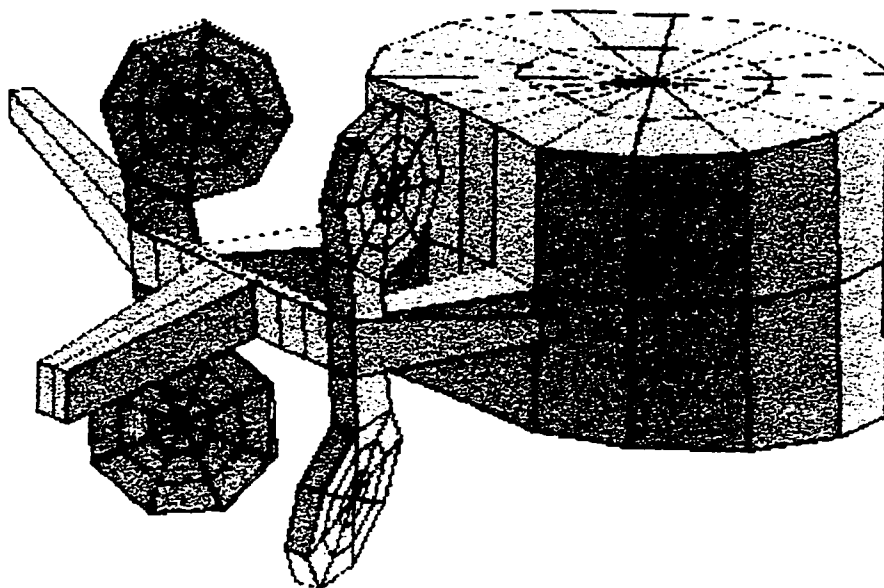


Figure 7-2. A typical lumbar vertebra in the mechanical model of the spine. Note that the pedicles are not anatomically correct and serve only as a means of attaching the vertebral body to the posterior elements. Otherwise, the pedicles have no influence on the mechanical behavior of the model. Each vertebra is modeled using 178 elements.

The brick elements used to model the vertebrae are given a high modulus ($E = 400$ GPa) and behave essentially as rigid body structures exhibiting negligible deformation compared to the softer interconnecting tissues and ligaments under normal physiological loads. The vertebral body elements form the kidney bean shaped columns that carry the majority of the axial loads within the spine. Non-parallel endplate surfaces, which give the vertebral bodies a slight wedge shape in the sagittal plane, were modeled as plane surfaces that directly transfer loads between the vertebral bodies

and intervertebral disc structures. These endplates are also insertion locations for the anterior and posterior longitudinal ligaments.

7.4 THE POSTERIOR ELEMENTS

The posterior elements of a single vertebra, including the pedicles, lamina, articular facet surfaces, and all associated processes, were modeled with 114 solid brick elements of the same type of elements used to construct the vertebral body. (Figure 7-2) The circular plane surfaces of the superior and inferior facets in each vertebra were modeled by 24 elements oriented in a radial pattern single layer. Each facet consists of 8 interior wedge shaped elements surrounded by 16 cube shaped brick elements. A superior lumbar facet is oriented such that the normal to the surface is oriented laterally outwards and slightly posteriorly from the vertebral arch. The surface of an inferior lumbar facet opposes the superior facet with the normal to the surface facing laterally inward and slightly anterior. The thoracic facets which gradually change from the position of the lumbar facet at T12, to a different orientation at T1 can be seen in Figure 7-1. The superior facet surface normal of T1 points posteriorly and slightly superiorly from the posterior arch while the inferior normal points anteriorly and slightly inferiorly. Mating facet surfaces are parallel to each other in the model's unloaded equilibrium configuration.

Each pedicle is composed of one brick element and connects the vertebra body to the lamina which is made up of 6 brick elements. These two components form the

posterior arch from which the articular, transverse, and spinous processes branch. In this model, the morphology of the pedicles in the mechanical model are not anatomically correct and serve only as a means of attaching the posterior elements to the vertebral body. This configuration does not affect the model's behavior since no ligament elements do not attach directly to the pedicles.

In each vertebra, 6 brick elements are used to model the superior and inferior articular processes. These processes directly branch off the lamina-pedicle junction and attach to the outer most radial elements on the superior and inferior edges of the circular plane facets. The elements represent the three-dimensional shape of the articular processes and rigidly attach the anatomically correct facet surfaces to the posterior arch.

The spinous processes are each modeled by two parallel brick elements extending posteriorly and slightly inferiorly from the symmetrical mid-line of the laminae. The transverse processes extend laterally and slightly posteriorly from the pedicle-lamina junctions on either side of the vertebra and require two elements per vertebra. Posterior endpoints of the spinous process and lateral endpoints of the transverse processes serve as attachment points for interconnecting ligamentous spring elements.

7.5 THE INTERVERTEBRAL DISCS

The intervertebral discs are modeled using a system of 49 spring elements forming a truss structure containing 17 vertically oriented and 32 diagonally oriented springs. (Figure 7-3) Each spring element, defined by two endpoint nodes, is capable of tensile or compressive loading. One vertically oriented spring joins the endplate centers together. All the other elements are located along the perimeter of the endplate surfaces.

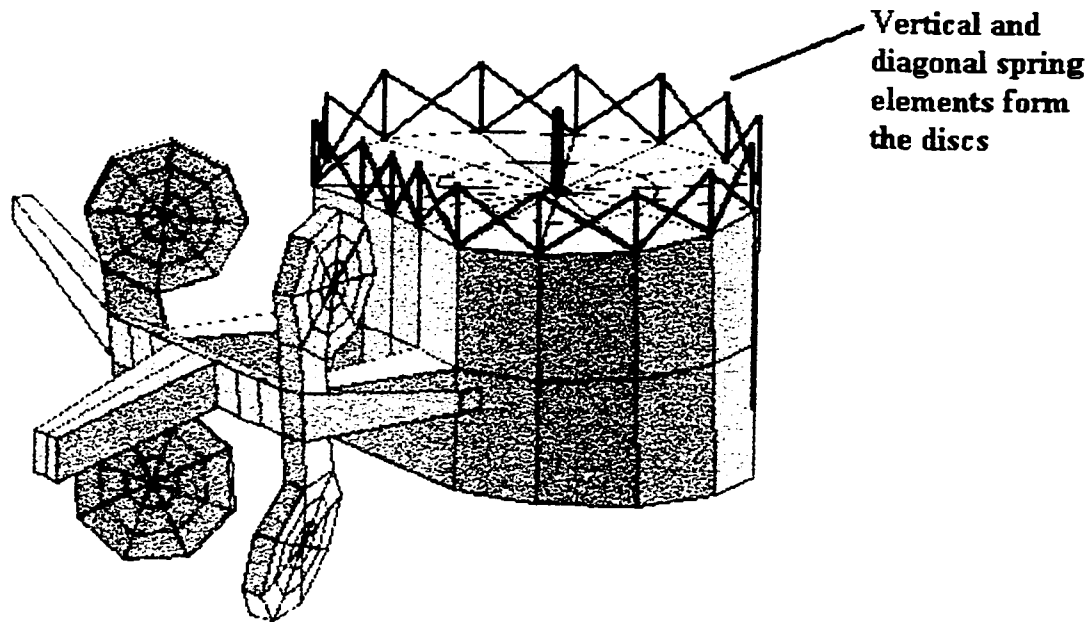


Figure 7-3. Intervertebral disc truss structure used to model disc behavior. The disc structure is composed of two node spring elements which interconnect adjacent vertebrae in a functional unit. This figure depicts only an inferior vertebra and disc. Note the single vertical spring located at the center of the vertebral body.

During bending, the stiffer center spring, acts as swivel joint between adjacent superior and inferior endplates, simulating the function of the nucleus pulposus. This is

achieved by giving the center spring an approximate stiffness 23 times higher than each vertical perimeter spring. This stiffness ratio was established empirically. The vertical spring elements interconnecting the perimeters of adjacent endplates primarily control and dictate the degree of "swiveling" or bending allowed between endplates. Diagonally oriented elements, also located along the endplate perimeters, primarily control the amount of rotation and shear. When subjected to axial loading, all three groups of elements, including the vertical center, vertical perimeter, and diagonal perimeter springs, undergo tensile or compressive loading. Spring elements were chosen to model the discs since overall disc behavior can be easily analyzed and manipulated by varying the stiffness' of the three groups of elements with the disc truss system. During the validation process of the intervertebral disc structure, lumbar or thoracic discs were evaluated in compression, bending, rotation, and shear.

7.6 THE SPINAL LIGAMENTS

The interconnecting spinal ligaments are each modeled using two node linear spring elements. (Figure 7-4a, 7-4b, and 7-4c) Spring elements can be made to behave like cable structures, capable of supporting only tensile, and not compressive loads. This inherent property makes the spring element an excellent choice for modeling ligament structures. Stiffness properties of individual spring elements can be easily varied to effectively simulate ligament structures. In this study, ligaments were modeled as linearly elastic, although the capabilities of these elements can include nonlinear and/or viscoelastic behavior.

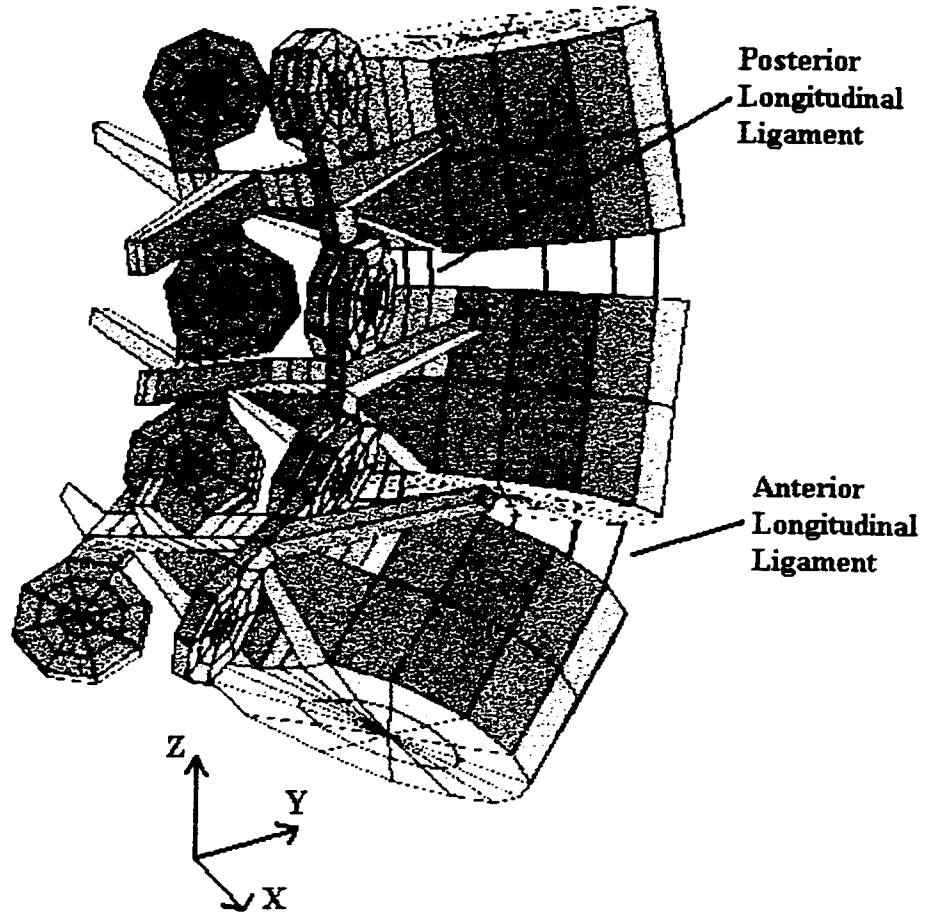


Figure 7-4a. Three vertebrae with only the anterior and posterior longitudinal ligaments in place.

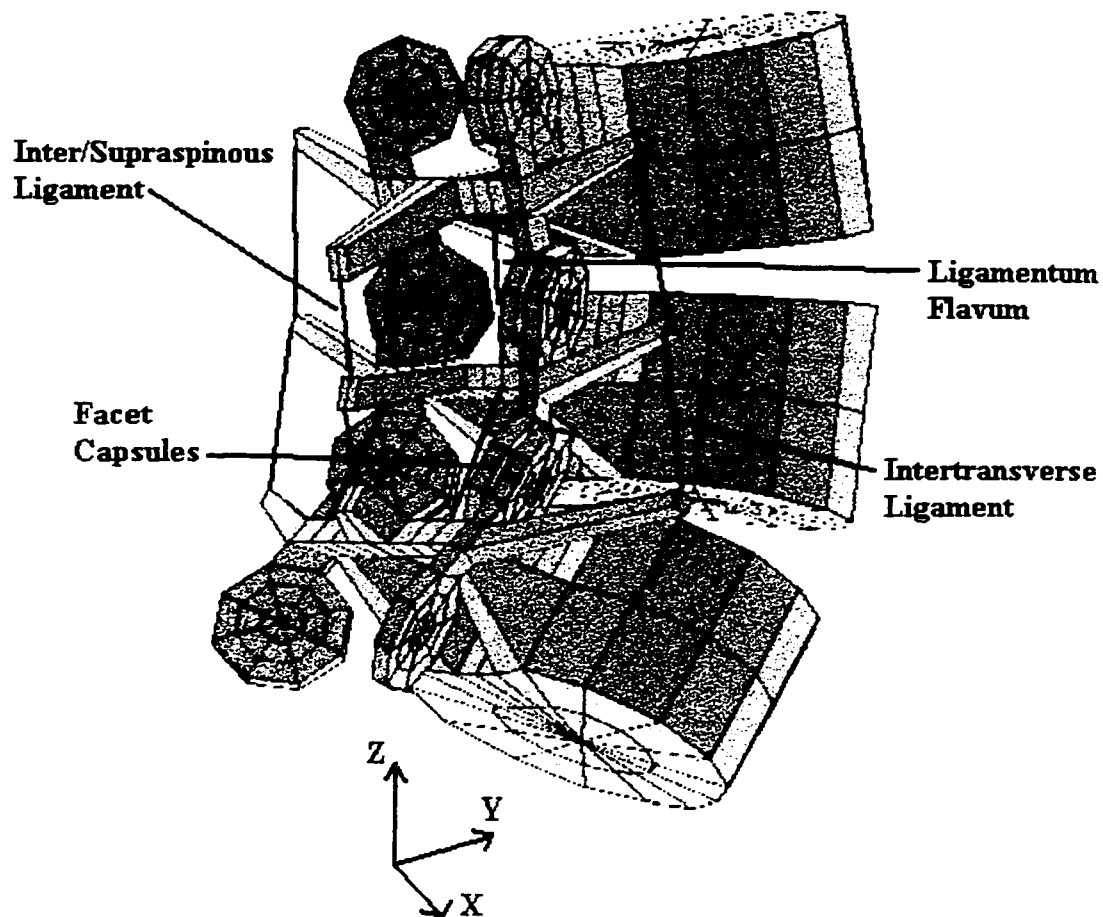


Figure 7-4b. Three vertebrae with only the inter/supraspinous ligament, intertransverse ligament, ligamentum flavum, and facet capsules in place. The facet capsules are represented by 8 spring elements interconnecting the perimeters of mating facet surfaces.

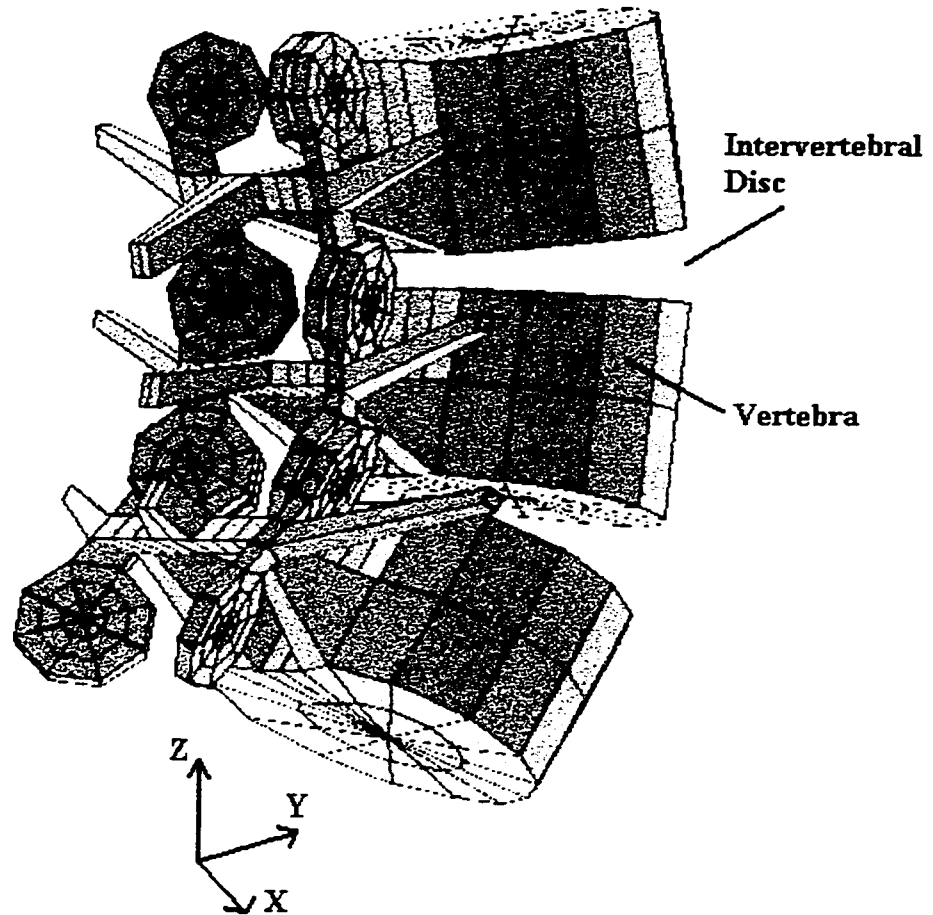


Figure 7-4c. Three vertebrae with only the intervertebral discs in place.

The anterior and posterior longitudinal ligaments are each constructed of three spring elements which insert into the anterior and posterior aspect of the vertebral body endplate surfaces respectively. Both ligaments are symmetrical about the vertebra's mid-sagittal plane providing control of flexion and extension movements of the spine. Uniform stiffness values were assigned to individual elements in both ligament structures to simulate band-like ligaments having uniform cross sectional thickness.

The intertransverse ligaments are each represented by a single linear spring element. This element interconnects the endpoints of transverse processes in neighboring vertebrae and aids in controlling lateral flexion movements of the spine. The anatomical transition from the interspinous ligaments structure to the supraspinous ligament is indistinct in the human spine. Both ligaments aid in controlling flexion, and to some degree, rotation of the spine. A single spring element was used to represent both interspinous and supraspinous ligaments. This element interconnects the endpoints of spinous processes in adjacent vertebrae. Locations of both transverse and spinous processes were previously described in Chapter 6 and are in agreement with results found in literature.

The ligamentum flavum is represented by 2 spring elements interconnecting adjacent vertebral laminae together in the normal spine model. The primary physiological functions of this ligament is to prevent hyperflexion of the spine, and protect the spinal cord within the spinal canal.

The articular capsules are each formed by eight spring elements interconnecting the perimeters of mating facet surfaces. These spring elements behave as linear elastic cable structures and control the amount of shearing or distraction between mating surfaces. When subjected to compressive loads, as in the case of a fully rotated or extended spine, facet ligaments become slack allowing facet surfaces to come into contact. During contact, the orientation of the mating facets at each spinal level is an

essential factor in determining the kinematics and mechanics of the spine. Typically, the orientations of lumbar facets are such that flexion or extension motions are permitted while vertebra rotations are limited. In contrast, thoracic facet surfaces permit vertebra flexion and rotation while extension movements are limited.

7.7 FACET “SUSPENSION” SYSTEM

In this model, the relative motion between vertebrae in each functional unit is limited by interconnecting spring or spar elements. Adjacent vertebrae move relative to one another about the intervertebral disc. Motion between adjacent rigid vertebrae is controlled by the truss system forming the discs, and the spinal ligaments interconnecting the endplates, process endpoints, and facet surfaces. To avoid the use of contact elements, simulating the necessary mechanics of facet surface contact was achieved using a “tree suspension” system. Contact elements would necessitate the use of at least 32 facet contact points and 32 facet target surfaces in the model. With contact elements in place, the chance of converged solutions for the spine model would greatly decrease. Computational time during runs would also increase due to the finer load step increments required for contact to occur between the contact points and target elements.

A facet suspension system was devised to simulate the contacting of facet surfaces. (Figure 7-5a and 7-5b) For each facet pair, a tree or pole like structure protrudes normally outwards from the superior facet center in the posterior direction

through the mating inferior facet of the superior vertebra. The tree serves to locate the ends of the cables and otherwise does not interfere in the mechanical behavior of the facets.

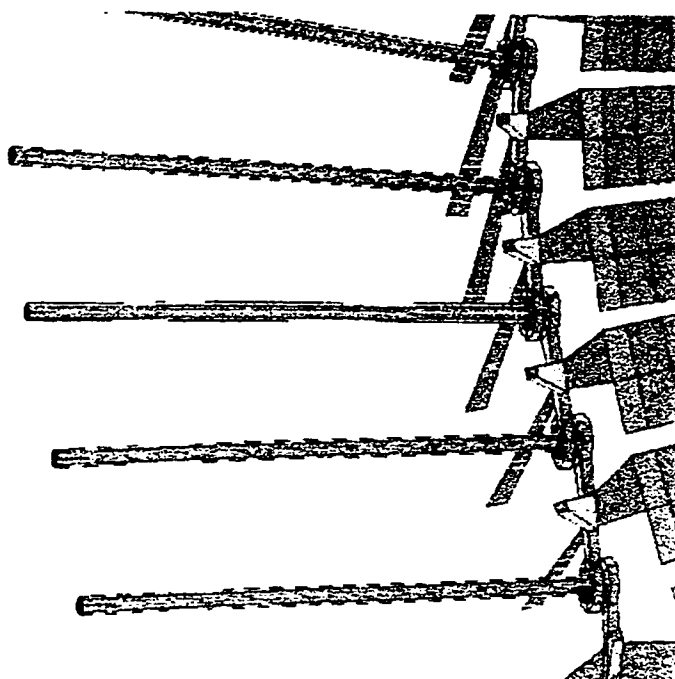


Figure 7-5a. Facet suspension system as seen in the lateral plane. 8 cable elements are used to "suspend" an inferior facet from a mating superior facet via pole structures protruding normally outwards from each superior facet surface.

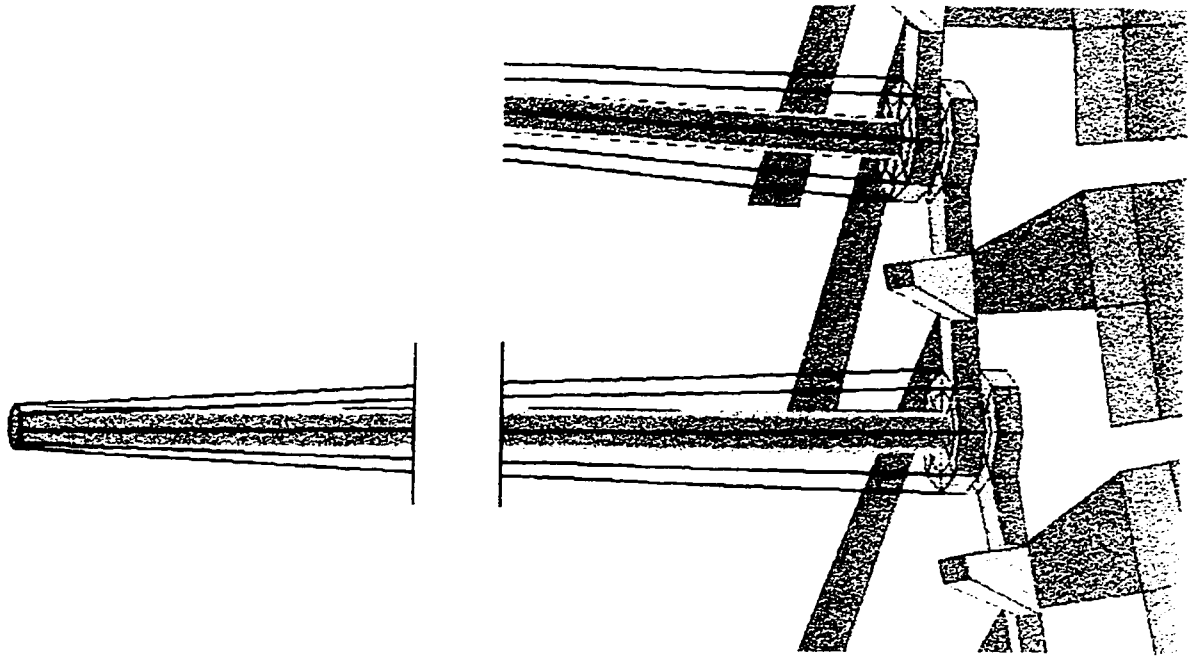


Figure 7-5b. Suspension cable elements (shown darkened) “suspending” the inferior facet of a superior vertebra over the superior facet of an inferior vertebra. The pole structure protruding through the facet of the superior vertebra does not interfere with any facet movements.

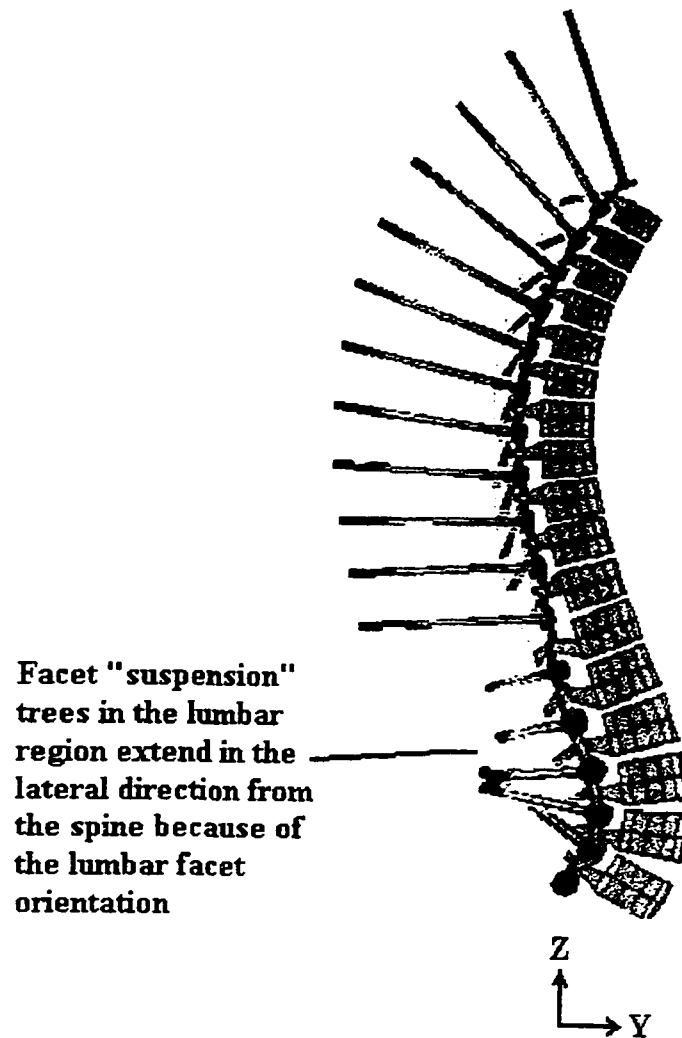


Figure 7.6 - Mechanical model shown in the mid sagittal view with facet tree structures and cable suspension elements. Facet tree structures visually describe the orientations of the facet surfaces.

Each tree is composed of 8 node brick elements and is solidly attached to the associated facet surface. The corresponding mating inferior facets of the superior vertebra is "suspended" from the end of the tree structure by a series of 8 cable elements. These cables do not support compressive loads and are sufficiently rigid to

prevent facet surfaces from passing through each other. The cable are unstretched in the model's unloaded equilibrium state.

Typical facets in the human body glide, touch, or part from one another during normal physiological movements. Little or no friction exists in the normal human facet joints because of the lubricating synovial fluid present in the articular capsules. With the model's suspension system, distraction between facets surfaces can occur where the suspension cable elements go slack. Gliding between facets also occurs where a suspended facet "swings above" its mating facet from the associated tree structure. The ratio of the length of a tree structure to the diameter of a typical facet surface is approximately 10. It was found that this ratio allows the model to simulate the relative motion between facet surfaces as parallel planes gliding over one another during normal physiological ranges of motion. During contact between mating facets, the suspension elements which are placed into tension, prevent the inferior facet of a superior vertebra, from passing through the superior facet of an inferior vertebra.

CHAPTER 8 - MATERIAL PROPERTIES

The mechanical properties of the interconnecting disc and ligament elements in the spinal model were based on values found in literature. Data on the interconnecting ligament properties were defined at each vertebral level. The compiled data for intervertebral discs were grouped to describe either a typical thoracic or lumbar disc.

8.1 THE VERTEBRAE

In building the model, the vertebrae were made to act as near rigid entities. The elements used to build the vertebrae were given a Young's Modulus value of 400 GPa, which is approximately 40 times greater than cortical bone in a vertebra. In comparison, spinal ligaments typically have modulus values of 10 to 30 MPa. The pedicles and articular processes in the model are used only as interconnecting structures between the vertebral body, posterior processes, and facet surfaces to locate ligament attachment points correctly, and are otherwise not anatomically correct. The cross sectional area of a pedicle in the model is less than that found in a normal human spine. This is because the pedicles are defined in part, by the corresponding nodal points describing the vertebral bodies. Subsequently, a high modulus of elasticity was used to eliminate any possible deformation upon loading, in the posterior elements of the model's vertebrae. When subjected to normal physiological loads, significant deflections of the model are limited to deformation in the ligaments and disc.

8.2 SPINAL LIGAMENTS

The load displacement paths of physiological ligaments are typically sigmoid in shape. (Figure 8-1) In order to represent this behavior, each interconnecting spinal element in the model, is characterized by a "two stage" linear load-displacement path. An interconnecting element behaves with a lower stiffness during initial displacements between ligament endpoint nodes. The linear load-displacement curve, corresponding to the element's initial stiffness, connects the origin of the load-displacement graph, with the point representing the beginning of the linear portion on the sigmoid curve. When a specified displacement is reached, a larger, secondary stiffness is utilized by the element for further deformations. This secondary stiffness, and the displacement point at which it is utilized by the model, corresponds with the linear region of the sigmoid curve of the associated physiological ligament. For all ligament elements, loading and unloading both take place along the same predefined load displacement path.

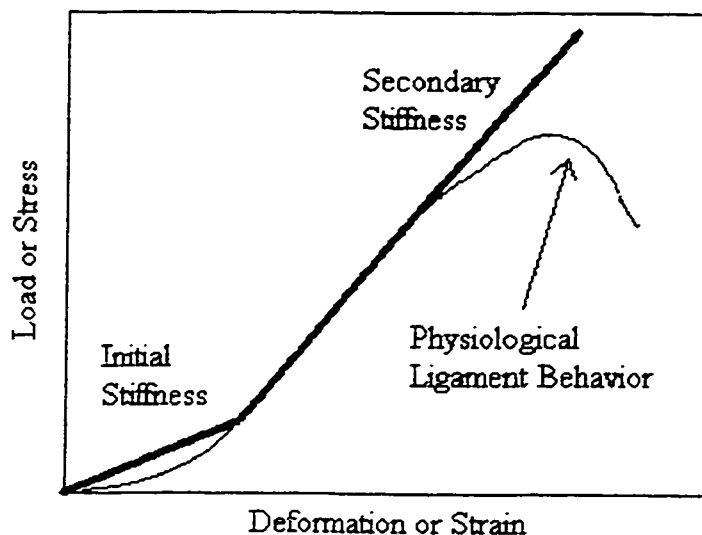


Figure 8-1. The sigmoid shaped load-displacement curve of a physiological ligament (thin line) is modeled using an element possessing two different stiffness values for two different ranges of displacement (thick line).

8.3 LIGAMENTS - "SECONDARY" STIFFNESS VALUES

The secondary stiffness values assigned to the interconnecting spinal elements, describe the linear "mid-range" of the sigmoid shaped load-displacement curves of the associated ligaments. These values are based on experimental data from four published studies. (4, 6, 20, 29) Of these studies, the primary results came from Pintar et. al. (29), Dumas et. al. (6), and Myklebust et. al. (20) The studies each documented load-displacement results for in vitro human spinal ligaments at each spinal level in the thoracolumbar spine. The stiffness values used in the model were then derived from these load-displacement results and assigned to each ligament element with an exception of the intertransverse ligaments.

Stiffness values for the intertransverse ligaments had not been recorded in any of these 3 studies, but were found in the remaining study by Chazal et. al. (4) For 5 spinal ligaments (anterior longitudinal ligament, posterior longitudinal ligament, ligamentum flavum, facet joints, and interspinous ligament), excluding the intertransverse ligament, Chazal's study consistently recorded averaged ligament stiffness values approximately 5 times greater than those found in the other 3 studies. For this reason, Chazal's data, with the exception of the stiffness values for the intertransverse ligaments, were excluded for use in the normal spine model. Chazal's study provided stiffness values for the intertransverse ligaments at vertebral levels T9-T10 (67.9 N/mm) and T7-T8 (61.5N/mm). These two values were averaged and scaled down by a factor of 5 to yield an intertransverse ligament stiffness of 12.9 N/mm. This was done since Chazal's study recorded on average, ligament stiffness values 5 time greater than the other three studies carried out by Pintar et. al. (29), Dumas et. al. (6), and Myklebust et. al. (20) The intertransverse ligament stiffness value of 12.9 N/mm was used at each level in the normal spine model.

The final stiffness values for the remaining ligament elements in the model were established by combining results from the three studies conducted by Pintar et. al. (29), Dumas et. al. (6), and Myklebust et. al. (20) For each ligament, the stiffness values from these three studies were averaged at each vertebral level. This data were then plotted as a function of vertebral level and fitted with a linear least squares regression

curve. The ligament stiffness values used for the model were then taken from each linear curve fit.

Both Chazal's and Myklebust studied the combined stiffness of the interspinous and supraspinous ligaments as a single value. This was done because both ligaments in the human spine intertwine and blend together to such a degree that only a single ligament is apparent during dissection. For this reason, the interspinous and supraspinous ligaments in the model are represented by a single element. The curve fitted data for ligament stiffness' can be seen in Figure 8-2 to 8-6.

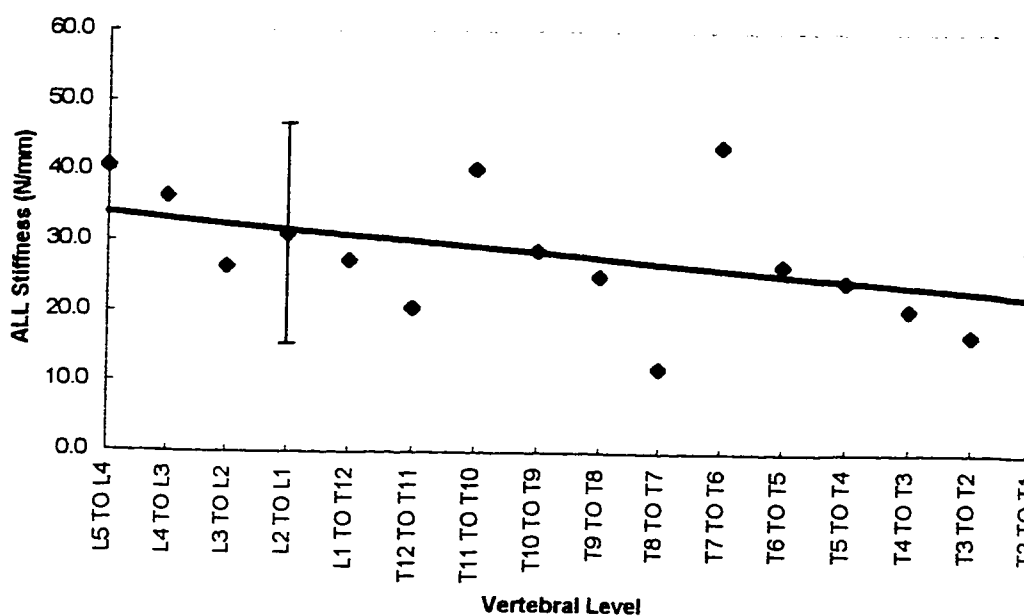


Figure 8-2. Anterior longitudinal ligament stiffness as a function vertebral level. Data was curve fitted using a linear least squares regression. A +/- one standard deviation range, typical of the data in the figure, is shown for L2 to L1. Sample size for the ALL ligament at L2 to L1 is 22.

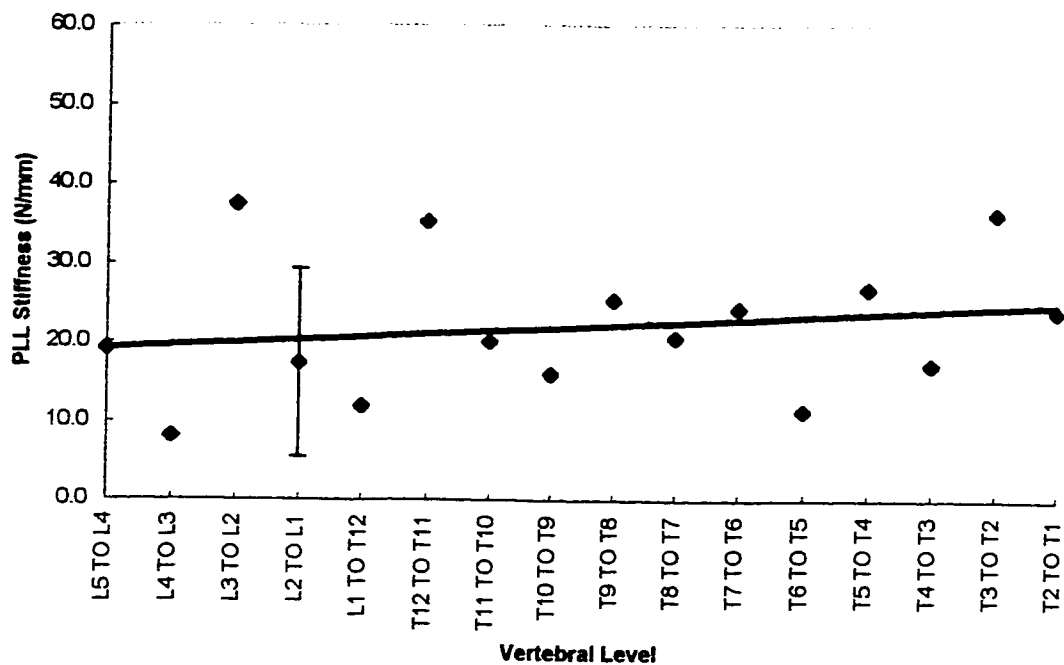


Figure 8-3. Posterior longitudinal ligament stiffness as a function vertebral level. A +/- one standard deviation range, typical of the data in the figure, is shown for L2 to L1. Sample size for the PLL ligament at L2 to L1 is 22.

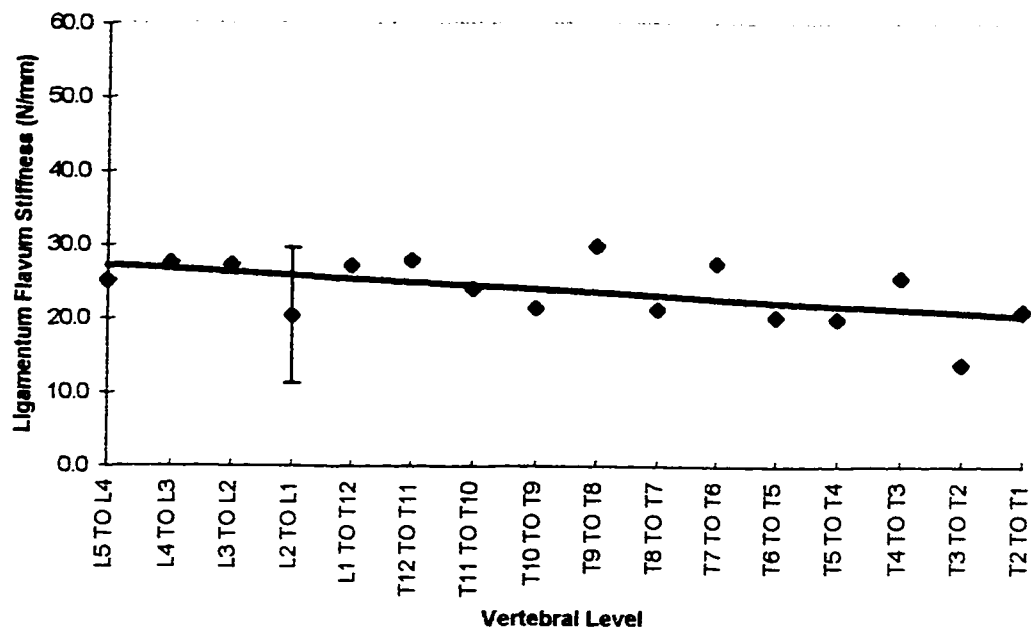


Figure 8-4. Ligamentum flavum stiffness as a function vertebral level. A +/- one standard deviation range, typical of the data in the figure, is shown for L2 to L1. Sample size for the ligamentum flavum at L2 to L1 is 22.

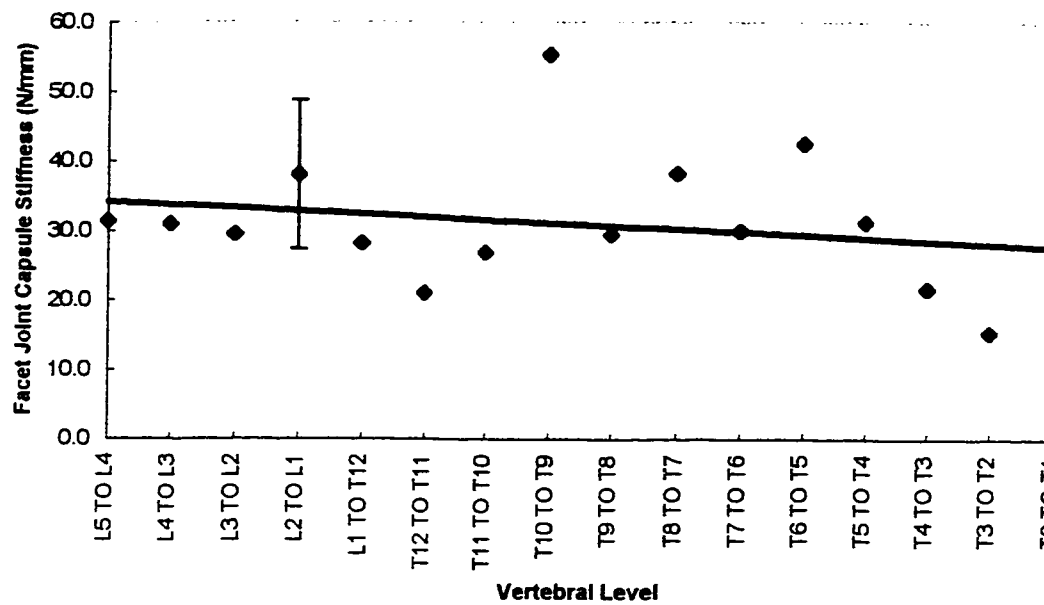


Figure 8-5. Joint capsule stiffness. The plotted data represents the stiffness values for both facet capsules tested as a bilateral unit with excised disc and spinal ligaments. A +/- one standard deviation range, typical of the data in the figure, is shown for L2 to L1. Sample size for the joint capsule data at L2 to L1 is 22.

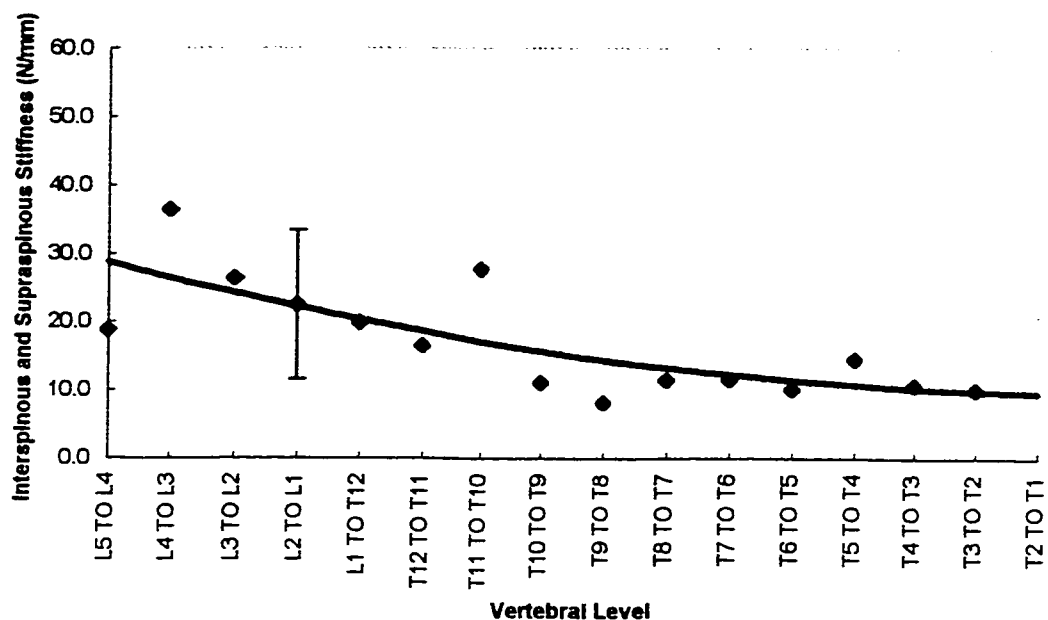


Figure 8-6. Interspinous and supraspinous ligaments with combined stiffness'. Data was curve fitted using a 2nd degree polynomial. A +/- one standard deviation range, typical of the data in the figure, is shown for L2 to L1. Sample size for the inter/supraspinous ligament at L2 to L1 is 44.

8.4 LIGAMENT INITIAL DISPLACEMENT STIFFNESS VALUES

The ligament stiffness values, used to characterize ligament element behavior when subjected to low loads and displacements, were based on a ligament study conducted by Chazal et. al. (4) Based on load displacement data taken from the study, the initial stiffness of a given ligament was expressed as a percentage of the ligament's linear mid-range stiffness. Each element's initial elongation value, for which the smaller initial stiffness is used, was taken directly from averaged data provided in Chazal's study. Once the initial elongation value for an element's deformation is exceeded, the larger, secondary stiffness value, is used to describe the elements behavior. Table 8-1

lists the ligament displacement limits and stiffness values (as a percentage of the associated ligament linear mid-range stiffness) for modeled ligaments undergoing small deformation within the initial region of the load displacement curve.

Table 8-1. Initial stiffness values for interconnecting ligaments

Ligament	Stiffness (expressed as a percentage of the linear mid-range secondary stiffness)	Displacement Limit (mm)
Anterior Longitudinal	Thoracic Region - 43% Lumbar Region - 40%	Thoracic Region - 0.83mm Lumbar Region - 1.52mm
Posterior Longitudinal	Thoracic Region - 49% Lumbar Region - 52%	Thoracic Region - 0.70mm Lumbar Region - 0.92mm
Joint Capsules	Thoracic Region - 50% Lumbar Region - 50%	Thoracic Region - 1.00mm Lumbar Region - 1.00mm
Ligamentum Flavum	Thoracic Region - 60% Lumbar Region - 57%	Thoracic Region - 0.75mm Lumbar Region - 1.60mm
Inter/Supraspinous	Thoracic Region - 59% Lumbar Region - 51%	Thoracic Region - 1.05mm Lumbar Region - 1.54mm
Intertransverse	Thoracic Region - 39% Lumbar Region - 39%	Thoracic Region - 0.80mm Lumbar Region - 0.80mm

8.5 INTERVERTEBRAL DISCS

The construction of the intervertebral discs in the model was described in Chapter 6. The mechanical properties of the spring elements in the disc model were

developed through an iterative procedure where the load-displacement behavior of the disc model was compared with disc stiffness properties from 4 studies found in literature. These comparisons were made within the natural range of motion (32) of a human intervertebral disc. In the validation procedure, the disc model was tested in compression, flexion/extension/lateral bending, shear, and axial rotation. Gross stiffness values of the disc model are presented and compared with literature results in Table 8-2.

Table 8-2. Stiffness parameters of an intervertebral disc

	Axial (N/mm)	Shear (N/mm)	Torsion (Nmm/deg)	Flexion Extension Bending (Nmm/deg)
Literature Results (*)	2400	100	2000	2270
Disc Model	2420	107	1700	2270

(*) Axial stiffness value derived from Virgin et. al., 1957 and Brown et. al., 1957

Shear stiffness value derived from Panjabi et. al., 1976 and Thompson, 1995

Torsional stiffness value derived from Farfan et. al., 1970

Flex/Ext/Bending stiffness value derived from Panjabi et. al. 1976 and Thompson, 1995

8.6 VALIDATION

Validation of the mechanical spine model was done by a comparison of stiffness values of the model's functional units with stiffness values given in literature (8, 16, 17, 18, 22, 23, 24, 31, 33). At the time of this thesis, experimental work for validation purposes could be found only for individual functional units. Load deflection studies on whole spinal segments were restricted to in vivo subjects using externally applied loads on the body and radiographs or MRIs.

Each functional unit in the model consists of two adjacent vertebrae and the associated interconnecting ligaments and disc. During testing, the inferior endplate perimeter nodes on the inferior vertebra were constrained from translation in all directions. The superior vertebra, having no constraints, was allowed to deflect when subjected to loading. Loads were applied to the superior vertebra to produce flexion, extension, lateral bending, or axial rotation movements. (Figure 8-7) After each test run, reactions for the given functional unit were checked at the constrained nodes to ensure the deformed functional unit had reached equilibrium upon convergence. Nodal displacements in the superior vertebral body of the loaded spinal unit were used to determine the gross resultant translation of the superior vertebra relative to the adjacent inferior vertebra. The load vs. deflection results were then translated to stiffness values and compared to existing literature results. Other available data derived from each test run included the force and "stretching" of each spinal ligament as a result of loading.

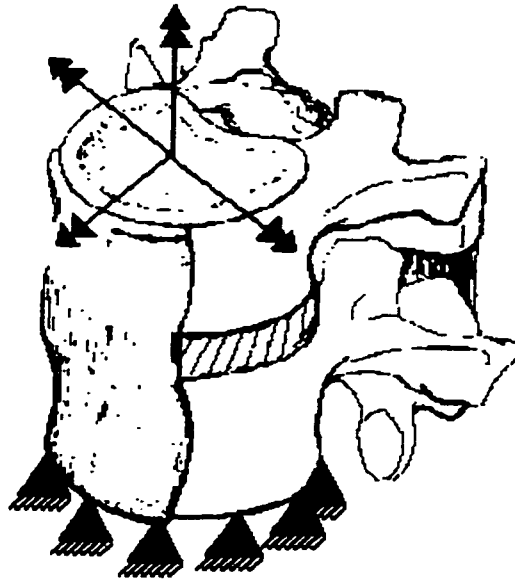


Figure 8-7 - Flexion, extension, axial rotation, and lateral bending loads were applied to the superior vertebra of each functional unit during the validation of the model. In each case, the base of the inferior vertebra was constrained.

Literature results provided stiffness values for thoracic or lumbar functional units in flexion, extension, lateral bending, and axial rotation. In most cases, the experimental stiffness' found in literature were not specific to any given vertebral level. The data from the various studies were mostly grouped as stiffness values for either the thoracic or lumbar regions of the spine. As a result, each functional unit in the model was only tested against either a thoracic or lumbar stiffness result depending on the vertebral level of the given functional unit.

CHAPTER 9 - RESULTS

At each spinal level, load-displacement results were determined for the given functional unit in flexion, extension, lateral bending, and axial rotation. Each pre-loaded functional unit was oriented in a normal upright spine in the standing position. Results for the lumbar region of the model are presented first, followed by the thoracic units. This is done because of the distinct variation between lumbar and thoracic vertebrae, particularly with facet orientation.

9.1 INITIAL TESTING ON THE L5 TO L4 AND L4 TO L3 UNITS

A trial study was performed on the L5 to L4, and L4 to L3 functional units using stiffness values taken from the physiological “mid range” of the interconnecting spinal ligaments and disc. Curve A in Figure 9-1 represents an interconnecting spinal structure where the mid-range behavior during deformation is linear and the overall shape is sigmoid. For this part of the study, the stiffness values from this linearly elastic region for the spinal ligaments and disc were used in defining the mechanical properties of the interconnecting elements within the L5/L4 and L4/L3 functional units. These values were previously discussed in Chapter 8. Curve B represents the behavior of the ligament and disc structures used in this trial study, where the linear stiffness of the curve was set equal to the mid-range linear stiffness of Curve A. No initial displacements were present in any interconnecting element in the model’s unloaded state.

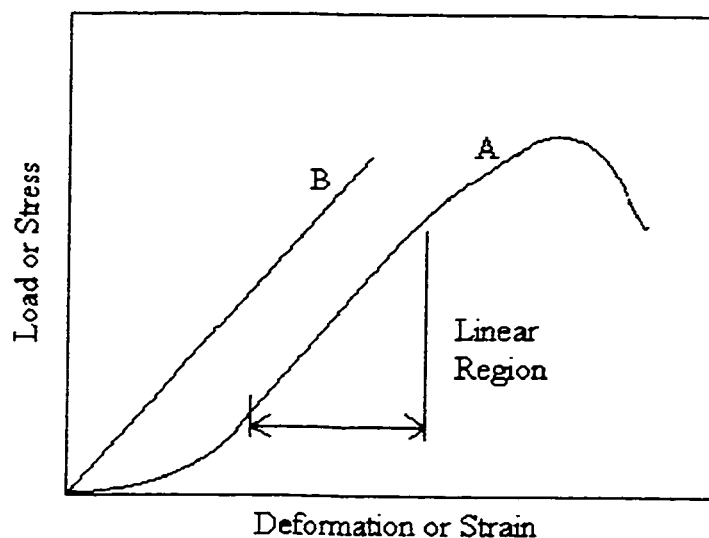


Figure 9-1. Representation of the sigmoid shaped load - displacement curve for ligament or disc structures shown in curve A. Curve B possesses a linear load displacement response with the same stiffness as the "mid-range" of curve A. In a trial study, the mechanical response of interconnecting elements in an L5/L4 and L4/L3 unit were set to behave like Curve B.

After testing, it was found that the response of the L5/L4 and L4/L3 trial units were too stiff compared with literature results. The lower stiffness of the ligaments and disc in the initial portion of deformation are essential for modeling correct load-displacement responses comparable to literature results, and have been incorporated into the version of the model described next. An example of the reduced deflection response of the L5 to L4 functional unit model in flexion, compared to figures based on functional unit stiffness values taken from literature, are shown in Table 9-1. The

results shown are for the L5/L4 functional unit subjected to a 5 Nm load applied to the vertebral body of L4 while the inferior endplate of L5 is rigidly fixed.

Table 9.1 - A comparison of the degrees of flexion for a modeled L5/L4 functional unit possessing ligaments and disc modeled with stiffness values characteristic of the linear mid-range of physiological interconnecting structures. Lower initial stiffness behavior of interconnecting structures, undergoing low displacements, were not accounted for in this model.

Applied flexion moment of 5 Nm to L4 vertebra in L5/L4 unit	Trial model	Markolf, 1972	Markolf, 1971	Oxland, 1992
	1° flexion	2.5° flexion	1.9° flexion	1.8° flexion

9.2 BI-LINEAR LUMBAR SPINAL MODEL

For the final lumbar model, the ligament and disc structures in each individual functional unit were modeled with a two stage linear stiffness. (Figure 9-2) During initial displacements, the elements behave with a lower initial stiffness, which increase to a greater stiffness once a specified displacement is reached. The finalized stiffness properties for the elements were determined from literature and were presented in Chapter 8. This element behavior was introduced to better represent the mechanical behavior of physiological spinal structures. With the two stage stiffness concept, the initial region of the load-displacement curve of an interconnecting element is represented by a linear model, beginning at the origin and ending at the linear portion of

the associated ligament's physiological sigmoid curve. (Figure 9-2) Once element displacement reaches the linear mid-range portion of the sigmoid curve, a secondary stiffness is used by the element undergoing increased loading.

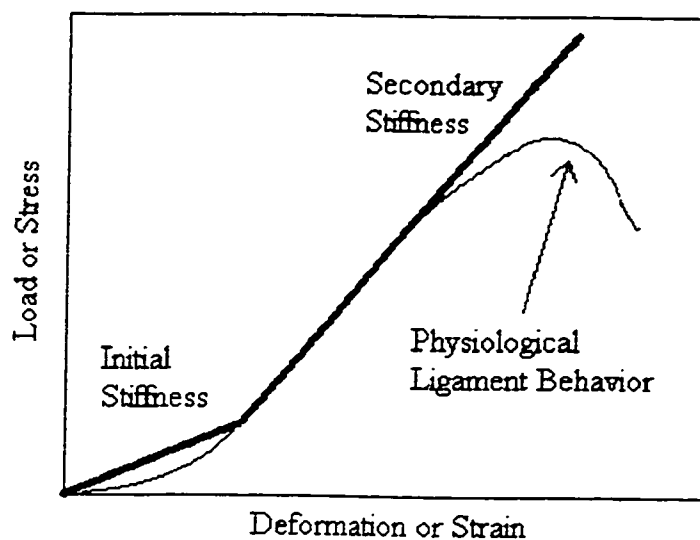


Figure 9-2. The thicker line represents the behavior of a typical disc or ligament while the thinner line represent the sigmoid shaped behavior of the actual physiological structure. The two stage stiffness behavior of the elements in the modeled functional units were used to better simulate the physiological behavior of human ligaments and disc structures.

The lumbar functional units were tested in flexion, extension, lateral bending and axial rotation. In each case, the inferior endplate of the inferior vertebra in the unit was constrained from movement while a moment was applied to the superior vertebra. Nodal displacements of the vertebral bodies were then used to determine the degrees of flexion, extension, bending, or rotation. The stiffness value of a functional unit in each

test was defined as the value of the applied moment, measured in Nm, over the deformation, measured in degrees. The average stiffness values presented, are taken from data results of units tested within the normal physiological range of motion as defined in literature (32). No initial deflection is present in the functional unit's unloaded state.

9.3 LUMBAR FLEXION

In flexion, each lumbar functional unit was tested within the normal lumbar physiological range of motion of 0° to 6° degrees rotation. Deformation was produced by applying loads to the superior vertebra of the functional unit while the inferior endplate of the inferior vertebra was constrained. Upon loading, no lateral displacements were noted in the superior vertebra. The amount of flexion was measured from the resulting nodal displacements of the superior vertebral body after each converged run, which was then used to determine the stiffness of the given lumbar unit. The flexion stiffness was then compared against literature results. Flexion stiffness values for the lumbar functional units range from 2.14 Nm/degree to 2.60 Nm/degree. The overall averaged flexion stiffness value for all lumbar units from L5/L4 to L1/T12, is 2.48 Nm/degree, with a population standard deviation of 0.19 Nm/degree. This average stiffness value in comparison to documented lumbar flexion stiffness results can be seen in Figure 9-3. Figure 9-4 shows a typical pre-loaded (dotted outline) and post-loaded (solid entity) functional unit in flexion.

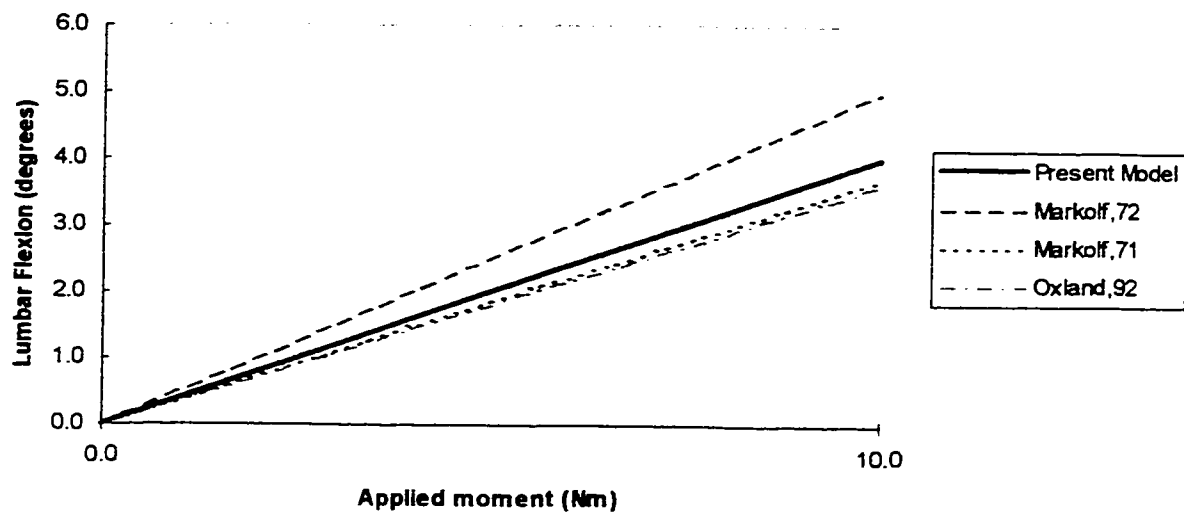


Figure 9-3. Stiffness comparison of lumbar functional units in the model to other studies.

Results from lumbar units were averaged for comparison purposes with other studies.

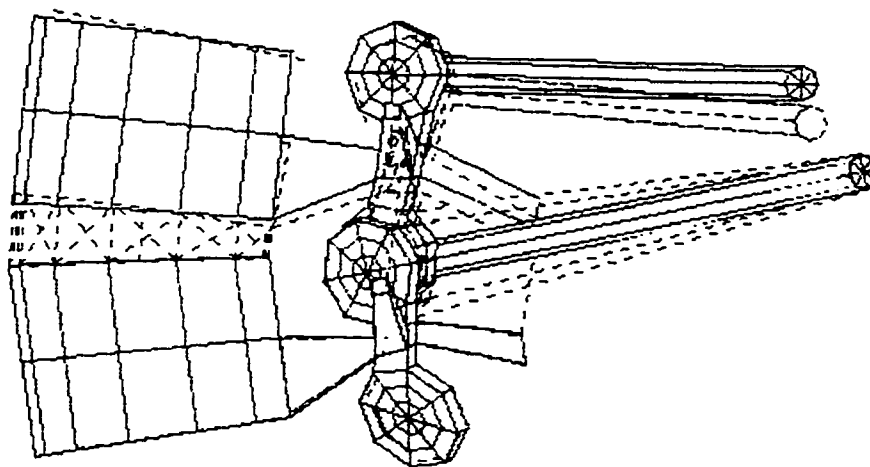


Figure 9-4. A lumbar functional unit in flexion. The dotted outline represents the pre-loaded state, while the solid entity depicts the post-loaded position.

Ligament deformation during flexion can be seen in Figure 9-5. The bar graph in Figure 9-5 represents the average distraction of the lumbar ligaments brought on by a 10 Nm moment during flexion. Standard deviation ranges of \pm one standard deviation are shown for each ligament. Any negative values denote a negative distraction amount, signifying an unloaded ligament.

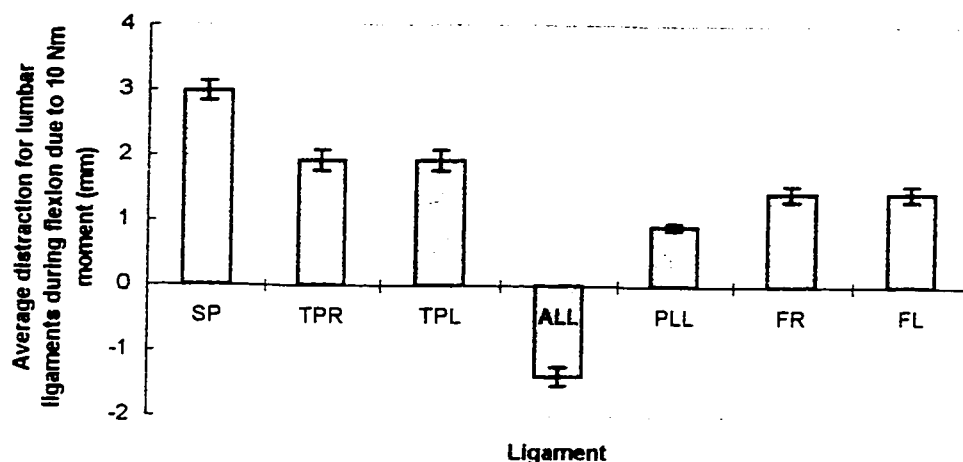


Figure 9-5. The average distraction in some lumbar ligaments during flexion due to an applied moment of 10 Nm. SP - inter/supraspinous ligament. TPR - right intertransverse ligament. TPL - left intertransverse ligament, ALL - anterior longitudinal ligament. PLL - posterior longitudinal ligament. FR - right facet capsule. FL - left facet capsule. Note only the ALL was unloaded during flexion. Standard deviation of \pm one standard deviation is shown for each ligament.

9.4 LUMBAR EXTENSION

Extension, like flexion, was also tested within the normal lumbar ranges of motion of 0° to 6° degrees rotation. In these test runs, 5 Nm extension loads were applied to the superior vertebra of the functional unit, while the inferior endplate of the

inferior vertebra was constrained. No lateral displacements of the superior vertebra occurred as a result of extension loading. Extension stiffness values for functional units in the lumbar region range from 1.63 Nm/degree to 2.17 Nm/degree. The average lumbar spinal unit extension stiffness is 1.98 Nm/degree with a population standard deviation of 0.20 Nm/degree. A load-flexion comparison graph of the average lumbar spinal unit in the model vs. literature results are shown in Figure 9-6. Figure 9-7 shows a typical lumbar functional unit in the model undergoing extension.

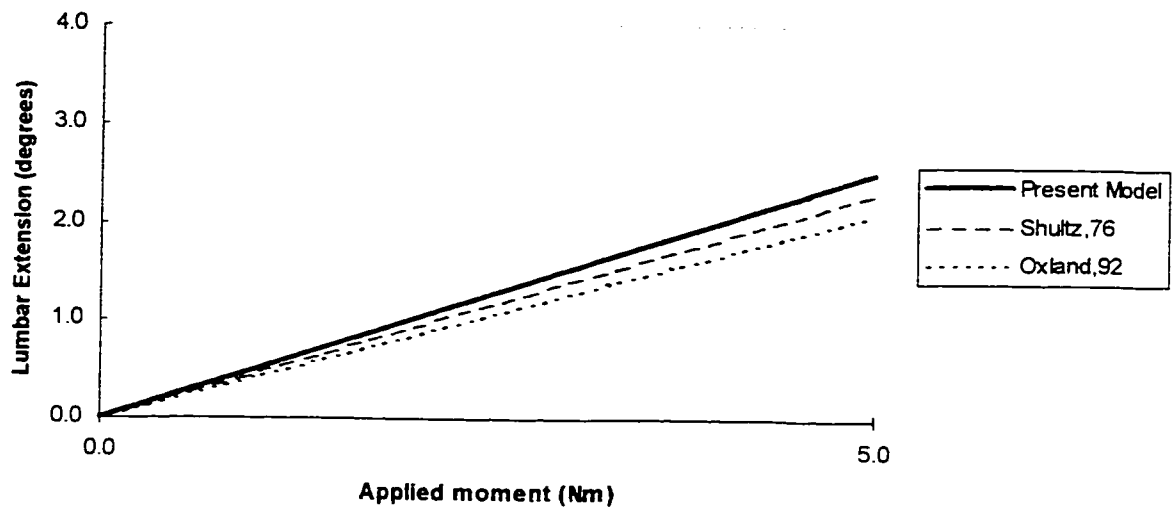


Figure 9-6. Lumbar functional units subjected to extension loading compared to other studies. The model's averaged lumbar extension results are shown as the thicker line.

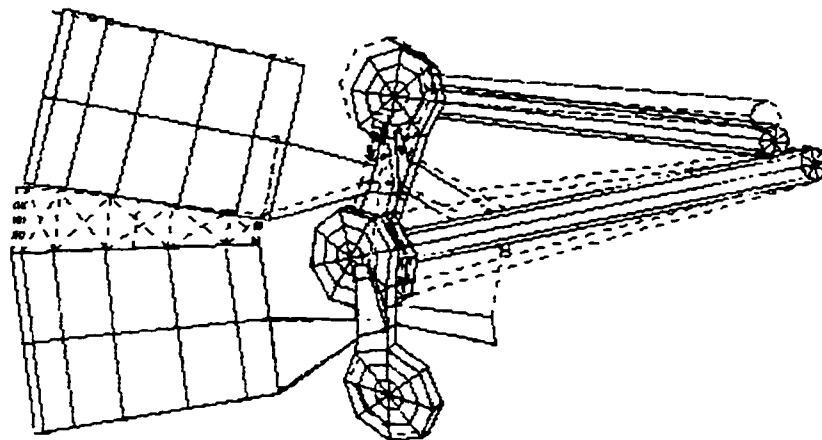


Figure 9-7. A lumbar functional unit in extension. The dotted outline represents the pre-loaded state, while the solid entity depicts the post-loaded position.

Average ligament deformation for the lumbar functional units during extension caused by a 5 Nm moment are shown in Figure 9-8. The bar graph shows that the only ligaments sustaining a tensile load during extension are the anterior longitudinal ligament and facet capsules. The facet capsular distraction was due to the sliding of the inferior facet in the unconstrained superior vertebra, downwards over the superior facet in the rigidly constrained inferior vertebra in a given functional unit.

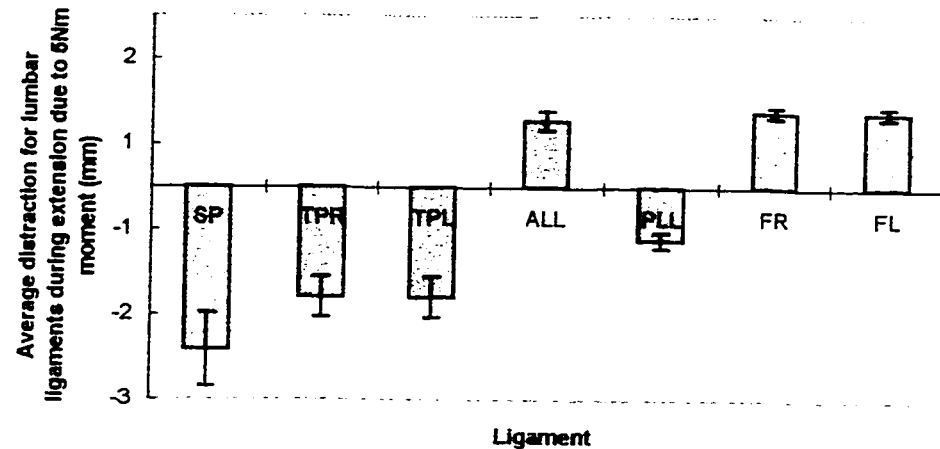


Figure 9-8. The average distraction in lumbar ligaments during extension due to an applied moment of 5 Nm. SP - inter/supraspinous ligament. TPR - right intertransverse ligament, TPL - left intertransverse ligament, ALL - anterior longitudinal ligament, PLL - posterior longitudinal ligament. FR - right facet capsule, FL - left facet capsule. Standard deviation of +/- one standard deviation is shown for each ligament.

9.5 LATERAL BENDING IN THE LUMBAR REGION

Lateral bending was produced by application of a moment to the superior vertebra in a functional unit. Lumbar spinal unit stiffness values in lateral bending range from 1.87 Nm/degree to 2.6 Nm/degree with an average of 2.17 Nm/degree. The population standard deviation for these stiffness values are 0.26 Nm/degree. A comparison of the average bending stiffness for the lumbar spinal units vs. literature results are shown in Figure 9-9. A pre-loaded and post-loaded lumbar functional unit seen in the frontal plane is shown in Figure 9-10.

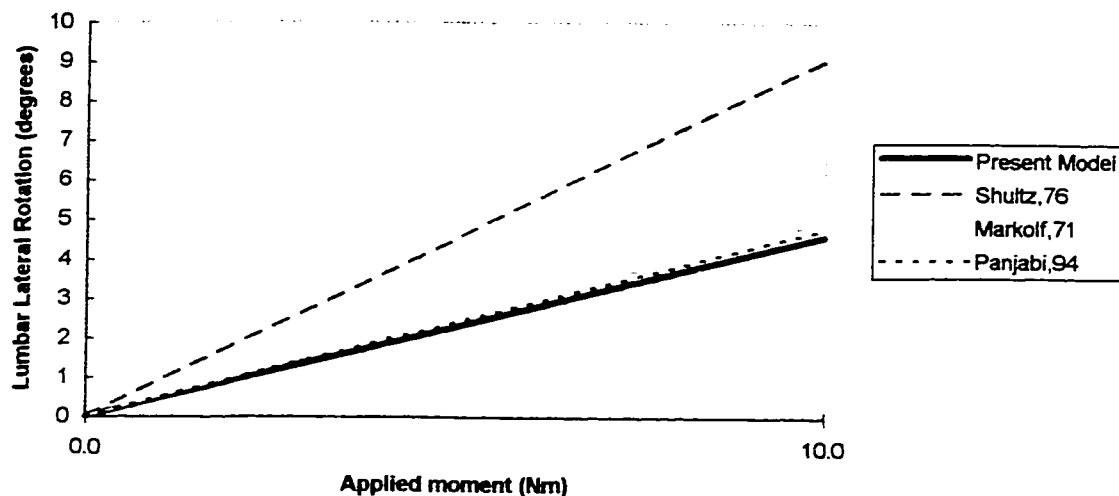


Figure 9-9. Lateral bending of the modeled lumbar functional units compared to other studies. The model's averaged lumbar lateral bending result are shown as the thicker line.

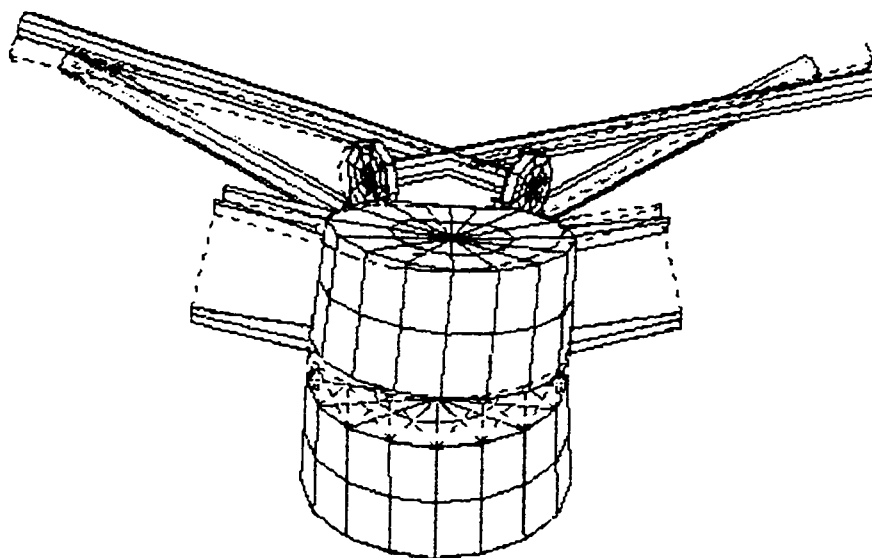


Figure 9-10. Lateral bending of a typical modeled lumbar functional units. Pre-loaded configuration is represented by dotted lines while post-loaded equilibrium position shown by solid entities.

At the end of each test run, a slight axial rotation was noted in every loaded functional unit accompanying the primary lateral bending movement. This type of coupled motion has been noted in antero-posterior radiographs of human spines in lateral bending, although quantified results on this behavior have not been found. As described in literature (39) and demonstrated by the model, a lateral bending movement is usually accompanied by a vertebral axial rotation in the contralateral direction. For example, if a normal spine, viewed from the posterior aspect, bends laterally towards the left, the spinous processes would in turn also point towards the left, in the direction of the bend. Although the contralateral rotation is the most common coupled motion found to occur with lateral bending, the magnitude, and even direction of the coupled rotation can be significantly changed by the posture of the spine (39). Contralateral rotations accompanying lateral bending in lumbar functional units are shown in Figure 9-11. In this figure, a 10 Nm moment was applied to each units to induce lateral bending. The resultant lateral bending rotation is plotted beside the accompanying axial rotation movement for each lumbar functional unit.

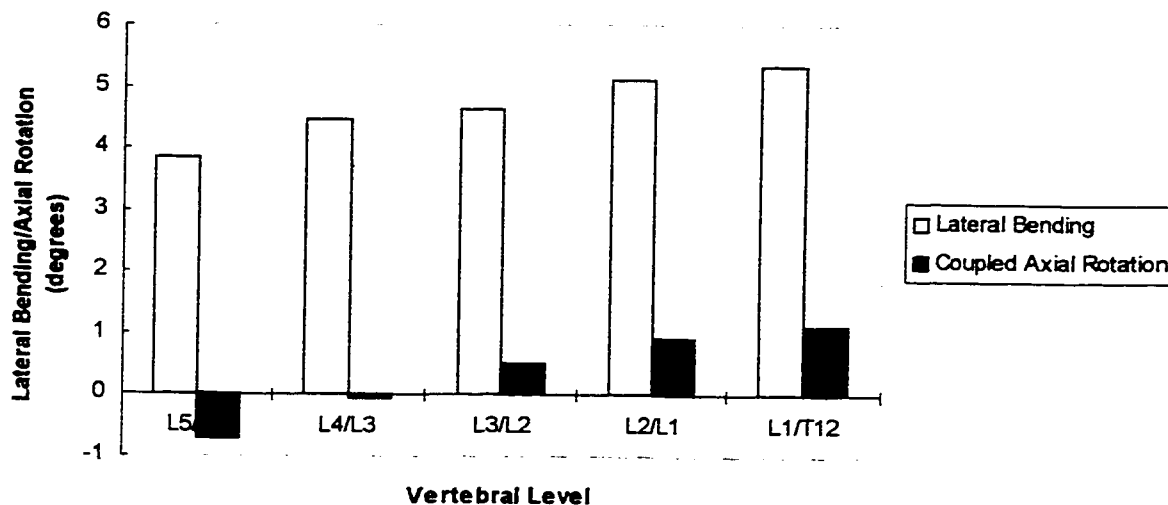


Figure 9-11. Lateral bending accompanied by coupled axial rotation in the lumbar spinal units as a result of an applied 10 Nm moment. Note that positive values signify contralateral rotation, whereas negative values signify the opposite.

Average ligament deformation for the lumbar functional units, as a result of lateral bending to the left, caused by a 10 Nm moment, are shown in Figure 9-12. From this figure, it can be seen that the ligaments furthest from the mid-sagittal plane of the vertebra undergo the most deformation and tensile loading; namely, the right intertransverse ligament (TPR), and the facet capsules (FR & FL).

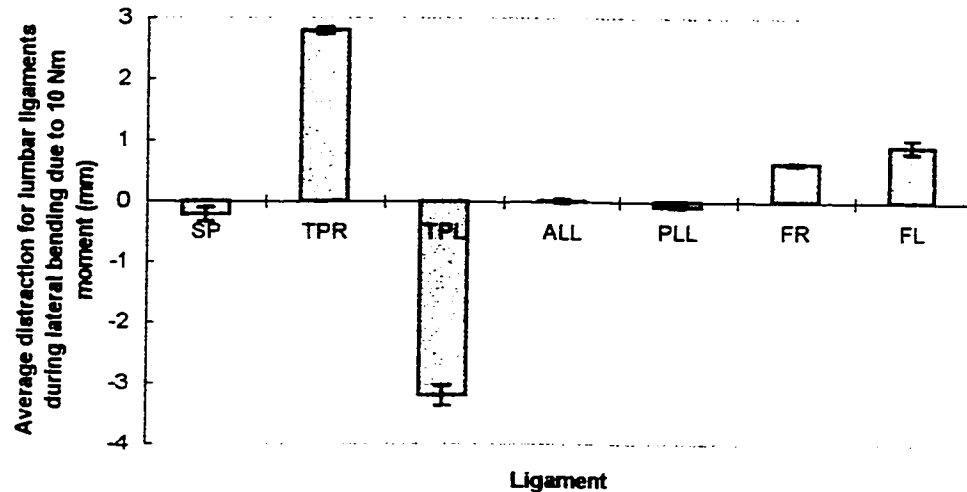


Figure 9-12. The average distraction in lumbar ligaments during lateral bending due to an applied moment of 10 Nm. SP - inter/supraspinous ligament. TPR - right intertransverse ligament, TPL - left intertransverse ligament. ALL - anterior longitudinal ligament, PLL - posterior longitudinal ligament. FR - right facet capsule. FL - left facet capsule. Standard deviation of +/- one standard deviation is shown for each ligament.

9.6 AXIAL ROTATION IN THE LUMBAR REGION

Axial rotation was produced by applying a moment to the unconstrained superior vertebra, while the associated inferior vertebra was held fixed. The axial rotation produced in each post-loaded functional unit was calculated within the transverse plane of the model using nodal displacements of the superior vertebra. The stiffness of lumbar functional units in axial rotation ranges from 2.91 Nm/degree to 4.35 Nm/degree. By excluding the lumbar unit L5 to L4, the axial rotation stiffness ranges from 4.04 Nm/degree to 4.35 Nm/degree. The overall average axial stiffness for

the lumbar region was 3.95 Nm/degree, with a population standard deviation of 0.53 Nm/degree. Figure 9-13 compares the model's axial load-rotation behavior with literature results, while Figure 9-14 depicts a typical lumbar functional unit undergoing axial rotation.

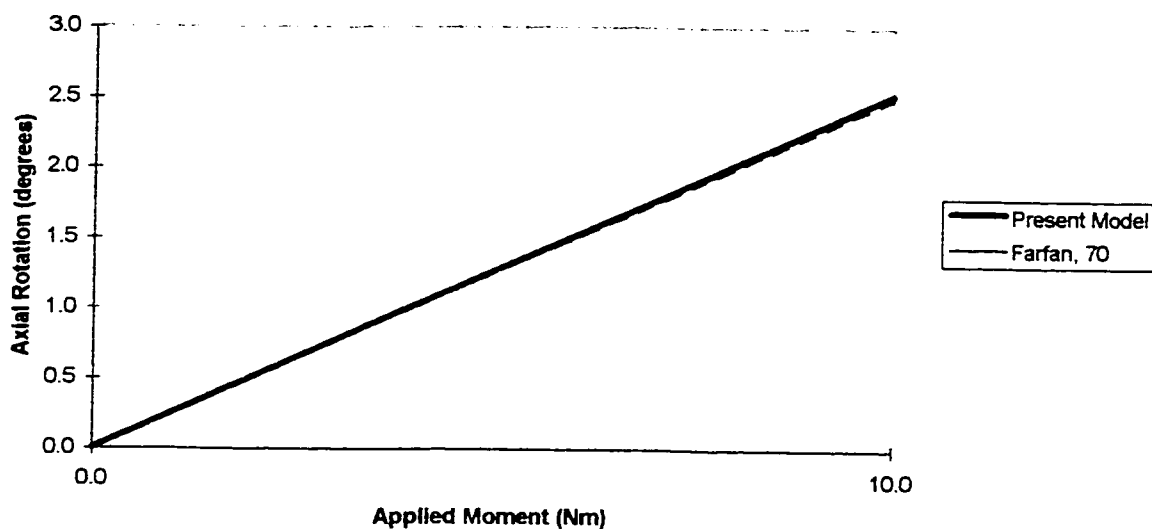


Figure 9-13. Axial rotation of the lumbar functional units compared to another study. The model's averaged lumbar axial rotations result is shown as the thicker line.

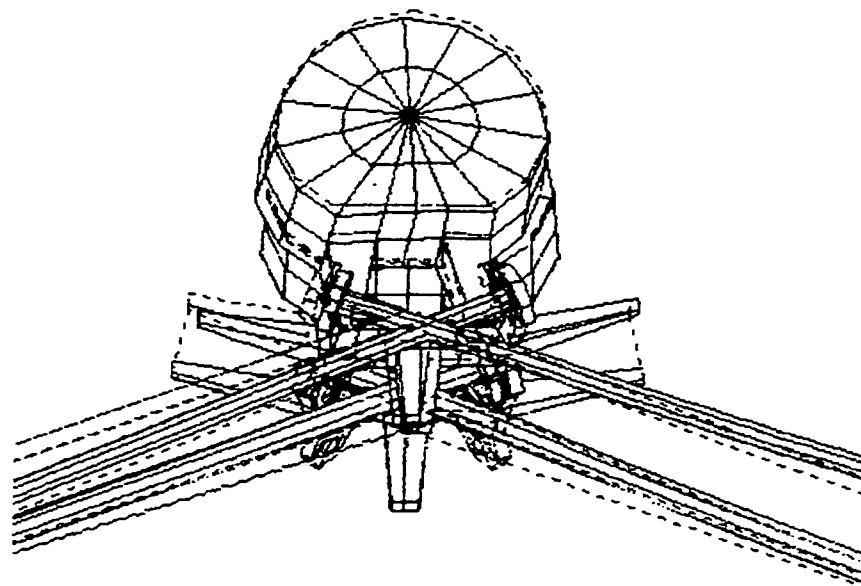


Figure 9-14. Axial rotation of a lumbar functional unit as seen in the transverse plane.

It is known that a coupling effect in human lumbar spines is seen where lateral bending produces a contralateral rotation. This study investigated the opposite effect of axial rotation producing lateral bending. It was found that if the lumbar spine, as viewed from the posterior aspect, rotated such that spinous processes would turn in towards the right, the spine would also bend laterally towards the right. This coupling effect was noted in all lumbar units except the L5/L4 functional unit. Induced lateral bending in this model, was thus brought on by an axial rotation in the contralateral direction. Figure 9-15 compares the induced lateral bending (towards the right) as a result of axial rotation towards the left (i.e. spinous processes turning in towards the right). The average ligament distraction during an axial rotation movement as a result of a 5 Nm applied moment, is shown in Figure 9-16. In this figure, it is evident that the

ligaments furthest away from the vertebral body experience the greatest amount of stretching.

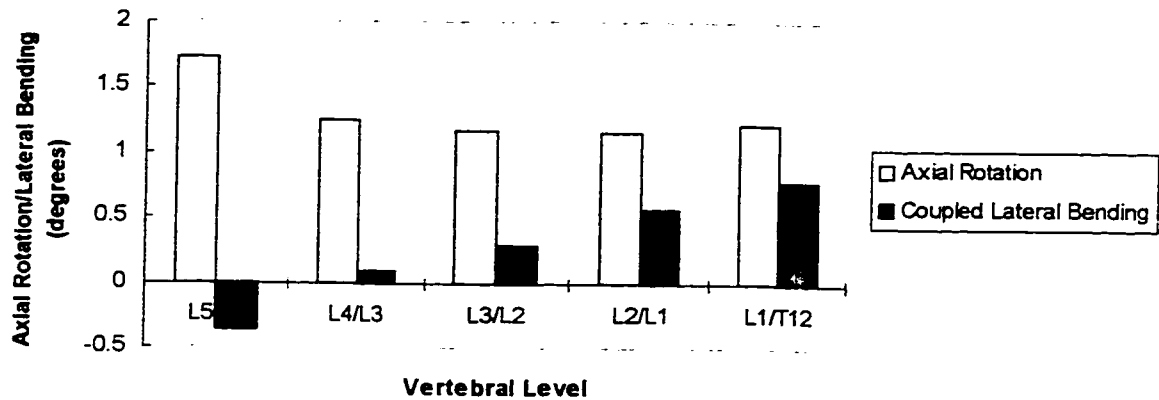


Figure 9-15. Axial rotation accompanied by coupled lateral bending in the lumbar spinal units as a result of an applied 5 Nm moment. Note that positive values signify axial rotation causing the superior vertebra's spinous process to turn in towards the right, and lateral bending where the superior vertebra also bends towards the right.

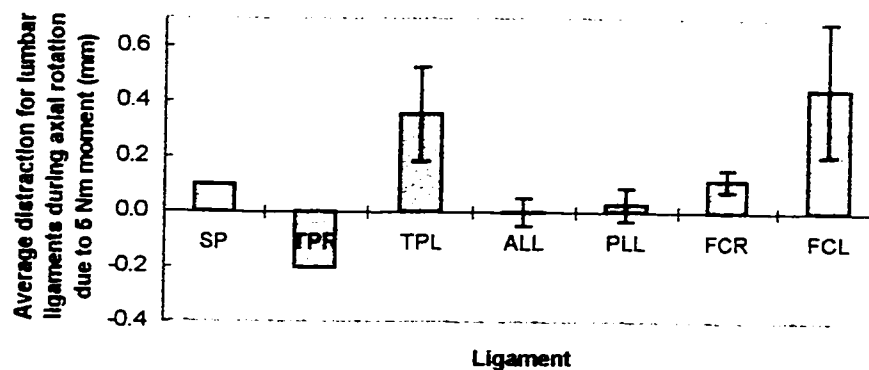


Figure 9-16. The average distraction in lumbar ligaments during axial rotation due to an applied moment of 5 Nm. SP - inter/supraspinous ligament. TPR - right intertransverse ligament, TPL - left intertransverse ligament, ALL - anterior longitudinal ligament, PLL - posterior longitudinal ligament, FR - right facet capsule, FL - left facet capsule. Standard deviation of +/- one standard deviation is shown for each ligament.

9.7 THORACIC SPINAL UNITS

The thoracic functional units, like those of the lumbar region, possess bilinear ligament and disc structures. The thoracic units were tested in flexion, extension, lateral bending and axial rotation. As with the lumbar units, each test consisted of fully constraining the inferior endplate of the inferior vertebra, while a moment was applied to vertebral body of the superior vertebra. Nodal displacements were then used at the end of each converged run to determine the degrees of flexion, extension, bending, or rotation.

9.8 THORACIC FLEXION

In flexion, each thoracic spinal unit produced nodal displacements within, or parallel to, the mid transverse plane of the superior vertebra. No lateral displacements were noted. Thoracic flexion stiffness values range from 1.68 Nm/degree to 2.63 Nm/degree. The overall averaged flexion stiffness value for the thoracic units from T12/T11 to T2/T1, is 2.1 Nm/degree, with a population standard deviation of 0.39 Nm/degree. A sample of the load displacement result for a typical thoracic spinal unit is shown in Figure 9-17. Note the comparatively higher degree of flexion occurring during the initial phase of loading as a result of using the bilinear ligament and disc structures. The model's average thoracic flexion stiffness, in comparison to other studies, is shown in Figure 9-18. Figure 9-19 shows a typical pre-loaded (dotted outline) and post-loaded (solid entity) thoracic functional unit in flexion.

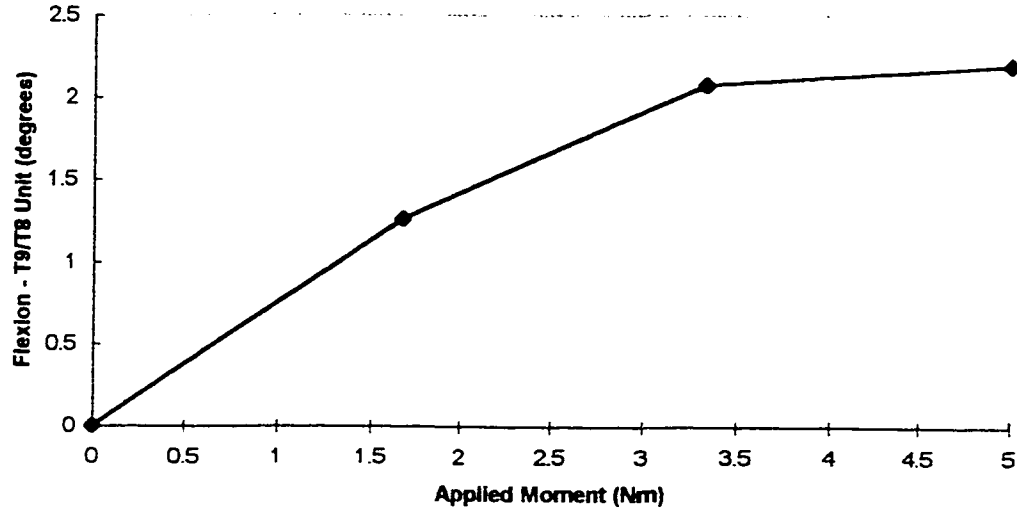


Figure 9-17. Load displacement result for a T9/T8 thoracic spinal unit in flexion with data taken at 3 load levels.

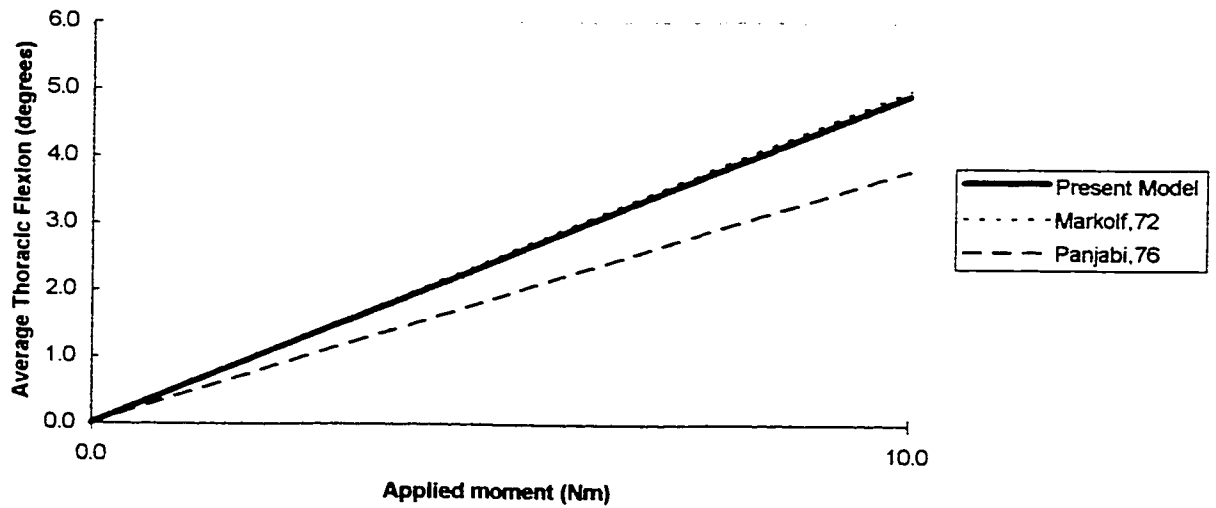


Figure 9-18. A stiffness comparison of thoracic functional units in the model to other studies. The model's averaged thoracic flexion result is shown as the thicker line.

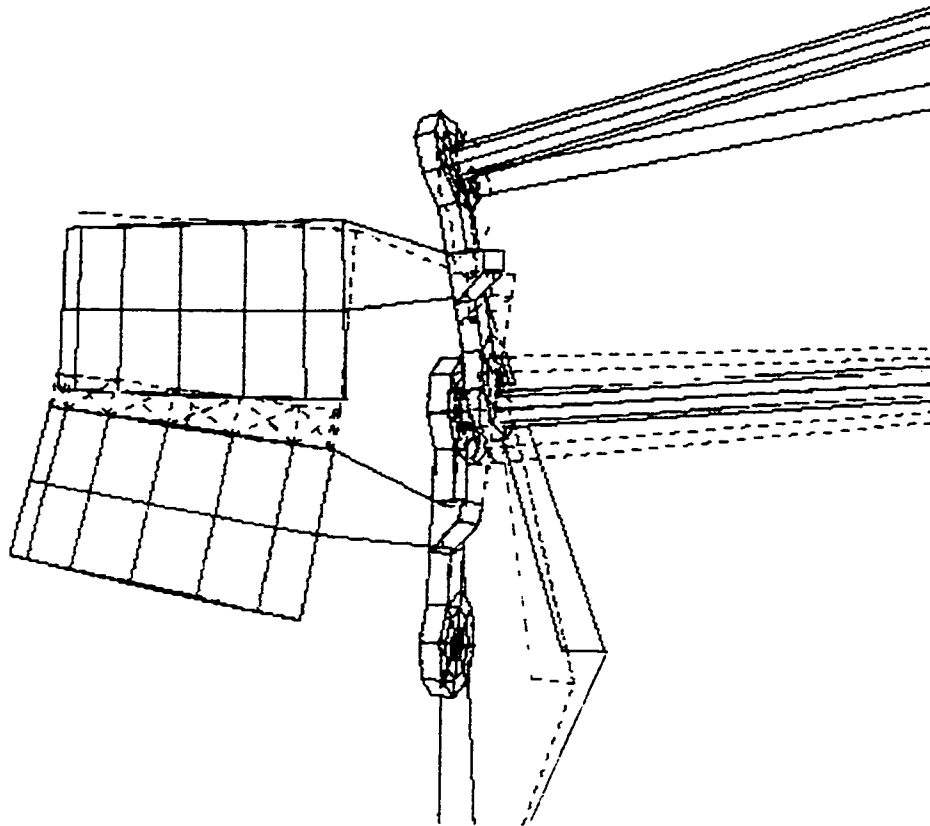


Figure 9-19. A thoracic functional unit in flexion. The dotted outline represents the pre-loaded state, while the solid entity depicts the post-loaded position.

Deformation of the thoracic ligaments during flexion are shown in Figure 9-20. The bar graph represents the average amount of distraction in thoracic ligaments in the post loaded equilibrium position during flexion due to a 10 Nm applied moment. Standard deviation ranges of +/- one standard deviation are provided for each ligament. Negative distraction signifies an unloaded ligament. From the graph, it can be seen that the ligaments furthest from the vertebral body especially the interspinous ligament, undergo more deformation.

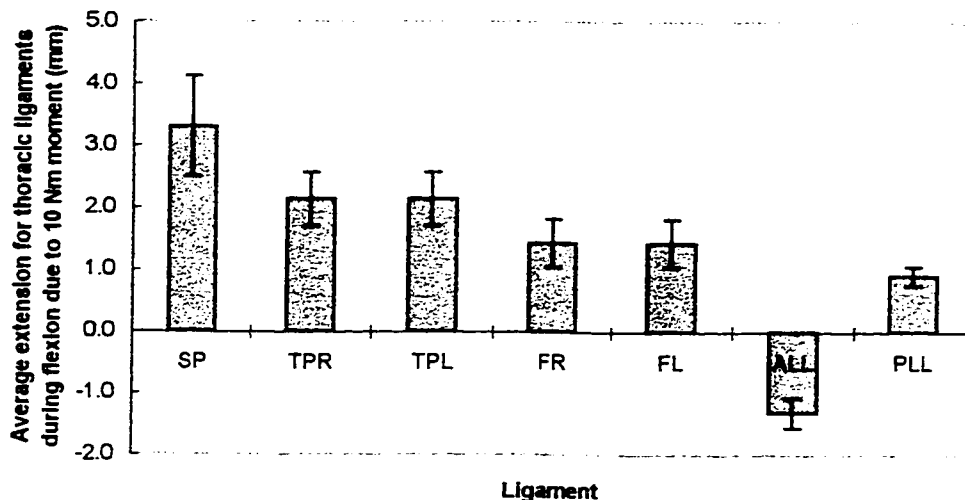


Figure 9-20. The average extension in some thoracic ligaments during flexion due to an applied moment of 10 Nm. SP - inter/supraspinous ligament. TPR - right intertransverse ligament. TPL - left intertransverse ligament. ALL - anterior longitudinal ligament. PLL - posterior longitudinal ligament. FR - right facet capsule. FL - left facet capsule. Note only the ALL was unloaded during flexion. Standard deviation range of +/- one standard deviation is shown for each ligament.

9.9 THORACIC EXTENSION

As with the flexion tests, extension movements produced no lateral displacements within the post loaded superior vertebra in each thoracic unit. Extension stiffness values for functional units in the thoracic region range from 1.29 Nm/degree to 2.07 Nm/degree. The average thoracic unit stiffness in extension is 1.59 Nm/degree with a population standard deviation of 0.30 Nm/degree. Figure 9-21 depicts a load displacement sample for a typical thoracic spinal unit. Again, movement decreases with

loading due to the presence of the bilinear elements. An average extension stiffness comparison of the thoracic units in the model vs. literature results is shown in Figure 9-22. Figure 9-23 shows a typical thoracic functional unit undergoing extension, induced by a 5 Nm moment applied to the superior vertebra of the spinal unit.

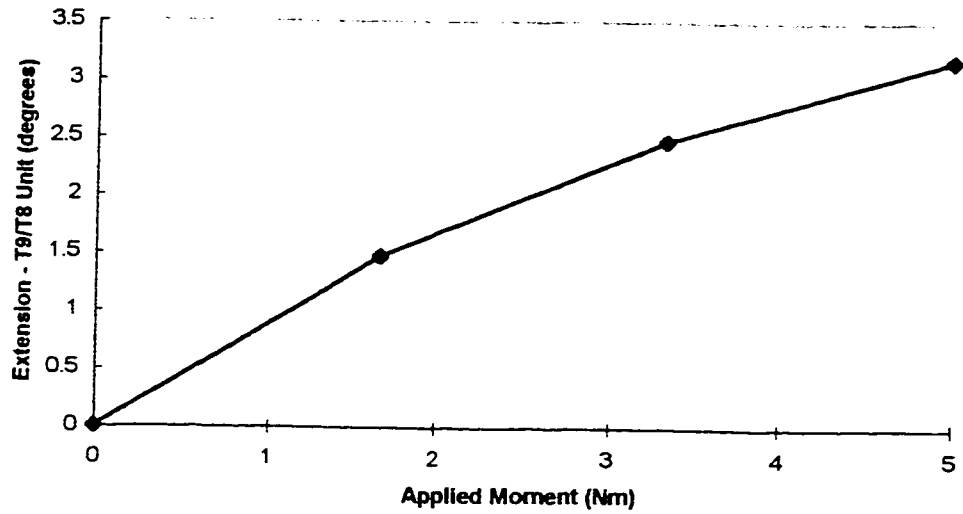


Figure 9-21. Load displacement result for a T9/T8 thoracic spinal unit in extension with data taken at 3 load levels.

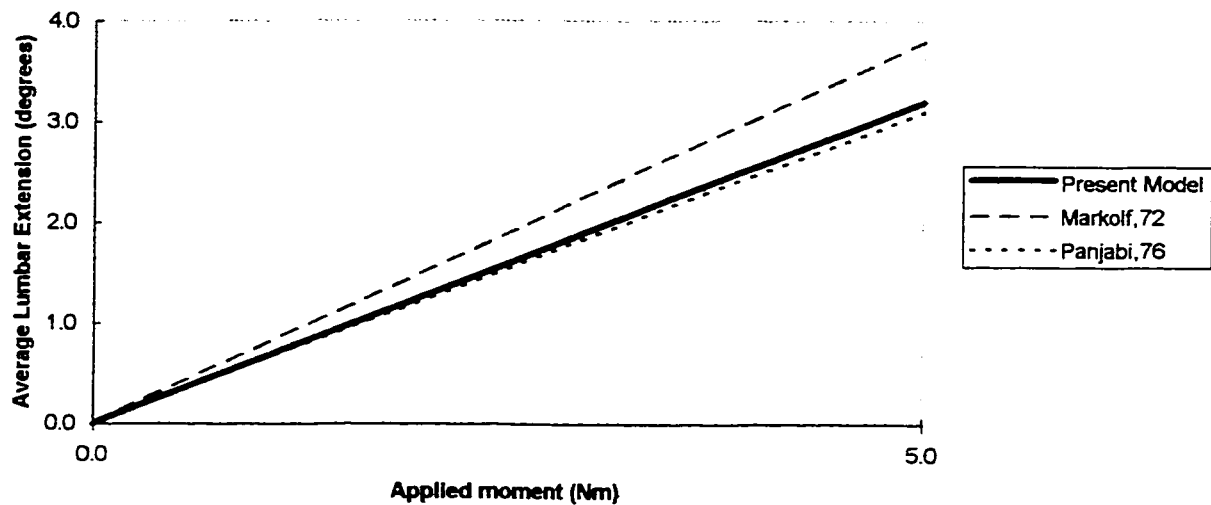


Figure 9-22. Extension comparison of thoracic functional units in the model to other studies.

The model's averaged extension results are shown as the thicker line.

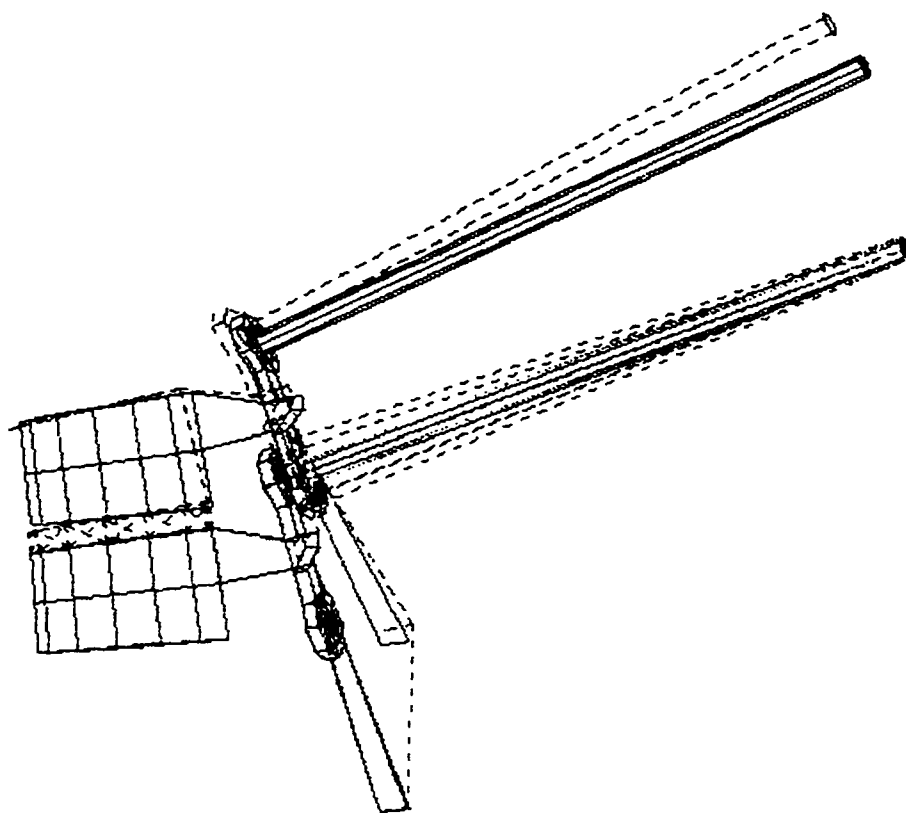


Figure 9-23. A thoracic functional unit in extension. The dotted outline represents the pre-loaded state, while the solid entity depicts the post-loaded position.

The average thoracic ligament deformation during extension as a result of a 5 Nm moment are shown in Figure 9-24. The anterior longitudinal ligament and facet capsules were the only ligament structures within the post loaded thoracic spinal units sustaining a tensile load. In the case of extension, the left and right facet capsular distraction was primarily due to a sliding of mating facet surfaces over one another, and not a separation between facets.

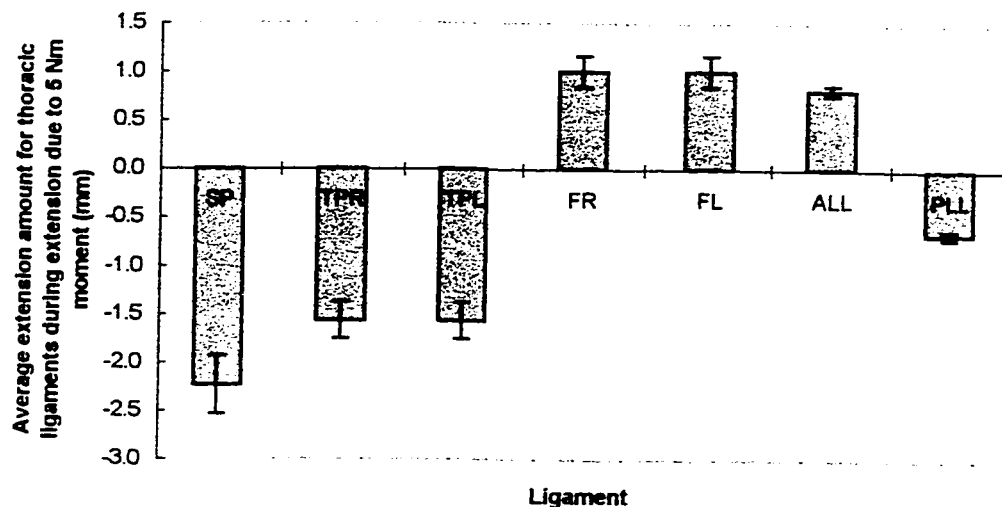


Figure 9-24. The average extension in thoracic ligaments during extension due to an applied moment of 5 Nm. SP - inter/supraspinous ligament. TPR - right intertransverse ligament. TPL - left intertransverse ligament. ALL - anterior longitudinal ligament. PLL - posterior longitudinal ligament. FR - right facet capsule. FL - left facet capsule. Standard deviation range of +/- one standard deviation is shown for each ligament.

9.10 LATERAL BENDING IN THE THORACIC REGION

In lateral bending, the thoracic spinal unit stiffness values range from 1.56 Nm/degree to 2.02 Nm/degree with an average of 1.74 Nm/degree. The population standard deviation is 0.16 Nm/degree. Overall, the bending stiffness decreases from the lower to the upper thoracic region. The lower initial stiffness during motion is apparent in Figure 9-25 which depicts the load-displacement result for the T9/T8 functional unit in lateral bending. Comparison of the average lateral bending stiffness for the modeled thoracic units vs. literature results are shown in Figure 9-26. Figure 9-27 depicts a pre-

loaded and post-loaded lumbar functional unit as seen from the posterior aspect. From this figure, the orientation, and relative sliding motion of the thoracic facets during lateral bending, can be seen.

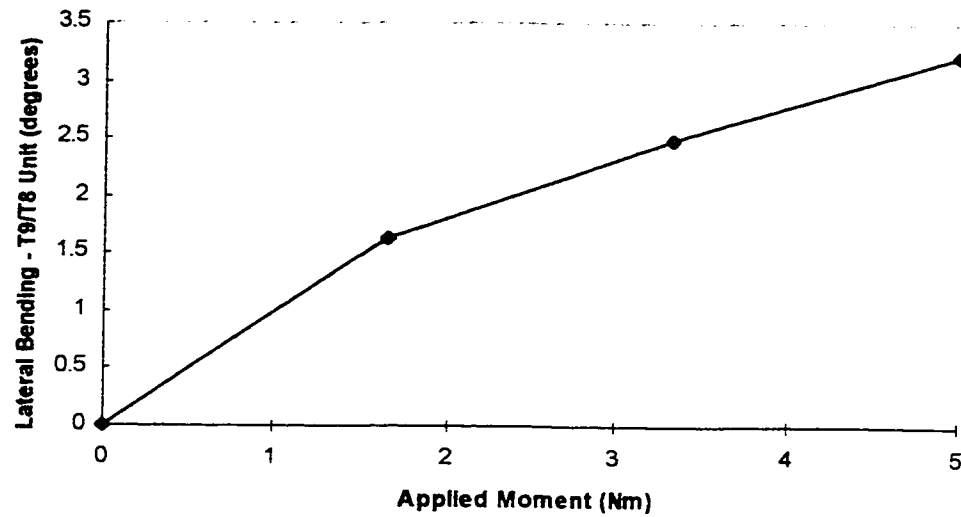


Figure 9-25. Load displacement result for a T9/T8 thoracic spinal unit in lateral bending with data taken at 3 load levels.

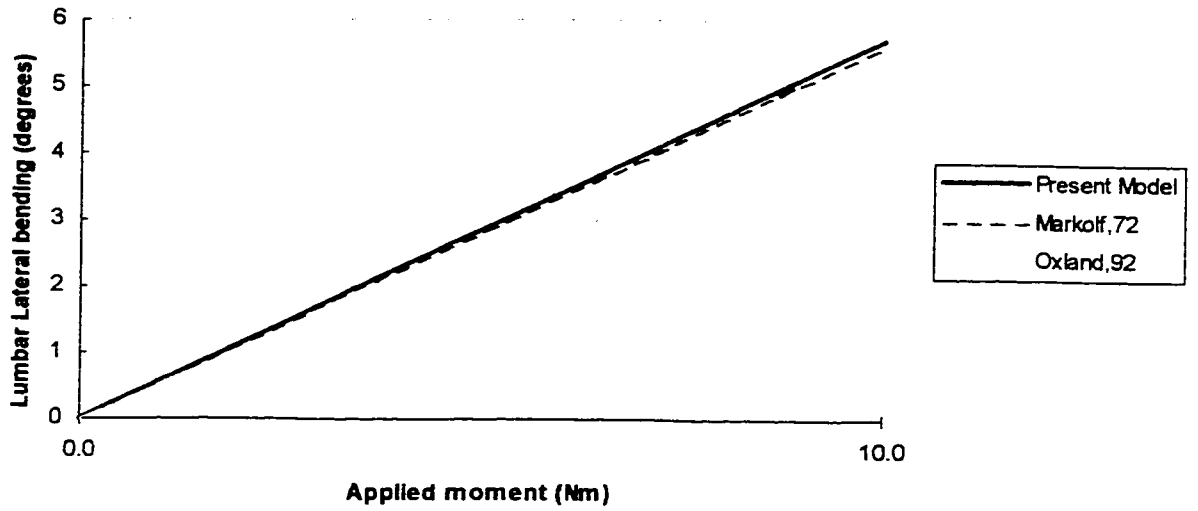


Figure 9-26. Lateral bending of the modeled thoracic functional units compared to other studies. The model's averaged results are shown as the thicker line.

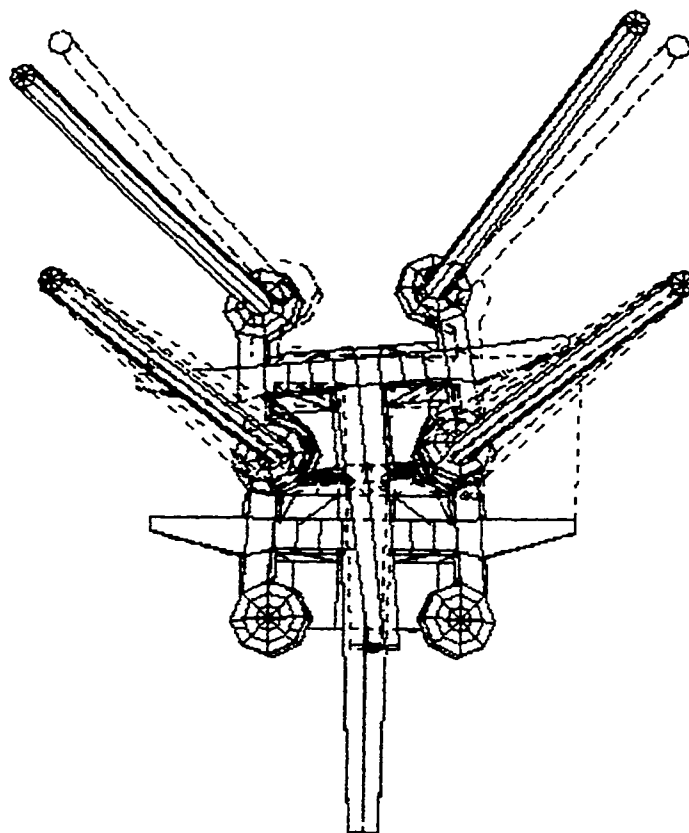


Figure 9-27. Lateral bending of a typical thoracic functional unit. Pre-loaded configuration is represented by dotted lines while the post-loaded equilibrium position is shown by the solid entities.

In contrast to the lumbar region, the thoracic spinal units have an induced lateral, instead of contralateral, axial rotation accompanying the primary lateral bending movement. With this rotation, as an example, a left lateral bending of the spine, as seen from the posterior aspect, causes the spinous processes to point posteriorly to the right. The coupling effect was greater near the lower thoracic spine, than at mid to upper regions. This coupled rotation, accompanying lateral bending is shown for selected lower and mid thoracic functional units in Figure 9-28. In this figure, a 10 Nm moment

was applied to induce lateral bending. The resultant lateral bending rotation is shown beside the accompanying axial rotation movement for the selected thoracic units. Note the greater degree of coupling effect in the lower thoracic units T12/T11, and T11/T10, for a given amount of lateral bending as compared to the mid-thoracic units from T7/T6 up to T5/T4.

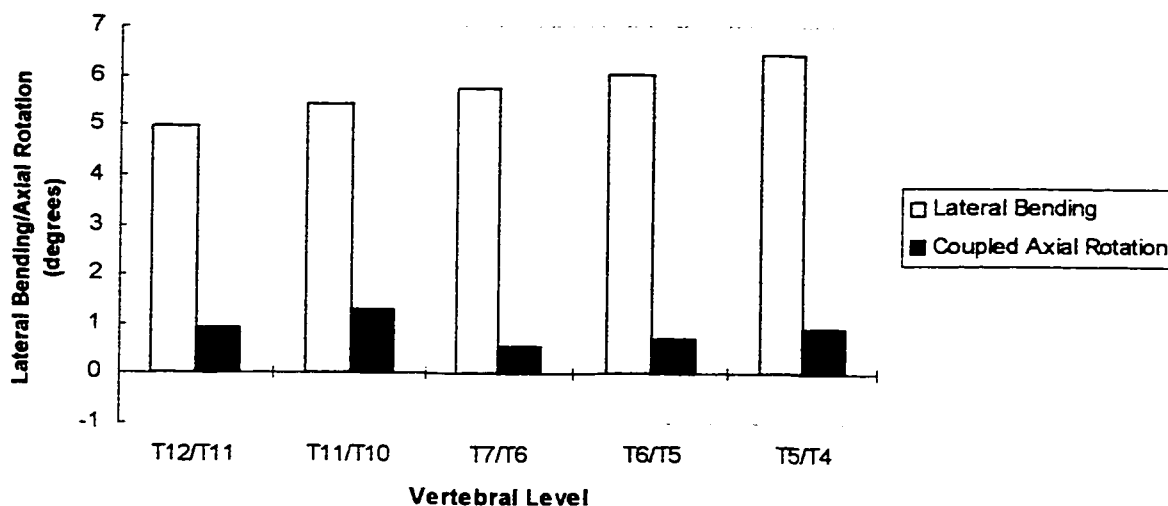


Figure 9-28. Lateral bending accompanied by coupled axial rotation in selected thoracic spinal units as a result of an applied 10 Nm moment.

Average values for ligament deformation for the thoracic functional units, as a result of lateral bending to the left induced by a 10 Nm moment, are shown in Figure 9.29. By using the information from Figure 9-29, and by looking at thoracic unit undergoing left lateral bending in Figure 9-27, it can be seen that the ligaments furthest from the mid-sagittal plane of the vertebrae undergo the greatest amount of deformation.

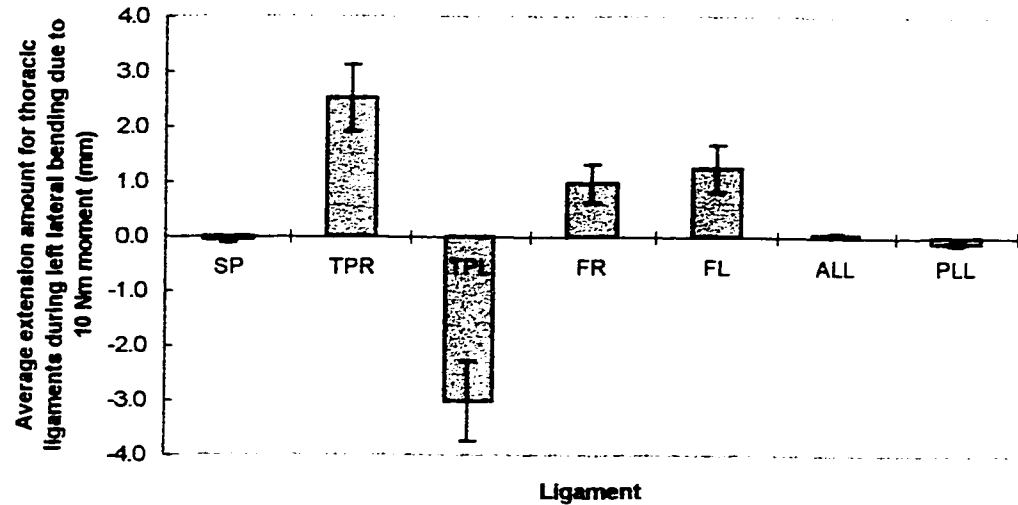


Figure 9-29. The average extension in thoracic ligaments during lateral bending due to an applied moment of 10 Nm. SP - inter/supraspinous ligament. TPR - right intertransverse ligament. TPL - left intertransverse ligament. ALL - anterior longitudinal ligament. PLL - posterior longitudinal ligament. FR - right facet capsule. FL - left facet capsule. Standard deviation range of +/- one standard deviation is shown for each ligament.

9.11 AXIAL ROTATION IN THE THORACIC REGION

As with the lumbar spine, axial rotation was measured within the transverse plane of the model. The axial rotational stiffness in the thoracic functional units range from 1.1 Nm/degree to 2.1 Nm/degree. The overall average axial stiffness was 1.7 Nm/degree, with a population standard deviation of 0.35 Nm/degree. In comparison, a study conducted by Panjabi (23, 24) documented thoracic axial rotational stiffness values in cadaver specimens ranging from 1.3 Nm/degree to 5.8 Nm/degree. This extremely wide range is attributed biological variations among the specimens. Panjabi's

study measured an average axial rotational stiffness of 1.9 Nm/degree in the mid-thoracic region. Another study conducted by Shultz (31) investigated the axial rotational stiffness for a T8-T9 functional unit. This unit subjected to moment loads of up to 5 Nm, responded with an average axial rotational stiffness of 1.8 Nm/deg. Figure 9-30 depicts a typical thoracic functional unit in the model undergoing axial rotation, while Figure 9-31 compares the model's average moment load-axial rotation behavior with literature results.

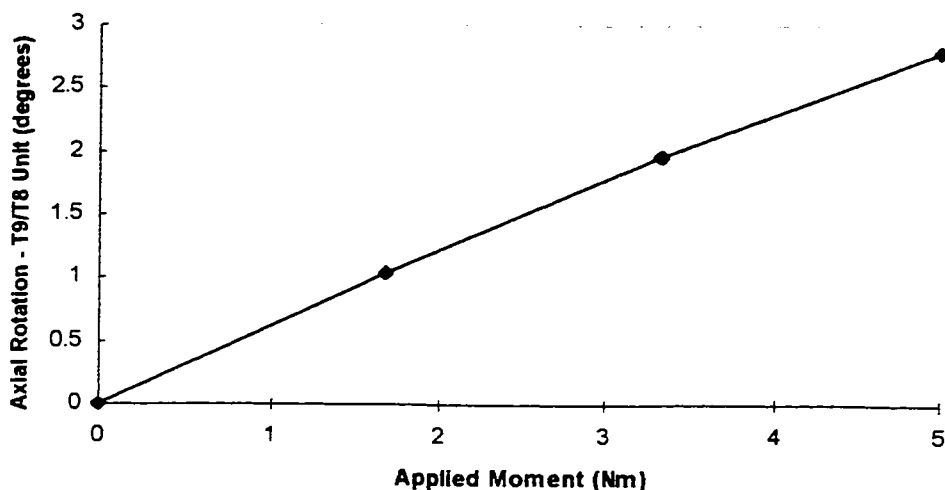


Figure 9-30. Axial rotation response of a thoracic functional unit subjected to moment loads.

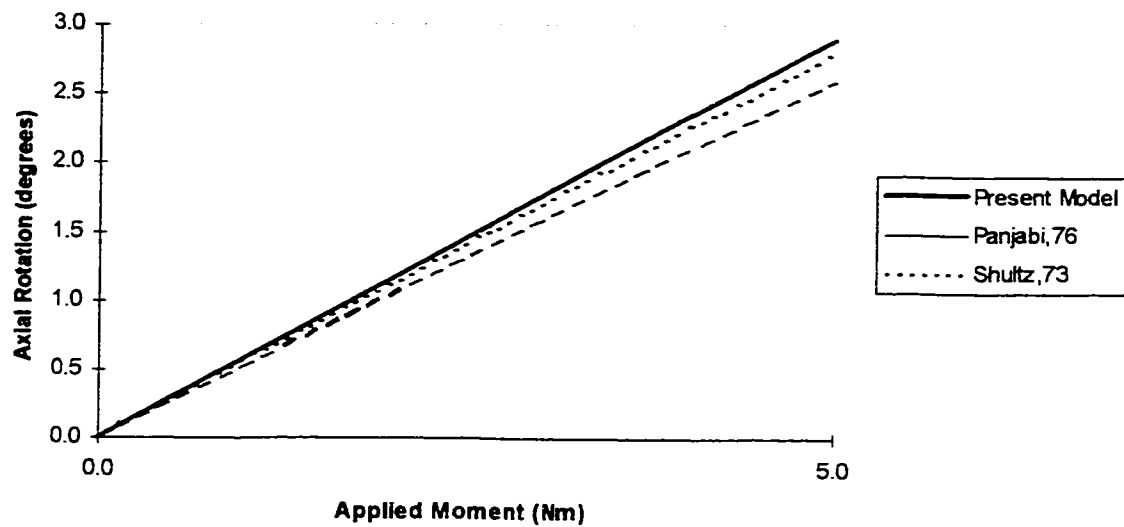


Figure 9-31. Average response of the thoracic functional units in axial rotation compared to other studies. The model is represented by the thicker line.

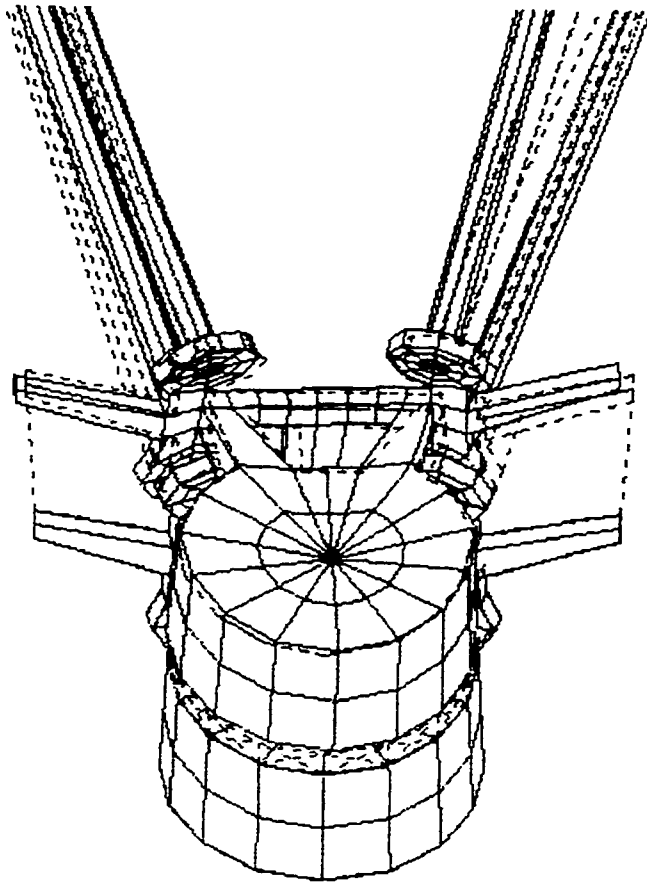


Figure 9-32. Axial rotation of a typical thoracic functional unit. Pre-loaded configuration is represented by dotted lines while the post-loaded equilibrium position is shown by the solid entities.

The effect of induced lateral bending due to thoracic axial rotation was investigated. In the lower thoracic spine from T12 to T8, rotational movements in functional units induced a bending response in the direction which the spinous processes point upon loading. For example, if axial rotation occurred such that the spinous process pointed posteriorly towards the right, the spinal unit would also bend towards the right. In contrast, a different coupling mechanism appeared in the mid and

upper thoracic spine, where axial rotations induced lateral bends in the direction opposite the spinous processes. Figure 9-33 compares the amount of lateral bending accompanying axial rotation in selected functional units in the thoracic spine. A positive bending values signifies coupling where the induced lateral bend, curves in the same direction as the spinous process. A negative bending values denote an opposite coupling reaction. Figure 9-34 shows the average amount of ligament distraction during axial rotation due to a 5 Nm moment. The amount of sliding occurring between thoracic facets during axial rotations is greater than lumbar facets. It is also apparent that the ligaments farther from the vertebral body undergo the greatest amount of stretching.

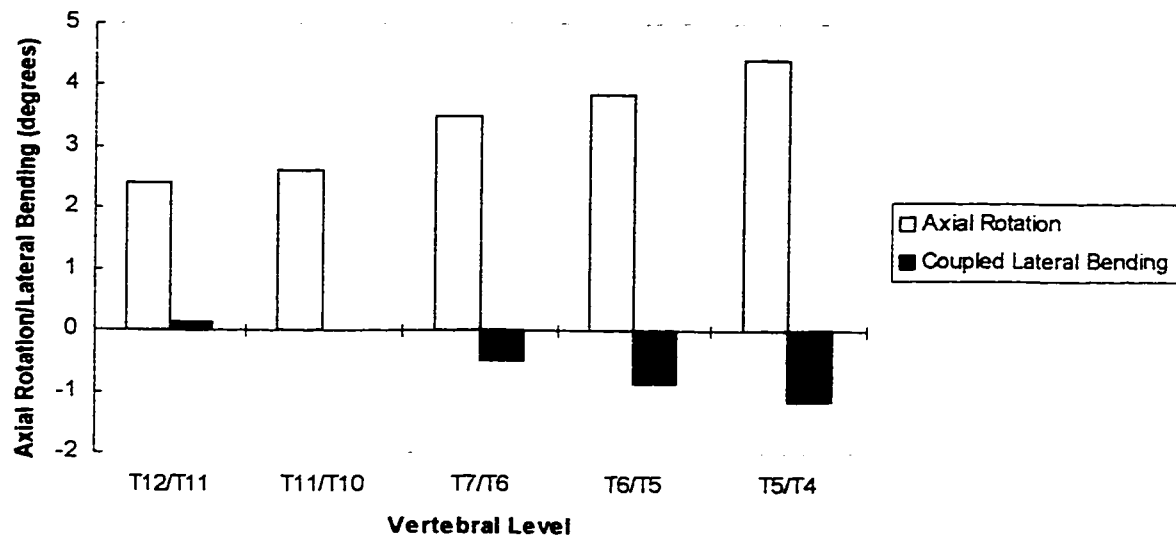


Figure 9-33. Axial rotation accompanied by coupled lateral bending in thoracic spinal units as a result of an applied 5 Nm moment.

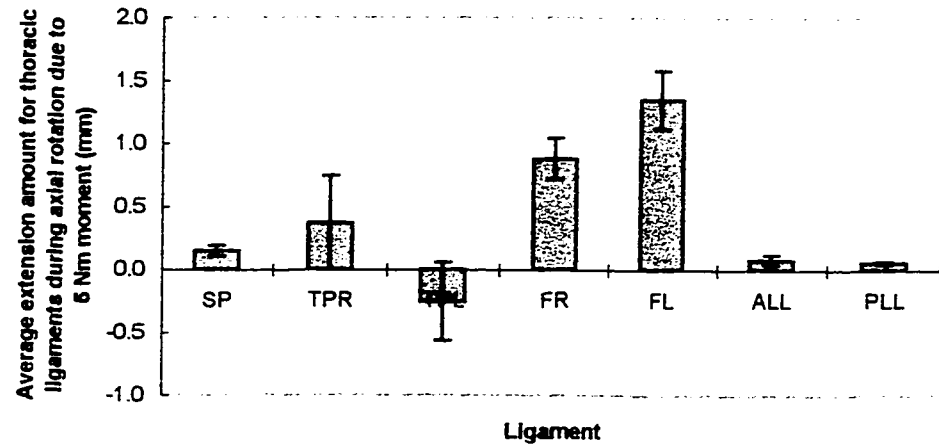


Figure 9-34. The average extension in thoracic ligaments during axial rotation due to an applied moment of 5 Nm. SP - inter/supraspinous ligament, TPR - right intertransverse ligament, TPL - left intertransverse ligament, ALL - anterior longitudinal ligament, PLL - posterior longitudinal ligament, FR - right facet capsule, FL - left facet capsule. Standard deviation range of +/- one standard deviation is shown for each ligament.

CHAPTER 10 - DISCUSSION OF RESULTS

In this thesis, a model of a “generic” thoracolumbar normal spine was created to simulate and predict the kinematic response of normal human spines. Using curve fitting techniques, the vertebrae morphology and ligament behaviors were established from empirical results taken from literature. The modeled intervertebral discs were constructed such that the gross overall behavior in axial compression/tension, flexion/extension, lateral bending, and axial rotation were in agreement with documented literature results. The mechanical response and behavior of the model is thus a product of geometric data and material properties based on empirical results. In no instance, were the mechanical properties of the model’s interconnecting spinal elements modified or altered to produce “correct” responses in functional units when subjected to known loads.

As seen previously, both lumbar and thoracic functional units in the model share stiffness values comparable to existing literature results in flexion, extension, lateral bending, and axial rotation movements. On account of the biological diversities present in the cadaver subjects and test specimens used in generating the data found in literature, the stiffness results themselves inherently contain a great deal of variation. Differences in an individuals’ spinal shape, size, structure, and composition are all contributing factors to the wide data ranges. Because of this, only averaged results

generated by the model's thoracic or lumbar functional units were compared with the literature results, rather than individual functional unit test results.

10.1 FLEXION OF LUMBAR AND THORACIC UNITS

In flexion, the thoracic functional units possess on average, 84% the flexion stiffness of the lumbar functional units. This can in part, be attributed to the lower ligament stiffness in the thoracic region, compared with the lumbar region. The posterior spinal ligaments, excluding the anterior and posterior longitudinal ligaments, interconnect the posterior elements of the spine. Resistance to flexion is partly due to the effectively positioned posterior ligaments, which as a result of insertion location, produce a considerable moment arm length. In Chapter 8, it was found that the tensile stiffness of all ligaments in the model, except the posterior longitudinal ligament, decreased from the lower lumbar to the upper thoracic region. The thoracic ligaments are all in all less stiff than their lumbar counterparts. This lower stiffness can be observed as increased ligament stretching in a thoracic functional unit, when compared with a lumbar unit, subjected under the same flexion loading. For instance, the average thoracic supraspinous ligament in the model elongates 10% more than the average lumbar supraspinous ligament in a functional unit subjected to an applied flexion moment 10 Nm.

10.2 EXTENSION OF LUMBAR AND THORACIC UNITS

In extension, the stiffness of the thoracic functional units was less than the lumbar units. The thoracic units possess on average, 80% the extension stiffness of lumbar units. In a spinal unit subjected to extension, the only ligaments experiencing any load were the anterior longitudinal ligament and the facet capsules. In both thoracic and lumbar facets, the ligament suspension tree structures prevented the facet surfaces from passing through one another, and instead, allowed the surfaces to “slide”. Excessive sliding of the facet surfaces were, in part, controlled by the surrounding facet capsular ligaments. The thoracic capsular ligaments extend, on average, 12% more than the lumbar capsular ligaments when subjected to a moment load of 5 Nm. Sliding between mating facet surfaces during extension is also approximately 12% more in thoracic functional units, and is partly due to the difference in facet surface orientation between thoracic and lumbar vertebrae. The remaining ligament placed in tension during extension was the anterior longitudinal ligament, which elongated approximately 5% more in thoracic functional units compared with lumbar units when subjected to moment loads of up to 5 Nm. Correspondingly, the most anterior region of the average thoracic intervertebral disc elongated 5% more than the average lumbar disc. The extreme posterior region of the intervertebral disc, lining the spinal canal in the typical thoracic unit, shortened on average, 6.5% more than the average lumbar unit undergoing a 5 Nm load.

10.3 LATERAL BENDING OF LUMBAR AND THORACIC UNITS

The lateral bending stiffness of the thoracic functional units are lower than that of lumbar functional units by approximately 80% on average. This stiffness difference between thoracic and lumbar units is reflected in the amount of facet capsular ligament elongation, where the average facet capsular distraction in a thoracic unit is 46% more than in a lumbar unit. Both left and right facet capsules in the thoracic and lumbar units stretch upon applied loading. The difference in the capsular elongation can be related to orientation dissimilarity between thoracic and lumbar facet surfaces. In the thoracic spine, the normal to facet surfaces point in either the anterior or posterior direction of the vertebra, almost parallel to the frontal plane. This orientation lends itself to the sliding of facet surfaces over one another in lateral bending. In contrast, the facet surface normals in a lumbar vertebra, which face one another in the sagittal plane, restrict movement in the lateral direction between adjacent posterior elements. During lateral bending, the ligaments close to the mid-sagittal plane of the vertebra changed very little from the pre-loaded to post loaded configuration in each spinal unit. In both thoracic and lumbar units, the anterior longitudinal ligament, posterior longitudinal ligament, and inter/supraspinous ligament exhibited little deformation.

The axial rotation induced by the coupling effect during lateral bending varied from the lumbar to thoracic region of the model. As mentioned previously, a contralateral rotation which denotes an axial rotation of the vertebra, opposite to the direction of bending, occurred in the mid to upper lumbar functional units during lateral

bending. In contrast, the thoracic region displayed an opposite behavior where the vertebra would axially rotate in the direction of bending (i.e. spinous processes rotate and point opposite the bending direction). This change in rotation direction occurred abruptly at the thoracolumbar junction, where an abrupt change in facet orientation took place. When looking at the morphology of vertebral components other than the facet surfaces, only “smooth geometrical transition” exist when moving from the lumbar to thoracic spine. For example, the vertebral bodies of the spine gradually decreased in size when moving from the lumbar to thoracic region. Likewise, the transverse process length also gradually change in length from the lumbar to thoracic spine. The only abrupt geometric change occurs at the thoracolumbar junction and pertains to the facet geometry and surface orientations. This suggests that the contrast in coupling behavior between the thoracic and lumbar regions is due to a difference in morphology of the facet surfaces, rather than the other remaining vertebral structures. Once more, the orientation of thoracic facet surfaces do not inhibit the sliding of facet surfaces over one another in lateral bending, whereas the facet surfaces in lumbar vertebrae confine movement in lateral directions between adjacent posterior vertebral elements.

10.4 AXIAL ROTATION OF LUMBAR AND THORACIC UNITS

The axial rotational stiffness of a thoracic functional unit is on average, 57% less stiff than a lumbar unit. This difference is primarily due to the contrast in facet morphology between thoracic and lumbar facets. Lumbar facets, as mentioned

previously in Chapter 6, are oriented almost parallel to the mid-sagittal plane of the spine. This orientation considerably restricts rotational movements between lumbar vertebrae in comparison to thoracic vertebrae. In both regions, the ligaments furthest from the mid-sagittal plane of the spine had the greatest amounts of deformation during axial rotation. Ligaments closest to the vertebral bodies, namely the anterior longitudinal and posterior longitudinal ligaments, underwent little deformation.

At each spinal level, the coupling of effect of axial rotation and induced lateral bending was investigated. Within the lumbar and lower thoracic region (with the exception of L5/L4), a lateral bending response in the direction opposite to the rotation was noted. If for example, the vertebrae rotate towards the left (spinous processes point to the right), the spine would then bend in response to the rotation, towards the right. The opposite pattern was observed in the mid and upper thoracic region. As mentioned in the previous section, the change in coupling behavior between the upper and lower spine coincides with a change in facet orientation between the lumbar and thoracic vertebrae. White and Panjabi (39) mentioned that the coupling effect between vertebrae could easily be affected by spinal posture. When looking at the normal spine model in the sagittal plane, the lordosis curvature in the lumbar region “encourages” contact between adjacent facet surfaces. This lordosis curvature is somewhat similar to a spine in full extension, where facet surfaces come into contact with one another. In contrast, the thoracic kyphosis curvature is somewhat similar to a spine in flexion where mating facet surfaces separate, as the spine bend towards the anterior aspect of

the body. The association of contacting facets in an extended spine (similar to the lumbar lordosis curvature) and non-contacting facets in a flexed spine (similar to the thoracic kyphosis curvature), possibly suggests, and reinforces the inference that the observed coupling response in the normal human spine is related to the facet joint geometry and orientation.

CHAPTER 11 - FUTURE WORK AND CONCLUSIONS

11.1 FUTURE WORK

The thoracolumbar spine model can be described as a compilation of three main components, the vertebral bodies, the interconnecting spinal ligaments, and the intervertebral discs. When the spine moves, deformation in the ligaments and disc are considerably greater than the comparatively rigid vertebrae. The mechanical properties of the interconnecting disc and ligaments thus contribute extensively to the overall behavior of the spine. The usage of bi-linear spring elements in the intervertebral disc structures and ligaments allows for accurate modeling of spinal behavior during normal ranges of motion, but yield inaccurate responses during higher displacements. For example, the existing spring elements representing the ligaments are incapable of modeling the traumatic phase of deformation. In this phase, ligament stiffness increases significantly over a short range until a peak is reached, at which point failure begins. Future applications of the model to these higher loading situations warrant the usage of non-linear elements. It is a general consensus that more accurate data and information is presently required pertaining to the geometry, morphology, and especially, the mechanical properties of physiological spinal structures. This limitation is the principal constraint for a more accurate and versatile model of the spine.

For validation purposes, the response of each modeled functional unit was tested against literature results. The validation would have been extended to partial or whole spinal segments, but the present scarcity of empirical information regarding

gross displacements of whole spinal sections prevent this. This lack of empirical information could be possibly due to experimental obstacles in testing human spines without ribs, intercostal membranes, muscles, or other physiological structures influencing the behavior of the spine. The spinal column by itself is considerably less stable when separated from its surrounding physiological structures. An example of this could be an excised spine's susceptibility to buckling when subjected to compressive loading. Further experimental testing on whole spines, and not just individual functional units, is therefore required for comparison purposes and further validation of the model. Eventually, a validation of the whole spinal model would be performed through a comparison of displacement results with *in vivo* spines. This type of testing would call for the development of appropriate modeling constraints to simulate the live physiological structures surrounding the spine.

This thesis lays the groundwork for the development of a scoliotic model of the human spine. In order to have a model capable of simulating the mechanics involved with spinal fixation, an understanding of the relationship between the morphology and mechanical properties of the scoliotic spine, in comparison to normal spine, must first be established. As of now, the majority of literature results regarding spine mechanics deal only with the normal spine configuration. Eventually, this pool of literature will expand to cover the scoliotic spine, providing the necessary data from which a scoliotic spine model could be built upon.

Data required to build a model capable of simulating the mechanics involved with scoliotic corrective surgery would include:

- Information describing the overall three-dimensional shape of the scoliotic spine.
- Quantitative data describing the geometry of individual scoliotic vertebrae. Some key parameters required, with respect to the scoliotic vertebral bodies, include the vertebral body height, width, depth, and wedge angle (in both the lateral and anterior-posterior plane). The geometric parameters needed for the posterior elements would include pedicle length and orientation, spinous and transverse process length and orientation, and facet surface geometry and orientation.
- Data describing the scoliotic ribs and rib cage. This would include information describing the morphology and mechanical properties of the ribs, sternum, and rib articulation joints and ligaments.
- A method of modeling the spinal instrumentation and the mechanics of the interface between the instrumentation and the scoliotic spine.

11.2 CONCLUSION

In this thesis, a mechanical model of the thoracolumbar spine was created. The model was constructed using geometric and morphologic data compiled from various sources in literature. Each functional unit in the model was validated through comparisons with existing studies conducted on excised spinal units. With this thesis, a few conclusions can be drawn:

- The implementation of bi-linear stiffness properties for the interconnecting spinal elements is necessary to produce functional unit loading responses consistent with literature results. The use of uni-linear stiffness properties taken from the elastic midrange of load-displacement curves produce excessively stiff functional units.
- The design and use of the facet “suspension tree” system for modeling articular facet surface to surface contact, provides an alternative to using computationally intensive contact elements.
- The validity of the model is maintained as long as interconnecting spinal structures undergo deformation amounts within normal ranges of motion.
- In most lumbar functional units, lateral bending gives rise to a coupling effect which produces axial rotation of the vertebrae in the contra-lateral direction. An opposite coupling effect is noted in the majority of the thoracic spine where lateral bending induces an axial rotation in the lateral

direction. This behavior is possibly linked with the difference in facet orientation between lumbar and thoracic vertebrae.

- The orientation of the facet surfaces in the thoracic spine allows for more axial rotation to occur when compared with the lumbar spine.
- Generally, ligaments furthest from the vertebrae bodies, undergo the greatest amount of distraction during spinal movements.

References

1. *ANSYS User's Manual - ANSYS Revision 5.2*. SAS IP, USA, 1995
2. Benzel E.C. *Biomechanics of Spine Stabilization*. McGraw-Hill, USA, 1995
3. Berry J., Moran J.M., Berg W.S., Steffee A.D. A Morphometric Study of Human Lumbar and Selected Thoracic Vertebrae. *Spine* Vol 12, No 4, pg 362, 1987
4. Chazal J., Tanguy A., Bourges M., Gaurel G., Escande G., Guillot M., and Vanneuville G. Biomechanical Properties of Spinal Ligaments and a Histological Study of the Supraspinous Ligament in Traction. *J. Biomechanics* Vol 18, No 3, pg 167-76, 1985
5. Describes JL., Aubin CE., Boudreault F., Skalli W., Zeller R., Dansereau J., Lavaste F. Modeling of Facet Joints in a Global Finite Element Model of the Spine: Mechanical Aspects. Correspondence, Ecole Polytechnique, Quebec, Canada
6. Dumas G.A., Beaudoin L., Drouin G., In Situ Mechanical Behavior of Posterior Spinal Ligaments in the Lumbar Region. An In Vitro Study. *J. Biomechanics* Vol 20, No 3, pg 301-10, 1987
7. Dumas G.A. Some Geometric Parameters of Spinal Facets. *Personal communication* Queen's University
8. Farfan H.F., Cossette J.W., Robertson G.H., Wells R.V., Kraus H. The Effects of Torsion on the Lumbar Intervertebral Joints: The Role of Torsion in the Production of Disc Degeneration. *J. Bone and Joint Surgery* Vol 52A, pg 468, 1970

9. Goel V.K., Kong W., Han J.S., Weinstein J.N., Gilbertson L.G. A Combined Finite Element and Optimization Investigation of Lumbar Spine Mechanics With and Without Muscles. *Spine* Vol 18, No 11, pg 1531-41, 1993
10. Goel V.K., Monroe B.T., Gilbertson L.G., Brinckmann P., Nat R. Interlaminar Shear Stresses and Laminae Separation in a Disc - Finite Element Analysis of the L3-L4 Motion Segment Subjected to Axial Compression. *Spine* Vol 20, No 6, pg 689-98, 1995
11. Kapandji I.A. *The Physiology of the Joints, Vol.3 - The Trunk and the Vertebral Column*. Churchill Livingstone, USA, 1974
12. Keim H *The Adolescent Spine*. Grune & Stratton Inc., USA, 1976
13. Kulak R.F., Schultz A.B., Belytschoko T., Galante J. Biomechanical Characteristics of Vertebral Motion Segments and Intervertebral Discs. *Orthopedic Clinics of North America* Vol 6, No 1, 1975
14. Lavaste F., Skalli W., Robin S., Roy-Camille R., Mazel C. Three-Dimensional Geometric and Mechanical Modeling of the Lumbar Spine. *J. Biomechanics* Vol 25, No 10, pg 1153-64, 1992
15. Lee M., Kelly D.W., Steven G.P. A Model of Spine, Ribcage, Pelvic Responses to a Specific Lumbar Manipulative Force in Relaxed Subjects. *J. Biomechanics* Vol 28, No 11, pg 1403-08, 1995
16. Markolf K.L. *Stiffness and Dampening Characteristics of the Thoracic-Lumbar Spine*. Proceedings of Workshop on Bioengineering Approaches to the Problems of the Spine, NIH, 1970

17. Markolf K.L. Deformation of the Thoracolumbar Intervertebral Joint in Response to External Loads: A Biomechanical Study using Autopsy Material. *J. Bone and Joint Surgery* Vol 54A, pg 675, 1972
18. Miller J.A.A., Shultz A.B., Warwick D.N., Spencer D.L., Mechanical Properties of Lumbar Spine Motion Segments under Large Loads. *J. Biomechanics* Vol 19, No 1, pg 79-84, 1986
19. Moore K.L. *Clinically Oriented Anatomy, 3rd Edition*. Williams & Wilkins, USA, 1992
20. Myklebust J.B., Pintar F., Yoganandan N., Cusick J.F., Maiman D., Myers M., and Sances A. Tensile Strength of Spinal Ligaments. *Spine* Vol 13, No 5, 1988
21. Netter F.H. *Atlas of Human Anatomy*. CIBA-GEIGY, USA, 1989
22. Oxland T.R., Lin R.M., Panjabi M.M. Three-Dimensional Properties of the Thoracolumbar Junction. *J. of Orthopaedic Research* Vol 10, No 4, pg 573-80, 1992
23. Panjabi M.M., Brand R.A., White A.A. Mechanical Properties of the Human Thoracic Spine as shown by Three-Dimensional Load-Displacement Curves. *J. Bone and Joint Surgery* Vol 58A, pg 642, 1976
24. Panjabi M.M., Brand R.A., White A.A. Three-Dimensional Flexibility and Stiffness Properties of the Human Thoracic Spine. *J. Biomechanics* Vol 9, pg 185-92, 1976
25. Panjabi M.M., Takata K., Goel V.J., Federico D., Oxland T., Duranceau J., Krag M. Thoracic Human Vertebrae - Quantitative Three-Dimensional Anatomy *Spine* Vol 16, No 8, pg 888, 1991

26. Panjabi M.M., Goel V.J., Oxland T., Takata K., Duranceau J., Krag M., Price M. Human Lumbar Vertebrae - Quantitative Three-Dimensional Anatomy *Spine* Vol 17, No 3, pg 298, 1992
27. Panjabi M.M., Oxland T., Takata K., Goel V.J., Duranceau J., Krag M. Articular Facets of the Human Spine - Quantitative Three-Dimensional Anatomy *Spine* Vol 18, No 10, pg 1298-1310, 1993
28. Panjabi M.M., Oxland T.R., Yamamoto I., Crisco J.J. Mechanical Behavior of the Human Lumbar and Lumbosacral Spine as shown by Three-Dimensional Load-Displacement Curves. *J. Bone and Joint Surgery* Vol 76A, pg 413, 1994
29. Pintar F.A., Yoganandan N., Myers T., Elhagediab A., and Sances A. Biomechanical Properties of Human Lumbar Spine Ligaments. *J. Biomechanics* Vol 25, No 11, pg 1351-56, 1992
30. Roberts S.B., Chan P.H. Elastostatic Analysis of the Human Thoracic Skeleton. *J. Biomechanics* Vol 3, pg 527-45, 1970
31. Schultz A.B., Belytschko T.B., Andriacchi T.P., Galante J.O. Analog Studies of Forces in the Human Spine: Mechanical Properties and Motion Segment Behavior. *J. Biomechanics* Vol 6, pg 373-83, 1973
32. Schultz A.B., Mechanics of the Human Spine, *Applied Mechanics Review* Vol 27, pg 1487-97, 1974
33. Schultz A.B., Warwick D.N., Berkson M.H., Nachemson A.L. Mechanical Properties of Human Lumbar Spine Motion Segments - Part 1: Response in

- Flexion, Extension, Lateral Bending, and Torsion. *J. of Biomechanical Engineering* Vol 101, pg 46-52, 1979
34. Scoles P.V., Linton A.E., Latimer B., Levy M., Digiovanni B.F. Vertebral Body Posterior Element Morphology: The Normal Spine in Middle Life. *Spine* Vol 13, No 10, 1988
35. Suwito W., Keller T.S., Basu P.K., Weisberger A.M., Strauss A.M., Spengler D.M. Geometric and Material Property Study of the Human Lumbar Spine Using the Finite Element Method. *J. Spinal Disorders* Vol 5, No 1, pg 50-59, 1992
36. *Taber's Cyclopedic Medical Dictionary - 17th Edition*. F.A. Davis, Philadelphia, 1993
37. Thompson J.M. *A Finite Element Model of the Rib Cage*. Thesis, University of Alberta, 1995
38. Ueno K., Liu Y.K. A Three-Dimensional Nonlinear Finite Element Model of Lumbar Intervertebral Joint in Torsion. *J. Biomechanical Engineering* Vol 109, 1987
39. White A.A. and Panjabi M.M. *Clinical Biomechanics of the Spine - 2nd Edition*. J.B. Lipincott Co., USA, 1990
40. Wilke HJ., Kettler A., Claes L.E. Are Sheep Spines a Valid Biomechanical Model for Human Spines? *Spine* Vol 22, No 20, pg 2365-74, 1997
41. Vertebral Body Centroid Data taken from Digitized Radiograph. Glenrose Hospital Research Center, Edmonton, Alberta